

# FY01 Supplemental Science and Performance Analyses,

Volume 1: Scientific Bases and Analyses  
Part 2 of 2



U.S. Department of Energy  
Office of Civilian Radioactive Waste Management

June 2001

CO1

## 8. WATER DIVERSION PERFORMANCE

### 8.1 INTRODUCTION

Section 8 describes the new information developed to produce a more realistic model for water diversion (principally by the drip shield) through the engineered barrier system (EBS). More specifically, this information is designed to quantify uncertainties and reduce conservatisms in the EBS water diversion for the *Total System Performance Assessment for the Site Recommendation* (TSPA-SR) (CRWMS M&O 2000 [DIRS 153246]). The new information provides supplemental models or analysis in the following areas: (1) drip shield fluxes, (2) evaporation of seepage from the drip shield, (3) invert evaporation/condensation inside the drip shield, (4) waste package fluxes, and (5) bathtub flow through the waste package. Table 8-1 summarizes the rationale for the supplemental models and analyses in these five areas and identifies the specific section that documents the new information.

**Evaporation of Seepage Contacting the Drip Shield (8.3.1)**—The evolution of waste package heat has the potential to evaporate a portion of in-drift seepage that might contact the drip shield. The model provides an estimate of the fraction of this heat needed to evaporate seepage as it contacts the drip shield. Drip shield evaporation depends on a number of parameters: waste package heat evolution, forced air ventilation of the preclosure period, natural ventilation during the postclosure period, and drip shield surface conditions. The fraction of heat is treated as a random variable with potentially more evaporation taking place in the higher-temperature operating mode. The TSPA model was based upon a flow splitting algorithm that included flux into breaches and away from breaches in the drip shield (CRWMS M&O 2000 [DIRS 153246] Section 3.6.2.1). No credit is taken for potential evaporation at the surface of the drip shield. Consideration of this process potentially reduces the amount of seepage available for transport through the EBS. Alternative thermal operating modes are addressed by assuming two different temperature and relative humidity distributions for the higher- and lower-temperature operating modes. The impact on the amount of seepage available for transport over the range of thermal operating modes can be inferred from the time histories of time-dependent fluxes through the EBS (drip shield, waste package, and invert).

**Model for Drip Shield Condensation (8.3.2)**—This model quantifies the condensate flux on the underside of the drip shield due to evaporation and addresses what fraction will fall on the waste package. It was developed for the original EBS flow abstraction, but was not included in subsequent calculations. This activity is only meant to supplement the rationale for screening out this process due to low consequence. Alternative thermal operating modes will not affect the conceptual model for condensation on the underside of the drip shield and waste package.

**Flux through the Drip Shield and Waste Package (8.3.3)**—The waste package degradation model (i.e., the WAPDEG V4.0 code) provides for predictions of the type, number, and timing of breaches in the drip shield and waste package. This information is used by the EBS water diversion abstraction to define the time-dependent fluxes that flow through (or are diverted around) the drip shield and the waste package. In this model, droplets fall randomly on a drip shield, and the model accounts for a random fraction of water that flows over the drip shield but is captured by breaches. The abstraction implemented in the TSPA-SR (CRWMS M&O 2000

Table 8-1. Summary of Supplemental Models and Analyses

Key Attributes of System	Process Model (Section of S&ER)	Topic of Supplemental Scientific Model or Analysis	Reason For Supplemental Scientific Model or Analysis			Performance Assessment Treatment of Supplemental Scientific Model or Analysis <sup>a</sup>		
			Unquantified Uncertainty Analysis	Update in Scientific Information	Lower-Temperature Operating Mode Analysis	Section of Volume 1	TSPA Sensitivity Analysis	Included in Supplemental TSPA Model
Long-Lived Waste Package and Drip Shield	In-Drift Moisture Distribution (4.2.5)	Condensation under drip shields	X			8.3.2	X	
		Evaporation of seepage	X		X	8.3.1	X	X
		Effect of breached drip shields or waste package on seepage	X		X	8.3.3	X	X
		Waste package release flow geometry (flow-through, bathtub)	X			8.3.4	X	

NOTE: S&ER = *Yucca Mountain Science and Engineering Report* ([DOE 2001 [DIRS 153849]).

<sup>a</sup> Performance assessment treatment of supplemental scientific model or analysis discussed in SSPA Volume 2 (McNeish 2001 [DIRS 155023]).

[DIRS 153246], Section 3.6.3.1) conservatively considered all of the seepage entering the drift as falling on the crown of the drip shield and that all fluid that drips onto the drip shield or waste package occurs at the same axial location as the breach. The analyses are not intended to address alternative thermal operating modes, but rather to quantify conservatism in the TSPA-SR (CRWMS M&O 2000 [DIRS 153246]).

**Model for Bathtub Flow Through the Waste Package (8.3.4)**—An alternative conceptual model to the flow-through geometry is the bathtub geometry, which allows seepage to collect in the waste package before being released to the EBS. This effect will be most important during the first 20,000 years. At longer durations (100,000 years or greater), the presence of multiple penetrations for multiple groups of waste packages makes a flow-through geometry the likely long-term configuration. This model provides estimates of the time delays for the bathtub versus the flow-through model and an approach to quantify the uncertainty and sensitivity of total system performance assessment (TSPA) results to the bathtub versus the flow-through conceptual model. Alternative thermal operating modes will not affect the conceptual model for flow through the waste package.

The EBS is designed to function with the natural barriers at the site to minimize water contact with waste packages and waste forms. The components that will perform this function include the drip shield, the waste package, the waste package pallet, the invert (consisting of a steel support structure with crushed rock ballast), and the steel ground support. Another aspect of EBS performance is to moderate the transport of released radionuclides from breached waste packages to the host rock at the drift floor. This will be accomplished for the case of a breached waste package under an intact drip shield using a diffusion barrier concept. For the case of a breached drip shield, transport will be moderated through partial performance by reducing the amount of water that contacts the waste package. Finally, free drainage from the drifts is important for EBS performance. Sufficient drainage capacity will prevent partial inundation of waste packages or their supports, promote diffusion barrier performance of the invert, and prevent saturated flow conditions that could lead to faster transport for released radionuclides through the EBS and the host rock.

After the waste packages are emplaced, radioactive decay of the waste will heat the drifts. This heating process may evaporate some (or all) of the groundwater near the drifts, thereby perturbing the natural flow pattern for percolation of water through the mountain. As the drifts cool and the natural flow pattern is reestablished, some of the water percolating through the mountain may seep into the drifts and contact some of the drip shields. Any water dripped onto intact drip shields is considered to be diverted to the invert, except that which is evaporated directly. Over time, the drip shields and waste packages are expected to degrade. Once this occurs water can contact the waste form, resulting in the mobilization and transport of radionuclides through the EBS. This water may be flowing or dripping slowly through the EBS. Alternatively, this water may form a continuous film of stationary liquid. Water, as a stationary film or a flowing liquid, must be present for mobilization of radionuclides in the waste form and their transport through the invert and into the unsaturated zone (UZ).

The EBS flow abstraction model implemented for this study differs from the original model in the following respects.

**Evaporation of Seepage Contacting the Drip Shield**—Waste packages emit substantial quantities of heat for a few thousand years after emplacement. This model allows a fraction of this heat to evaporate seepage as it contacts the drip shield. The fraction of heat is treated as a random variable, with potentially more evaporation taking place in the higher-temperature operating mode.

**Flux through the Drip Shield and Waste Package**—The type, number, and timing of breaches in the drip shield and waste package are predicted by the *WAPDEG Analysis of Waste Package and Drip Shield Degradation V4.0* model (CRWMS M&O 2000 [DIRS 151566]). This information is used by the EBS flow abstraction to define the time-dependent fluxes that flow through (or are diverted around) the drip shield and the waste package. In this model, droplets fall randomly on a drip shield, and the model accounts for the fact that a fraction of the water that flows over the drip shield may be captured by breaches.

**Model for Drip Shield Condensation**—This model was developed for the original flow abstraction, but not included in subsequent calculations. It is implemented in this study. As discussed in Section 8.2, the basis for the conclusion is the low evaporation rates from the invert, which would be the principal source of water for drip shield condensation.

**Bathtub Model for the Waste Package**—This model allows liquid to accumulate in waste packages. This bathtub effect can occur when there are corrosion patches on the drip shield and the top surface of the waste package, but no penetrations on the bottom surface of the waste package. Water is eventually released from such a waste package when a breach forms on the bottom half.

The EBS flow abstraction model implemented in the TSPA-SR model (CRWMS M&O 2000 [DIRS 153246]) is described next. Each of the submodels summarized above is described in subsequent sections.

## **8.2 REVIEW OF TOTAL SYSTEM PERFORMANCE ASSESSMENT-SITE RECOMMENDATION TREATMENT**

The source of inflow to the EBS is the seepage flux into the drift that results from the downward infiltration of fluid through the existing fracture system at Yucca Mountain. The seepage flux is conceptualized to fall vertically downward onto the drip shield from discrete fractures above the roof of the drift, as represented in *Abstraction of Drift Seepage* (CRWMS M&O 2001 [DIRS 154291]) for EBS flow and transport.

The seepage flows through the EBS along eight pathways, as shown in Figure 8.2-1. These pathways are:

1. Seepage flux entering the drift—This is the liquid flow into the EBS.
2. Flow through the drip shield—Liquid flux through the drip shield begins once patches form due to general corrosion. Patches are defined from the results of the WAPDEG V4.0 model as void areas penetrating through the drip shield. The number of patches through the drip shield is calculated by the WAPDEG V4.0 model (CRWMS M&O 2000 [DIRS 151566], Section 6.5.1) independently of the EBS flow

abstraction. The nominal size of a patch is fixed for the WAPDEG V4.0 calculations for a generic waste package (CRWMS M&O 2001 [DIRS 153940], Section 4, Table 1). It is currently defined to be  $7.21 \times 10^4 \text{ mm}^2$ . The liquid flux through any patches in the drip shield is proportional to the seepage flux entering the drift multiplied by the ratio of the axial length of all patches in the drip shield to the total axial length of the drip shield.

3. Diversion around the drip shield—The portion of the flux that does not flow through the drip shield is modeled as bypassing the invert and flow directly into the UZ. This approach is consistent with a pseudo-steady flow because the sum of the fluid volume entering the drip shield (Pathway 2) and the fluid volume diverted around the drip shield (Pathway 3) must equal the fluid volume entering the EBS (Pathway 1) for a steady-state system. Diversion directly to the UZ is also reasonable because diverted flow does not contact the waste form and is not contaminated with radionuclides. It is, therefore, ignored by the EBS transport abstraction.
4. Flow through the waste package—The fluid flow through the waste package is based on the presence of patches due to general corrosion. The number of patches through the waste package is calculated by the WAPDEG V4.0 model independently of the EBS flow abstraction. The nominal size of a patch is fixed for the WAPDEG V4.0 calculations; it is currently defined to be  $2.346 \times 10^4 \text{ mm}^2$  (CRWMS M&O 2000 [DIRS 153940], Section 4, Table 1). The area of each stress corrosion crack,  $4.08 \times 10^{-6} \text{ m}^2$  (CRWMS M&O 2000 [DIRS 153940], p. 51), is estimated from gap width calculations in the *EBS Radionuclide Transport Abstraction* (CRWMS M&O 2000 [DIRS 153940], Section 6.3.1.2.1) based upon residual stresses in the welded lids of the waste package in *Stress Corrosion Cracking of the Drip Shield, the Waste Package Outer Barrier, and the Stainless Steel Structural Material* (CRWMS M&O 2000 [DIRS 151564], Figure 13). This area corresponds to a hole with an elliptical cross section that is 1.6 inches long by 0.005 inches wide (CRWMS M&O 2000 [DIRS 153940], Section 6.3.1.2.1). The liquid flux through any patches in the waste package is proportional to the seepage flux falling on the waste package multiplied by the ratio of the axial length of all patches in the waste package to the total axial length of the waste package. The seepage flux falling on the waste package is equal to the liquid flux through the drip shield plus a condensation flux for unanticipated conditions in which condensation would form under the drip shield.
5. Flow diversion around the waste package—The portion of the flux that does not flow through the drip shield and into the waste package is modeled as bypassing the waste form and flow directly to the invert.
6. Evaporation from the invert condensation underneath the drip shield—The magnitude of the evaporative flux from the invert is based on the thermal-hydrologic abstraction (CRWMS M&O 2001 [DIRS 154594]). If the drip shield is cooler than the invert, then all the evaporative flux is modeled as dripping on the waste package. If the drip shield is hotter than the invert, then no evaporative condensation flux drips on the waste package. The magnitude of the evaporative flux and the temperatures of the drip shield and invert are precalculated and abstracted to provide runtime input data

for the EBS model in the TSPA-SR (CRWMS M&O 2000 [DIRS 153246], Section 3.6.2.1). The rationale for this approach is explained in the *EBS Radionuclide Transport Abstraction* (CRWMS M&O 2000 [DIRS 153940], Section 6.3.3). Analysis results from the *Water Distribution and Removal Model* (CRWMS M&O 2001 [DIRS 152016], Section 6.4) show that condensation is not likely to occur before 10,000 years. At times after 10,000 years, the evaporation rates in the invert are insignificant, less than  $0.013 \text{ m}^3/\text{year}/\text{m-drift}$  (CRWMS M&O 2001 [DIRS 154594], Section 6.4.6).

7. Flow from the waste package to the invert—All flux from the waste package flows to the invert, independent of breach location on the waste package. The presence of the emplacement pallet is ignored, and the waste package is modeled as lying on the invert so that a continuous liquid pathway for diffusive transport exists at all times.
8. Flow through the invert into the UZ—All fluid and mass flux into the invert is immediately released into the UZ, consistent with the quasi-static assumption for flow through the EBS.

These pathways are time-dependent because of thermal effects and corrosion. At early times, when the waste package internal temperature is above the boiling point of water in the higher-temperature operating mode, the spent nuclear fuel (SNF) will remain dry and advective transport is impossible. At later times, corrosive processes will create time-dependent breaches in the drip shield and waste package. Breaches in both the drip shield and the waste package must exist before advective flow can transport radionuclides out of the waste package. These pathways are also location-dependent. For example, all pathways will have zero advective flux in the non-dripping areas of the repository.

The most important element of the EBS flow abstraction is the flow-splitting algorithm, which determines the fluid volume that flows through the drip shield or waste package and the remainder that flows around the drip shield or waste package. This algorithm assumes that the liquid flux through any patches or pits that penetrate the drip shield or waste package is proportional to the ratio of the total length of all penetrating patches or pits in the axial direction to the total axial length of the drip shield or waste package. This algorithm is equivalent to assuming that a patch or pit will collect all fluid that drips or flows onto the drip shield or waste package at the same axial location as the patches or pits. It assumes that drips on the right-hand side of a drip shield or waste package would contribute to the flow through a patch or pit on the left-hand side. This is not physically possible because the droplets cannot flow uphill, against the direction of gravity.

Inputs to the flow abstraction are taken primarily from other elements of the TSPA. These inputs include:

- The flux of fluid into the EBS, as defined by the seepage flow abstraction (CRWMS M&O 2001 [DIRS 154291], Section 6.5; CRWMS M&O 2000 [DIRS 123916], Section 6.3)

- The temperature, relative humidity, saturation, and evaporative flux from the invert, as defined by the abstraction of thermal hydraulic calculations (CRWMS M&O 2001 [DIRS 154594], Section 6.3)
- The timing, size, number, and location (upper or lower surface) of breaches in the drip shield and waste package, as defined by results from WAPDEG V4.0 analyses (CRWMS M&O 2000 [DIRS 151566]).

Outputs from the flow abstraction include the time-dependent fluxes through the drip shield, waste package, and invert. These fluxes are used by the EBS transport abstraction to determine the mass of radionuclides released to the UZ.

The EBS flow abstraction for the TSPA-SR (CRWMS M&O 2000 [DIRS 153246]) is based on a reasonable approach that attempts to bound the average response of the EBS. It is based on typical flow processes, such as the advective flow of liquid water through the EBS and the potential for evaporation from the invert and condensation of water vapor on the underside of the drip shield. The use of reasonable bounds was employed because of potentially large uncertainties in the response of a very complex engineered system over long periods of time. Following are the noteworthy conservatisms in the flow abstraction.

**Seepage Through the Drip Shield Is Assumed to Always Fall on a Waste Package**—The current potential repository design has a small axial gap between adjacent waste packages. It is possible that the seepage through the drip shield between adjacent waste packages will fall directly to the invert, avoiding the waste package entirely. Also, it is possible that flow that occurs through the drip shield outside the waste package footprint would fall directly to the invert and avoid the waste package. These possibilities are conservatively ignored. Both these are minor conservatisms when the spacing between adjacent waste packages and the gap width between the waste package and the drip shield are small compared to the length of the waste package.

**Seepage Is Assumed to Wet the Drip Shield and Waste Package Randomly**—The pathways for seepage into the drifts are fractures or fracture sets. As a result, seepage will vary spatially and temporally over the waste packages. Therefore, the response of groups of waste packages is represented as averages for performance assessment. In addition, breaches are considered to be located so that it will collect all fluid that drips onto the drip shield or waste package at the same axial location as the breach. This representation conservatively ignores the fact that fluid dripping onto the lower portion of the drip shield or waste package will not flow through a breach high on the drip shield or waste package. It also conservatively ignores the fact that seepage on the left half of a drip shield or waste package cannot flow through a breach on the right half. Breach location is, therefore, conservative by a factor of approximately two for the calculation of fluid flows into the drip shield and waste package.

**Release of Radionuclides Through Advective Transport Is Independent of the Location of Breaches on the Waste Package**—Advective transport out of the waste package is based on a flow-through model that is independent of the location of penetrations through the drip shield or waste package. This means that advective transport will occur even if a waste package has only

one penetration, or if it has one or more penetrations on its upper surface and none on its lower surface.

**Evaporation Within and on the Waste Package Is Ignored**—Diffusive transport will cease if the heat from the waste form can evaporate any thin liquid films on the waste form. Advective transport will cease if the heat from the waste form can evaporate the small seepage flux onto and into the waste package. The potential for evaporation to eliminate radionuclide transport is conservatively ignored in the EBS abstractions. This is a minor conservatism for diffusive releases from the waste package. As discussed in Section 7.2.2, the best estimate of the thermal aging model, based on available data, indicates that thermal aging of Alloy 22 base metal would not progress to a significant level in the first 10,000 years (CRWMS M&O 2000 [DIRS 147639], Section 6.2). The earliest breach of any waste package occurs after 10,000 years, and the mean waste package lifetime is tens of thousands of years (CRWMS M&O 2000 [DIRS 153246], p. xviii).

Each of the new submodels developed for this study is described in the following sections. Evaporation of seepage is presented in Section 8.3.1. Section 8.3.2 presents the drip shield condensation model. New waste package and drip shield flux models are presented in Section 8.3.3. A bathtub waste package flow model is presented in Section 8.3.4.

### **8.3 UNCERTAINTY ANALYSES**

#### **8.3.1 Evaporation of Seepage**

##### **8.3.1.1 Goal of the Model**

In this model, the source of inflow to the EBS is the seepage flux into the drift that results from the downward infiltration of fluid through the existing fracture system at Yucca Mountain. The seepage flux is conceptualized to flow from discrete fractures above the roof of the drift, falling vertically downward onto the drip shield and waste package. A significant portion of the seepage that contacts the drip shield may evaporate, thus reducing the amount of seepage ultimately available for transport. The goal of this model is to calculate the amount of seepage flux that evaporates as a function of time and reduce the amount of liquid seepage moving through the EBS accordingly.

##### **8.3.1.2 Identification of Unquantified Uncertainties in Total System Performance Assessment-Site Recommendation**

The potential for evaporation to reduce seepage is conservatively ignored in the EBS abstractions. In the nominal scenario, the earliest breach of any waste package occurs after 10,000 years (CRWMS M&O 2000 [DIRS 147639], Section 6.2). The mean waste package lifetime is tens of thousands of years (CRWMS M&O 2000 [DIRS 153246], p. xviii). Evaporation will be most significant when in-drift temperatures are elevated after repository closure, and would affect mass transport only modestly. However, in the unlikely event that waste packages or drip shield might degrade due to juvenile failures, evaporation has the benefit of providing defense-in-depth. For this reason, evaporation effects on seepage were added to the TSPA abstraction models developed in Volume 2 (McNeish 2001 [DIRS 155023], Sections 3.2.6 and 4.2.6).

The effectiveness of evaporation on decreasing the seepage flow available for advective transport is uncertain, primarily because of representational model uncertainty. Heat from the waste package is transferred to the drip shield, then to the drift wall, by conduction, convection, and thermal radiation. The portion of this heat flux that goes to evaporating seepage is uncertain with respect to location and timing.

### 8.3.1.3 Model for Evaporation of Seepage

The approach taken to account for the potential evaporation rate of the incoming water at the top of the drip shield after emplacement is based on the evaporation model presented in the *Abstraction of NFE Drift Thermodynamic Environment and Percolation Flux* (CRWMS M&O 2001 [DIRS 154594], Section 6.3.10).

The evaporation rate at the top of the drip shield is bounded by the amount of heat available to vaporize water on the upper portion of the drip shield. This heat flow rate into the upper portion of the drip shield is used to determine the maximum volumetric flow rate of incoming seepage water that can be completely vaporized at this location.

The evaporation rate is computed according to the following steps. An energy balance is performed on the upper surface of the drip shield. The energy balance relates the heat input at this location to the maximum amount of incoming water that can be completely vaporized by the heat flow. Also, it relates to the effect of evaporative cooling for liquid that would fall directly on the drip shield, as discussed in Section 8.3.2.3. The energy balance is (CRWMS M&O 2001 [DIRS 154594], Section 6.3.10, Equation 4):

$$q_{ds} = \rho_l Q_{EVAP} h_{fg} \quad (\text{Eq. 8-1})$$

where

- $q_{ds}$  = heat input to the drip shield [W]
- $\rho_l$  = density of the incoming water [ $\text{kg}/\text{m}^3$ ]
- $Q_{EVAP}$  = drip shield evaporation which equals the maximum rate that water can be vaporized by the heat at this location [ $\text{m}^3/\text{s}$ ]
- $h_{fg}$  = latent heat of vaporization [J/kg].

The seepage rate into the drift is considered to be non-episodic, and the seepage is modeled as falling randomly on the upper surface of the drip shield. In the energy balance equation, the incoming water reaches the top of the drip shield at the vaporization temperature of the drip shield, which neglects heating by radiation, convection, or convection of liquid water (typically small compared to latent heat exchange).

The heat input at the drip shield,  $q_{ds}$ , can be rewritten in terms of the waste package heat output. The representative heat flow (by thermal radiation) from the top waste package to the underside of the top portion of the drip shield is some fraction  $\chi$ , nominally one-half of the total waste package heat generation rate ( $q_{wp}$ ). Thermal radiation is the dominant mode of heat transfer in a no-backfill emplacement drift. Implementing this and rearranging the energy balance equation,

the maximum evaporation rate is (CRWMS M&O 2001 [DIRS 154594], Section 6.3.10, Equation 5):

$$Q_{EVAP} = \frac{\chi q_{wp}}{\rho_l h_{fg}} \quad (\text{Eq. 8-2})$$

The waste package heat generation rate,  $q_{wp}$ , is evaluated for an average commercial SNF waste package (Figure 8.3.1-1). The non-commercial waste package heat output is based on DOE high-level radioactive waste (Figure 8.3.1-2). Implementation of an average waste package heat generation rate implies that the waste packages are close enough together that the radiant heat exchange and the (axial) heat flux through the drip shield is uniform.

The energy balance equation can be evaluated using temperature-dependent or constant (evaluated at an appropriate average temperature) fluid properties. To reduce the complexity of the model, constant fluid properties are used at an average incoming fluid temperature of 60°C. Calculations show that this is reasonable, with a negligible difference between evaporation rates obtained with constant and temperature-dependent properties (CRWMS M&O 2001 [DIRS 154594], Section 6.3.10).

#### 8.3.1.4 Implementation of Seepage Evaporation Model

The actual fraction of total heat flux emitted that is available for evaporating seepage is uncertain because of several factors. Heat flux is variable over the length of a waste package and drip shield, with the center of the waste package and drip shield likely being hotter than the edges. This variability is influenced by waste package spacing, with closely spaced waste packages tending to have less variation in heating from the center to the edges. Drips are modeled as falling randomly on the drip shield. If drips fall on a portion of the drip shield where the heat flux is low, such as near the ends of a waste package, the effective rate of evaporation will be lower compared to drips falling on a higher heat flux region, such as near the center of the package. In addition, evaporation effectiveness may be reduced if all the seepage is concentrated in a single stream, as opposed to several randomly spaced smaller drips, since smaller drips require less heat flux for evaporation. In addition, smaller drips will tend to experience more evaporation because they fall from the drift wall to the drip shield, thus reducing the seepage that actually impinges on the drip shield. To account for these uncertainties, the expression for evaporation rate is modified by introducing a random number from zero to one,  $f_{evap}$ . This parameter determines the fraction of potential evaporation that may occur. Using this parameter, the effective evaporation rate per waste package is determined using an approach similar to the drip shield evaporation (CRWMS M&O 2001 [DIRS 154594], Equation 5):

$$Q_{EVAP} = \frac{(1/2)q_{wp}}{\rho_l h_{fg}} f_{evap} \quad (\text{Eq. 8-3})$$

In the present treatment,  $f_{evap}$  is a random number that ranges from 0 to 1 in the higher-temperature operating mode (1.45 kW/m) and from 0 to 0.8 in the lower-temperature operating mode (1.12 kW/m). These heat loadings are presented in Table 2-1. The latter upper bound is considered to be equal to the ratio of the linear thermal loading, that is, 1.12/1.45, or approximately 0.8.

The net amount of seepage that is potentially available for sheet flow across the drip shield is given by the difference between the seepage flow onto the drip shield minus the seepage evaporated, as discussed in Section 8.3.3.3.1. This net amount of sheet flow not evaporated ( $Q_{SFNE}$ ) is given by:

$$Q_{SFNE} = Q_{SF} - Q_{EVAP} \quad (\text{Eq. 8-4})$$

where  $Q_{SF}$  is the sheet flow of water onto the top part of the drip shield [in  $\text{m}^3/\text{yr}$ ] as determined by the drip shield flux model. Note that  $Q_{SFNE}$  may range from zero to a value of  $Q_{SF}$ . In the latter case, all water that flows onto the drip shield evaporates.

### 8.3.2 Drip Shield Condensation Model

#### 8.3.2.1 Goal of Model

The drip shield condensation model is used to quantify the amount of condensate that may form on the underside of the drip shield and fall on the waste package.

#### 8.3.2.2 Identification of Unquantified Uncertainties in Total System Performance Assessment-Site Recommendation

As noted in Section 8.2 (Item 6), the formation of condensate on the underside of the drip shield due to evaporation is not included because analyses indicated that the effect of this process on repository performance would be insignificant.

If condensate forms on the underside of a drip shield, it will form during the cooling period. For condensate to form underneath the drip shield, the partial vapor pressure at the invert interface underneath the drip shield must be greater than the saturation vapor pressure at the drip shield. Thermal hydrology results show the potential for this condition to occur at times later than 1,000 years (CRWMS M&O 2001 [DIRS 152016], Section 6.4). Two key uncertainties in the process of drip shield condensation are: (1) how much water condenses on the drip shield (if condensation occurs) for the given thermal-hydrologic environment, and (2) what fraction of this condensate will fall on the waste package rather than flow downward along the sides of the drip shield. These uncertainties are addressed together by considering that the rate of condensation is proportional to the rate of evaporation from the invert where the proportionality constant, denoted  $f_c$ , is a random number between 0 and 1. This is written as:

$$q_{cond} = E_{invert} f_c \quad (\text{Eq. 8-5})$$

where  $E_{invert}$  ( $\text{m}^3/\text{yr}/\text{m-drift}$ ) is the evaporation rate in the invert as provided by the results in the *Abstraction of NFE Drift Thermodynamic Environment and Percolation Flux* (CRWMS M&O 2001 [DIRS 154594], Section 6.3.10). This flux value,  $q_{cond}$ , is converted to a condensate flow rate underneath the drip shield  $Q_{CWP}$  using:

$$Q_{CWP} = q_{cond} L_{WP} \quad (\text{Eq. 8-6})$$

where  $L_{WP}$  is the length of the waste package, equal to 5.17 m for commercial SNF (e.g., a 21-PWR waste package) and 3.59 m for high-level waste (HLW) (e.g., a 5-DHLW/DOE SNF Short waste package) (BSC 2001 [DIRS 154461], Item 3, Table 9).

### 8.3.2.3 Implementation of the Drip Shield Condensation Model

A conceptual model for drip shield condensation based on a simple node network has been developed that provides qualitative information for the formation of drip shield condensation. Figure 8.3.2.3-1 presents a conceptual model for EBS sensible and latent heat flow paths and drip shield condensation. The conceptual model treats the waste package, the drip shield, the invert, the air spaces between the waste package and the drip shield, and between the drip shield and the drift wall. It considers the latent heat exchange from evaporation off of the invert and potential film condensation underneath the drip shield.

The decay heat produced by the waste package during the postclosure period is the principal driver for EBS processes within the drift. The flow of heat from the waste package into the surrounding environment creates temperature differences, which result in thermal gradients for heat transfer by convection and radiation and liquid and vapor transport.

Heat is transferred from the waste package to the drip shield above and the invert below by thermal radiation and convection. These same mechanisms transfer heat from the drip shield to the drift wall. Conduction and mass transport carry the heat from the invert and drift wall into the surrounding rock.

#### 8.3.2.3.1 Sensible Heat Transfer Within the Annulus

The following discusses methods used to estimate the heat transfer for radiation, convection, and conduction within the EBS. Radiative heat transfer can be modeled for gray bodies through modification of the Stefan-Boltzmann equation between two surfaces, such as concentric cylinders (Incropera and DeWitt 1996 [DIRS 107784], p. 739) that account for geometry above and below the drip shield.

The nature of the thermal radiation varies with temperature and relative humidity. The degree to which the gas participates in the radiative heat transport varies as a function of the water vapor density. At low water vapor pressures, the water vapor is relatively transparent and intersurface radiation heat transport (waste package to drip shield, drip shield to drift wall) dominates. As the water vapor density increases, the water begins to participate; a portion of the energy radiated from the hot surface is absorbed by the water vapor, which radiates to the cold surface. The net effect is to diminish the relative contribution of thermal radiation to the intersurface heat transport (Siegel and Howell 1992 [DIRS 100687], pp. 572 to 573).

Several convection cells (Figure 8.3.2.3.1-2) that are symmetrical about the vertical mid-plane characterize the free convective heat transfer in the annular space between long, horizontal concentric cylinders (Incropera and DeWitt 1996 [DIRS 107784], p. 512). If the inner test cell or waste package is heated to a temperature  $T_{WP}$  and the drip shield is cooled to a temperature  $T_{DS}$ , fluid ascends and descends along the inner and outer cylinders, respectively (Incropera and DeWitt 1996 [DIRS 107784], p. 512). The effective thermal conductivity is the value that a stationary fluid should have to transfer the equivalent amount of heat as the moving fluid, the

effective thermal conductivity is a function of the Prandlt and Raleigh numbers (Incropera and DeWitt 1996 [DIRS 107784], pp. 512 and 509).

The nature of the convective pattern varies with the temperature difference between the bounding surfaces. Just after incipient gas motion, large roll cells form in the gas. Thermal and viscous boundary layer thicknesses are on the same order as the cavity dimensions, making the temperature of the gas dependent on its location in the cavity. Rising gases above the heat source (inner cavity: waste package; outer cavity: top of drip shield) are hotter than descending gases (inner cavity: drip shield sides; outer cavity: drift walls).

As the driving temperature differences increase, laminar flow instabilities form above the waste package and the top of the drip shield. The large roll cells begin to divide into smaller cells. These processes begin to homogenize the gas temperatures within the roll cells.

When the temperature differences are sufficiently large, the large-scale roll cell structure becomes completely transient. Cell breakdown and oscillation combine to make the bulk of the gas nearly isothermal. Under these conditions, the local heat transfer between a bounding surface and the gas is a function of the local conditions: local wall temperature, wall inclination, and gas temperature.

The velocities associated with the large-scale roll cells will increase with an increasing temperature difference in the region above the base of the waste package. However, between the waste package and the invert, the temperature gradient favors fluid stability for heating from above. Only the cooling from the drip shield walls would drive any large-scale roll cells. This should cause a small amount of counterflow in the region below the waste package.

The invert is composed of crushed tuff and has a thermal conductivity less than that of the surrounding rock because of its higher porosity and predominantly air-filled voids, as presented in the *Water Distribution and Removal Model* (CRWMS M&O 2001 [DIRS 152016], Table 4-5 and Attachment XIV.1). The various analyses show that the invert is at a somewhat higher temperature than the wall. If the invert were a perfect thermal insulator, the top surface would have the same temperature as the adjacent air. If the gas within the drip shield is nearly isothermal and drip shield cooling is sufficiently strong due to latent heat transfer (evaporative cooling), the invert surface temperature might exceed the temperature at the top of the drip shield. Although this scenario is very unlikely, as discussed below, the temperature difference is one of the requirements for condensation under the drip shield.

#### **8.3.2.3.2 Invert Evaporation**

Water vapor and heat are carried away from the immediate vicinity of the invert surface by the turbulent bulk flow of parcels of air containing quantities of heat and vapor. These parcels are carried upward in a chaotic manner, exchanging their contents with other parcels, which, in turn, are carried away from the surface. The net result is a transport of heat and water vapor between two heights: the invert surface and some height within the annulus. This turbulent flux is proportional to the vapor concentration or temperature difference (Jury et al. 1991 [DIRS 102010], p. 173). The difference in vapor pressure between the invert surface and the annulus is called the saturation pressure deficit. The heat transfer coefficient,  $h_H$ , and the water

vapor transfer coefficient,  $h_v$ , are considered to be equal according to the similarity hypothesis, which is reasonably accurate under most conditions at the surface (Jury et al. 1991 [DIRS 102010], p. 172). During the transient drying of the invert, control of the evaporation can pass from the temperature-humidity conditions of the annulus to the soil resistance of the invert. Also, vapor pressure lowering can be effected by osmolality. The rate of evaporation from a wet, bare soil surface is limited by internal conditions within the annulus. In contrast, water loss from a soil with a dry surface layer is regulated primarily by soil water resistances that limit the rate at which water moves upward to the evaporating surface, as described by the Penman Equation (Jury et al. 1991 [DIRS 102010], p. 153). In this latter case, the water evaporation rate will likely be less than the maximum potential loss dictated by the conditions within the annulus through the use of the Penman Equation.

Note that in the conceptual model described above, an upward latent heat flux from the surface (as governed by the Penman Equation) occurs outside the footprint of the waste package, and would result in latent heat exchange to the annulus. Heat transfer directly below the waste package represents heating from above. Vertical heat transfer in this zone would be conduction dominated with little convective enhancement. As the driving temperature difference increases, the fraction of heat that moves downward through the invert decreases.

### **8.3.2.3.3 Film Condensation Underneath the Drip Shield**

According to Incropera and DeWitt (1996 [DIRS 107784], p. 568), latent heat transfer by drop-wise condensation is an order of magnitude larger than that for film condensation. Therefore, if condensation occurs, it would occur initially by film condensation. As discussed below, the basis for this is that film condensation is an effective latent heat transfer mechanism relative to evaporation from the invert.

Condensation will occur on the inner surface of the drip shield if the drip shield temperature,  $T_{DS}$ , is less than the saturation temperature,  $T_{sat}$ , which is set to equal to the annulus temperature,  $T_{AN}$ . In modeling the heat transfer due to condensation, the drip shield can be approximated as a cylindrical surface. Incropera and DeWitt (1996 [DIRS 107784], pp. 560 to 568) present solutions for film based upon Newton's Law of Cooling. The rate of condensation below the drip shield equals the rate of evaporation from the invert outside the waste package footprint.

According to the nonlinear relation for heat transfer by radiation and convection, the invert temperature is highly dependent upon the heat flux partitioning under the drip shield. Larger fractions of the heat traveling downward through the invert will produce higher invert temperatures and lower drip shield temperatures. The network model shows that smaller fractions of heat traveling vertically downward will produce lower invert temperatures and higher drip shield temperatures. Therefore, to determine if condensation under the drip shield is possible, some knowledge of the heat flux partitioning produced by the combined mechanisms of thermal radiation and gas convection, as they can be studied with the simple network model presented above, is necessary.

The EBS Pilot Scale Test #3, conducted at the Atlas Facility in North Las Vegas, Nevada, consisted of a simulated quarter-scale waste package and drip shield resting on an invert of crushed tuff. The temperature, relative humidity; and flow data (DTN: SN0003L1011398.003

[DIRS 149765]) collected from this test provides information for validating the numerical models described above that form the basis of the EBS performance assessment model.

The most significant observations from EBS Pilot Scale Test #3 (BSC 2001 [DIRS 154479], Section 5) were:

- After heater power-up, temperatures approached steady state-conditions within a period of 3 to 5 days.
- Temperature differences were observed along the waste package surface due to natural convection.
- The coolest temperatures on the drip shield were higher than the coolest parts of the invert.
- No condensation of water was observed below the drip shield.

The test observations are consistent with recorded drip shield temperatures above the waste package (BSC 2001 [DIRS 154479], Figure 35) and at the point where the drip shield rests on the invert (BSC 2001 [DIRS 154479], Figure 38). The latter data, which reflects the invert temperature, shows that for the conditions simulated in the test, relative humidities increased during dripping. In comparing the dewpoint temperatures with the drip shield temperature, at no point were the two equal.

EBS Pilot Scale Test #3 provides important information on the concept of a drip shield to effectively protect simulated waste packages from infiltrating water under heated conditions at the one-quarter scale. No drip water or condensation was seen under the drip shield or on the waste package for conditions simulated in the test. The relative humidity at the top of the test cell stayed at about 85 percent, and under the drip shield it was about 65 percent. Based on temperatures and relative humidity, the water vapor pressure appeared to be approximately the same at these locations, with slight variations as a function of temperature variations.

As noted previously, in order for condensate to form underneath the drip shield, the partial vapor pressure at the invert interface underneath the drip shield must be greater than the saturation vapor pressure at the drip shield. The vapor pressures at the drip shield and invert are reduced somewhat by the presence of dissolved salts. In addition, the vapor pressure at the invert is reduced somewhat by capillary pressure. These effects on vapor pressure are rather complex, as discussed above, and no attempt will be made to include them in the model described here.

The conceptual model presented above shows that drip condensation is not anticipated to occur because the drip shield temperature is higher than the invert temperature. A possible scenario for drip shield condensation is that seepage impinging on the top surface of the drip shield cools the drip shield sufficiently to satisfy the dewpoint temperature on the inner surface of the drip shield. However, in the pilot scale test described above, the infiltration condition evaluated was higher than 300 mm/yr (BSC 2001 [DIRS 154479], Section 2.3.1), which is much higher than the anticipated percolation rates for the repository as presented in the *Water Distribution and Removal Model* (CRWMS M&O 2001 [DIRS 152016], Section 5.1.6). Therefore, cooling of the

drip shield by evaporation off the upper surface is not expected to result in drip shield condensation.

If TSPA results show that drip shield condensate is potentially important, then a more detailed model incorporating some of the features discussed above would be warranted. In the present implementation approach, condensate on the drip shield forms if:

$$T_{DS} \leq T_{invert} \quad (\text{Eq. 8-7})$$

where  $T_{DS}$  and  $T_{invert}$  are the temperatures of the drip shield and invert [ $^{\circ}\text{C}$ ], respectively. If this condition is satisfied, the condensate flux value is calculated using the flux equation in Equation 8-6.

### **8.3.3 Drip Shield and Waste Package Flux Models**

#### **8.3.3.1 Goal of Model**

The drip shield and waste package limit the amount of water contacting the waste forms during the postclosure period. The drip shield and waste package seepage flux models are used to quantify the amount of seepage that penetrates a breached drip shield and waste package.

#### **8.3.3.2 Identification of Unquantified Uncertainties in Total System Performance Assessment-Site Recommendation**

The EBS flow abstraction conservatively modeled all of the seepage as entering the drift falls on the crown of the drip shield as discussed in detail in the *EBS Radionuclide Transport Abstraction* (CRWMS M&O 2000 [DIRS 153940], Section 5.1). For seepage to contact the drip shield, droplets must form and fall from the rock roof. Other modes of flow, such as film flow on the drift wall, are possible, and may divert some or all of the seepage influx around the wall of the opening without dripping. This latter flow mode was conservatively ignored. In addition, the drip shield and waste package seepage flux models conservatively modeled any breach as located so that it will collect all fluid that drips onto the drip shield or waste package at the same axial location as the breach (CRWMS M&O 2000 [DIRS 153940], Section 5.1). These conservatisms were implemented in part to obviate the need to explicitly account for uncertainty in flux calculations.

To provide a more reasonable and less conservative estimate of flow onto the drip shield, drips will be modeled as falling randomly on the upper surfaces of the drip shield or waste package. Therefore, the probability of a drip intercepting a breach is given by the ratio of projected breach area to upper drip shield or waste package surface area. The probability that a drip will not intercept a breach is the complement of this probability. The fraction of non-intercepting drips that ultimately penetrate the drip shield and waste package is an uncertain quantity and has been identified as an uncertainty that will be quantified.

#### **8.3.3.3 Model for Drip Shield and Waste Package Flux**

In the present treatment, seepage is modeled as comprised of drips that fall randomly on the upper surface area of the drip shield, rather than along the crown of the drip shield. If a random

drip falls onto a breach, it is modeled as penetrating the drip shield. If a drip does not fall onto a breach, a fraction of this drip may splatter or flow into a neighboring breach. The fraction of seepage that penetrates the drip shield resulting from splatter and flow is treated as uncertain. The total seepage penetrating the drip shield is therefore that fraction of the seepage that directly intercepts breaches and that fraction of the seepage that splatters or flows into breaches. After seepage penetrates the drip shield, it may be assumed to fall on the upper half of the waste package or form film flow on the underside of the drip shield. The modeling approach and considerations used for the drip shield are also used to calculate the seepage through the waste package, the difference being that the corresponding waste package breach and projected areas are used.

### 8.3.3.3.1 Drip Shield Flux Model

The probability ( $P_{FDIB}$ ) of flow droplets impinging directly onto the breach and displacing water is given by the ratio of the projected breach area ( $A_{B,DS}$ ) to the projected drip shield surface area ( $A_{DS}$ ):

$$P_{FDIB} = \frac{A_{B,DS}}{A_{DS}} \quad (\text{Eq. 8-8})$$

Here, projected area refers to the area seen in a plan view of the drip shield looking downward from the crown of the emplacement drift. To simplify the present treatment,  $A_{B,DS}$  is considered to be equal to the actual breach area on the upper surface of the drip shield. This is slightly conservative because the actual breach area is always greater than the projected breach area on the upper curved surface of the drip shield. The probability as evaluated above is therefore slightly higher for a random drip to intercept the breach. The complementary probability of a drip not directly intercepting a breach is given by  $(1 - P_{FDIB})$ . The lengths of the waste packages for commercial SNF and HLW are 5.17 m and 3.59 m, respectively, (BSC 2001 [DIRS 154461], Item 3, Table 9). The width of the drip shield is 2.51 m (CRWMS M&O 2000 [DIRS 153940], Table 1). The  $A_{DS}$  is equal to  $2.51 \text{ m} \times 5.17 \text{ m} = 12.98 \text{ m}^2$  for commercial SNF waste packages and  $2.51 \text{ m} \times 3.59 \text{ m} = 9.01 \text{ m}^2$  for HLW waste packages. Waste package length is used to calculate the areas.

The total amount of seepage penetrating a drip shield is given by the sum of the seepage flow directly into breaches ( $Q_{FDIB}$ ) and sheet or splattering flow into breaches ( $Q_{SFIB}$ ). The partitioning of flow, discussed below, is illustrated by the conceptual drip shield flux model in Figure 8.3.3-1 and the event tree in Figure 8.3.3-2. The following flow definitions are presented:

- $Q_{SEEP}$  = Seepage flow into the drift
- $Q_{DS}$  = Flow on the top part of the drip shield
- $Q_{ODS}$  = Flow outside the drip shield
- $Q_{FDIB}$  = Seepage flow directly into breaches
- $Q_{SF}$  = Sheet flow onto drip shield
- $Q_{SFNE}$  = Sheet flow not evaporated
- $Q_{EVAP}$  = Drip shield evaporation
- $Q_{SFIB}$  = Sheet or splattering flow into breaches
- $Q_{SFAB}$  = Sheet flow away from breaches

The following probabilities are defined:

- $P_{FDS}$  = Probability of flow directly onto the drip shield
- $P_{FDIB}$  = Probability of flow droplets impinging directly onto the breach and displacing water
- $P_{EVAP}$  = Probability of drip shield evaporation
- $P_{SFNE}$  = Probability of sheet flow not evaporated (depends on temperature and relative humidity)
- $P_{SFIB}$  = Combined probability of sheet flow into breaches and water moving through the crevices to the underside of the drip shield (depends on temperature and relative humidity)

The first level of the event tree is the flow partitioning of the in-drift seepage ( $Q_{SEEP}$ ) that flows directly onto the top part of the drip shield ( $Q_{DS}$ ) and that falls outside the footprint of the drip shield ( $Q_{ODS}$ ) (shown by the dotted lines on Figure 8.3.3-1). Flow outside the drip shield flows directly to the invert without contacting the drip shield. The probability ( $P_{FDS}$ ) can be estimated by the simple ratio of the drip shield footprint to the tunnel footprint. The second level of the event tree is that water drops could fall directly onto breaches and potentially displace droplets by impact through the drip shield. This model for flow is described in the *Water Distribution and Removal Model* (CRWMS M&O 2001 [DIRS 152016], Section 6.1.1.2). Drops falling directly on the patches (saturated and unsaturated) result in kinetic energies that convert to pressure pulses (impulsive force) that break the capillary and gravitational force equilibrium if water is present. This causes some or all of the water to be displaced out of the crevices.

The spreading from the primary and secondary drops produces a thin film of water on the drip shield that very slightly thickens away from the crest (CRWMS M&O 2001 [DIRS 152016], Section 6.1.1.2). This is defined as sheet flow on the drip shield ( $Q_{SF}$ ). It is assumed that splashing and spreading cause the dripping water to be uniformly distributed on the drip shield. For sheet flow onto the drip shield ( $Q_{SF}$ ), a portion of the sheet flow ( $Q_{EVAP}$ ) may evaporate, as discussed previously. The evaporation rate on the drip shield depends deterministically on the temperature and relative humidity environment, which in turn would depend on variations in thermal and hydrological properties of the EBS and the surrounding media. This results in a probability  $P_{EVAP}$  and the complementary probability ( $P_{SFNE}$ ) of sheet flow water that is not evaporated.

As discussed in the *Water Distribution and Removal Model* (CRWMS M&O 2001 [DIRS 152016], Section 6.1.1.2), the breaches or crevices in the drip shield can be characterized for potential for capillary suspension. Crevices of various sizes will be developed in the drip shields due to pitting and crevice corrosions (i.e., by general corrosion and stress corrosion). Crevices in the drip shield can draw water from the thin film due to capillary suction and gravitational forces. The direction of the capillary force changes from downward to upward during the filling process, as discussed in the *Water Distribution and Removal Model* (CRWMS M&O 2001 [DIRS 152016], Section 6.1.1.2, Figure 6-3), which shows that the contact angle of water in the capillary increases from less than  $90^\circ$  to greater than  $90^\circ$  to accommodate the weight increase. The capillary force acts against gravity in holding the water in place when the contact angle is greater than  $90^\circ$ . The maximum contact angle is reached at  $180^\circ$ , which corresponds to a

maximum water holding capacity. Water content in the crevices can vary from saturated to partially-saturated to not capable of holding water (CRWMS M&O 2001 [DIRS 152016], Table 6-1) as the aperture sizes increase.

Film flows over saturated crevices have little impact on water held in the crevices due to the effects of capillarity. However, film flows into the partially-saturated crevices can cause pendant drops to be formed and released on the underside of the drip shield in a discrete manner.

The above discussion highlights some of the complexities in evaluating the potential for water to be imbibed into crevices for sheet flow. These complexities can be represented by the probability  $P_{SFIB}$ , which represents the combined probability of sheet flow occurring over breaches in the drip shield above the waste package and water moving through the crevice to the underside of the drip shield.

The event tree (Figure 8.3.3-2) provides the basis for assessing the probability for flow through the drip shield from seepage flow directly into breaches ( $Q_{FDIB}$ ) and for sheet flow outside the drip shield into breaches ( $Q_{SFIB}$ ), respectively:

$$Q_{FDIB} = P_{FDIB} \cdot P_{FDS} \cdot Q_{SEEP}$$

$$Q_{SFIB} = P_{SFIB} \cdot P_{SFNE} \cdot (1 - P_{FDIB}) \cdot P_{FDS} \cdot Q_{SEEP} \quad (\text{Eq. 8-9})$$

The conceptual model for flow through the drip shield provides a qualitative illustration for assessing advection through the drip shield. While actual probabilities may be assigned conservatively through selection of probabilities, the conceptual model indicates that droplets impacting on crevices would be low-probability events with high consequence for advection; while drip shield flow into breaches may occur with a somewhat higher probability, the consequence (depending on the environment) might be low.

### 8.3.3.3.2 Waste Package Flux Model

The modeling approach outlined in the preceding section for the drip shield is applied directly to the waste package as shown in Figure 8.3.3-2b. The following flow definitions are presented:

$Q_{CDS}$	= Condensate flow rate underneath the drip shield
$Q_{WP}$	= Flow onto waste package
$Q_{OWP}$	= Film flow on the inside of the drip shield or outside the waste package
$Q_{WPDFIB}$	= Waste Package flow directly into breaches
$Q_{WPSF}$	= Sheet flow onto waste package
$Q_{WPSFNE}$	= Waste package sheet flow not evaporated
$Q_{WPEVAP}$	= Waste package evaporation
$Q_{WPSFIB}$	= Waste package sheet flow into breaches
$Q_{WPSFAB}$	= Waste package sheet flow away from breaches

The following probabilities are defined:

- $P_{FOWP}$  = Probability of flow directly onto the waste package
- $P_{WPFIDIB}$  = Probability of flow droplets impinging directly onto the waste package breach and displacing water
- $P_{WPSFNE}$  = Probability of waste package sheet flow not evaporated (depends on temperature and relative humidity)
- $P_{WPSFIB}$  = Probability of sheet flow into waste package breaches (depends on temperature and relative humidity)

Once flow has occurred through the drip shield, there is a large probability that film flow will occur on the inside surface of the drip shield without flow dropping onto the waste package. This results in a low probability of flow ( $P_{FOWP}$ ) directly onto the waste package. As discussed in the results of EBS Pilot Scale Test #3 (BSC 2001 [DIRS 154479], Section 5), no drip water or condensation was observed under the drip shield or on the waste package for conditions simulated in the test. The water that had flowed through the interface of the metal strap and the drip shield, and through the interface between the drip shields, formed a thin film near the interface and flowed on the inside surface of the drip shield without contacting the waste package surface. While this observation does not apply in general to corrosion crevices and the narrow range of test conditions in the EBS Pilot Scale Test #3, it nevertheless shows that water flows are anticipated to dominantly form thin films.

The event tree presented for the waste package flux model indicates a very similar approach to the partitioning of waste package flow for the given temperature and RH environment. The total amount of seepage entering the waste package by advection is therefore respectively:

$$Q_{WP} = P_{WPFIDIB} P_{FOWP} \cdot (Q_{FDIB} + Q_{SFIB} + Q_{CDS})$$

$$Q_{WPSFIB} = P_{WPSFIB} \cdot P_{WPSFNE} \cdot (1 - P_{WPFIDIB}) \cdot P_{FOWP} \cdot (Q_{FDIB} + Q_{SFIB} + Q_{CDS}) \quad (\text{Eq. 8-10})$$

As in the case of the drip shield model, probability of flow droplets impinging directly on the waste package breaches and displacing water is given by:

$$P_{WPFIDIB} = \frac{A_{B,WP}}{A_{WP}} \quad (\text{Eq. 8-11})$$

where  $A_{B,WP}$  is the total breach area on the upper half of the waste package and  $A_{WP}$  is the projected area of the upper half of the waste package. As before, the probability of occurrence,  $f_{WP}$ , is assigned as a random number between zero and one.  $A_{WP}$  is equal to 8.07 m<sup>2</sup> and 7.29 m<sup>2</sup> for commercial SNF and HLW packages, respectively (length and diameter dimensions are taken from BSC 2001 [DIRS 154461], Item 3, Table 9).

#### 8.3.3.4 Implementation of Drip Shield and Waste Package Seepage Flux Models

The implementation of the drip shield model and waste package flux models require estimates of the various probabilities for flow. As noted previously, several of the probabilities can be

estimated by geometric factors, while others require more complex technical analysis. For some of the factors, conservative assumptions are made regarding probabilities in the absence of technical analysis or test data. Figure 8.3.3-3 presents information on geometric factors used in the drip shield model.

As discussed in the previous section, the probability of flow directly onto the drip shield ( $P_{FDS}$ ) can be estimated by the simple ratio of the drip shield footprint to the tunnel footprint, or by the ratio of the projected width of the drip shield ( $D$ ) to the tunnel diameter ( $D_T$ ). The probability of flow droplets impinging directly onto breaches and displacing water ( $P_{FDIB}$ ) is assigned by the ratio of the breached area of the drip shield ( $A_{B,DS}$ ) to the projected area of the drip shield ( $A_{DS}$ ) as is presented in Equation 8-8.

The probability of sheet flow into breaches ( $P_{SFIB}$ ) can in part be estimated by noting that sheet flow could occur from the crown of the drift shield to the sides of the drip shield. If a characteristic length ( $L$ ) is calculated based upon the square of the breached area of the drip shield ( $\sqrt{A_{B,DS}}$ ), then an estimate of  $P_{SFIB}$  would be the product of  $L$  and  $D/2$  divided by the area of the drip shield ( $A_{DS}$ ). To account for the fact that in-drift seepage drips on the drip shield below the location of the crevice, the  $P_{SFIB}$  can be multiplied by a random number ( $f_{DS}$ ) varying from zero to 1.

The *Water Diversion Model* (CRWMS M&O 2000 [DIRS 131108], Section 6.2.4) provides an analysis of the occurrence and flow of water through capillary tubes or parallel crevices. As the drip shield becomes wetter, a fraction of the voids will be filled with water and become available for flow. The tendency for water to be drawn in through the drip shield depends on the moisture potential on the inside surface of the drip shield. The moisture potential, in turn, depends on the relative humidity ( $RH$ ) and absolute temperature ( $T$ ) on the inside surface of the drip shield. At equilibrium, the water vapor potential equals the liquid water potential (Jury et al. 1991 [DIRS 102010], p. 60). Since the vapor and liquid phases are at about the same elevation, the relative humidity can be expressed as (Jury et al. 1991 [DIRS 102010], p. 60):

$$RH = \exp\left(\frac{M_w \psi}{\rho_w R T}\right) \quad (\text{Eq. 8-12})$$

$$\psi = \frac{\rho_w R T}{M_w} \ln(RH) \quad (\text{Eq. 8-13})$$

where

- $\psi$  = Moisture potential (bar)
- $\rho_w$  = Mass density of water ( $\text{kg/m}^3$ )
- $T$  = Temperature (K)
- $M_w$  = Molecular weight of water (0.018 kg/ mole)
- $R$  = Universal Gas Constant (8.314 Joule/(mole-K))
- $RH$  = Relative Humidity.

Figure 8.3.3-4 presents a plot of the relationship of the moisture potential ( $\psi$ ) to relative humidity from the equation above. The moisture potential ( $\psi$ ) is a strong function of relative

humidity (Equation 8-13), or the ratio of the vapor pressure ( $P_v$ ) on the inside of the drip shield to the saturated vapor pressure ( $P_{vsat}$ ) at absolute temperature ( $T$ ).

The *Water Diversion Model* (CRWMS M&O 2000 [DIRS 131108], Section 6.2.4) requires information on the flow geometry of the breaches in the drip shield to provide a flow analysis. However, at present the WAPDEG V4.0 model (CRWMS M&O 2000 [DIRS 151566], Section 6.5.1) only predicts the occurrence of patches ( $A_{B,DS}$ ), and no information exists on the flow geometry or distribution of crevice sizes for a deteriorating drip shield that could be applied to assessing the modification to probability. However, the analysis presented above suggests that the occurrence of flow is a strong nonlinear function of moisture potential or relative humidity. With this in mind, the modification probability for sheet flow into breaches ( $P_{SFIB}$ ) can in part be conservatively assigned as the ratio of vapor pressure to the saturated vapor pressure or the relative humidity. The modification to probability  $P_{SFIB}$  would be near one for a relative humidity of 100 percent, reflecting the potential retention and flow of water in crevices. At a lower relative humidity, such as 50 percent, the percentage of crevices retaining flow water would certainly be less than 50 percent, and a 50 percent relative humidity would tend to overestimate the probability for sheet flow into breaches.

The discussion above shows there will be a strong tendency for flow to occur in films on the inside surface of the drip shield, which would lower the probability  $P_{FOWP}$ . However, for large crevices in an environment of 100 percent saturation, there is a far higher probability for water to form droplets through crevices in the drip shield. A conservative approach to evaluating flow would be again to assign the probability  $P_{FOWP}$  on the basis of the relative humidity, which would tend to overestimate  $P_{FOWP}$  on the basis of the technical analysis presented above.

The same principles for assigning probabilities for the drip shield flux model apply to assigning probabilities for the waste package flux model. Since the waste package would have different temperature and RH environments, the overall probability for waste package flow would be lower.

### **8.3.4 Bathtub versus Flow Through Waste Package Model**

#### **8.3.4.1 Goal of Model**

The EBS flow abstraction model initiates advective flow through a waste package as soon as a single general corrosion patch forms anywhere on its surface (assuming that the drip shield already has failed and that the package is located in a region with seepage). There is no long-term buildup and retention of liquid within the waste package. There is also no significant resistance to flow through the waste form. This approach maximizes the immediate release and mobilization of radionuclides into the local groundwater environment, and is referred to as the flow-through geometry.

The approach is physically unrealistic because advective flow cannot occur through a single patch on the waste package when considering the bathtub effect. Also, water would be stored for some residence time on the waste package. The degree of conservatism in the approach will depend, in part, on the time delay between the first patch and the next patch that forms a continuous flow pathway through the waste package. In general, the onset of advective flow

through a waste package will be delayed until there is at least one patch on both the upper and lower surfaces of the waste package. This delay time was (conservatively) ignored in the TSPA-SR (CRWMS M&O 2000 [DIRS 153246], Section 3.6.1.1).

An alternative conceptual model to the flow-through geometry is the "bathtub" geometry. The bathtub geometry allows seepage to collect within the waste package before being released to the EBS when a patch forms in the lower half of the waste package. In theory, the patch failure scenario for a bathtub geometry could result in the sudden release of a large pulse of radionuclides. The bathtub effect will be most important during the first 20,000 years after repository closure (CRWMS M&O 2000 [DIRS 153940], Section 6.6). Patches are not anticipated, as discussed in Section 8.3.4.3. In this situation, there may be penetrations through the top of the waste package while the bottom surface remains intact, leading to retention of liquid water. At longer durations, such as 100,000 years or more, the presence of multiple penetrations for multiple groups of waste packages makes a flow-through geometry the likelier long-term configuration.

The goal of this model is twofold: (1) provide estimates of the time delays for the bathtub versus the flow-through model for the waste package, and (2) provide an approach to quantify the uncertainty and sensitivity of TSPA results to the bathtub versus flow-through conceptual model.

Alternative thermal operating modes will not affect the conceptual model for flow through the waste package.

#### **8.3.4.2 Identification of Unquantified Uncertainties in Total System Performance Assessment-Site Recommendation**

Prior to the TSPA-SR calculations (CRWMS M&O 2000 [DIRS 153246]), the response of the bathtub geometry was evaluated for a primary case and for three secondary cases (CRWMS M&O 2000 [DIRS 153940], Sections 6.6.1 and 6.6.2). The primary case includes consideration of two types of radionuclide release mechanisms: dissolution rate-limited and solubility-limited. The results for the primary case are based on a closed form analytic solution with constant values of inflow rate, dissolution rate, and solubility. The three secondary cases consider a step change in inflow rate (such as would occur from a climatic change), a change in groundwater chemistry, and a step change in flow geometry (such as would occur if a patch suddenly failed beneath the waterline). The basic geometry and flow pattern for the bathtub geometry is shown in Figure 8.3.4-1.

The general conclusion from the comparison of the flow-through and bathtub geometries is that the bathtub model often introduces a time delay in the release of radionuclides in comparison to the flow-through model (CRWMS M&O 2000 [DIRS 153940], Section 6.6.3). The flow-through model is therefore conservative in relation to the bathtub geometry for these cases. However, the flow-through model is not clearly conservative in all cases. For example, a pulse (additional mass) of radionuclides is released from a bathtub geometry if a (second) patch opens instantaneously beneath the water line. In this case, the flow-through model is not clearly conservative.

The uncertainty in radionuclide release due to the use of a flow-through versus bathtub geometry for the waste package was not quantified for the TSPA-SR (CRWMS M&O 2000 [DIRS 153246]). Several factors led to this decision: (1) the flow-through model is conservative for early arrival of radionuclides, (2) sorption in the unsaturated and saturated zones will tend to smooth out any discrete pulse released by the bathtub geometry, and (3) the repository is represented as 30 groups of waste packages, so a single bathtub failure for one group is averaged out by the response of the other groups. However, the concerns about the potential nonconservatism of the pulse release from the bathtub geometry make it advantageous to consider this alternative conceptual model for releases from the waste package.

### **8.3.4.3 Quantification of Previously Unquantified Uncertainty**

The WAPDEG V4.0 model (CRWMS M&O 2000 [DIRS 151566]) provide detailed information about the growth of patches, pits, and stress corrosion cracks on the surface of the drip shield and waste package. The WAPDEG V4.0 model is appropriate because it encompasses the full variability in waste package response due to corrosion rates, package-to-package variability, and environmental factors.

WAPDEG V4.0 output includes the time of first failure for patches, pits, and stress corrosion cracks in the drip shield and on the upper and lower surfaces of the waste package. This information is ideal for estimating the delay in release from a waste package if a bathtub geometry forms. For example, if the upper surface of the waste package fails before the lower surface, then fluid will collect in the waste package until a patch forms on the lower surface. Similarly, there is no bathtub delay time if the lower surface of the waste package fails before (Case 2001 [DIRS 155053], p. 1) the upper surface.

This analysis focuses on the formation of patches for two reasons. First, pits are not anticipated to form in the drip shield and waste package for the in-drift environment. Second, advective flow through stress corrosion cracks is expected to be negligible because their small size and the presence of a meniscus or corrosion products in the cracks will reduce the advective flux through cracks to insignificant levels compared to a patch. Patches are then the main advective pathway through the waste package.

Patch location on the waste package will influence the magnitude of any pulse release of radionuclides caused by a sudden failure in the lower surface. For example, a patch that forms at the bottom of the waste package will tend to maximize the pulse released by the bathtub effect. On the other hand, a patch high on the side of the waste package is unlikely to release a pulse, but will merely delay releases until the waste package fills to its level and begins to overflow.

In the following analysis, the patch location is considered to be at the crown for a top patch and at the bottom for a patch on the lower surface of the waste package. This approach provides a reasonable estimate of the variability in delay times for the bathtub versus flow-through models. It also is most relevant to the case for a pulse release that was identified as potentially nonconservative for the flow-through model. WAPDEG V4.0 output data (Case 2001 [DIRS 155053], p. 2) identify patches on the upper and lower surface, but do not provide information on their azimuthal location.

Output data (Case 2001 [DIRS 155053], p. 2) from a WAPDEG V4.0 calculation for 100 realizations have been analyzed to determine potential delays from a bathtub geometry. Each realization considers 400 waste packages, each of which provides a different time delay for the bathtub effect in the waste package. Analysis of the frequency and magnitude of the bathtub delay time in the 400 realizations is useful because: (1) it provides quantitative estimates of the time delays for the bathtub versus the flow-through model for the waste package, and (2) the WAPDEG V4.0 output provides distributions that can be sampled to determine the sensitivity of TSPA results to the bathtub versus flow-through models.

WAPDEG V4.0 output (Case 2001 [DIRS 155053], p. 2) includes the times for first failure of the top of the drip shield, of the top and bottom of the outer barrier of the waste package, and of the top and bottom of the inner barrier of the waste package. Since the outer barrier always fails before the inner barrier, its presence is ignored here. The following definitions provide the delay time for the bathtub effect:

$$\begin{aligned}
 T_{accum} &\equiv \text{Max}(t_{fail,DS}, t_{fail,topWP}) \\
 T_{flow-thru} &\equiv \text{Max}(t_{fail,DS}, t_{fail,topWP}, t_{fail,bottomWP}) \\
 T_{delay} &\equiv T_{flow-thru} - T_{accum}
 \end{aligned}
 \tag{Eq. 8-14}$$

where

- $T_{accum}$  = time when fluid begins to accumulate in the waste package
- $T_{flow-thru}$  = time when a flow-through geometry first forms
- $T_{delay}$  = the bathtub delay time
- $t_{fail,DS}$  = time of first failure of the drip shield
- $t_{fail,topWP}$  = time of first failure of the top surface of the waste package
- $t_{fail,bottomWP}$  = time of first failure of the bottom surface of the waste package.

The first definition states that a continuous pathway through the top surfaces of all barriers is required for seepage to accumulate within the waste package. The second definition states that flow-through cannot begin until failures in both the top and bottom surfaces of the waste package are present. The third equation defines the time delay between when water starts to accumulate and when an advective flow can occur through the waste package. This is the time delay due to the bathtub effect.

Figure 8.3.4-2 presents the delay times from a single WAPDEG V4.0 realization as a cumulative distribution function (CDF). The maximum bathtub delay time is 60,400 years (Case 2001 [DIRS 155053], p. 3). About half of the bathtub delay times are zero because failure of the top or bottom surfaces of the waste package is equally likely on the surfaces of the waste package. In this situation, the bottom of the inner barrier fails before the top of the inner pseudo-barrier in approximately half the realizations, so there is no bathtub effect for these cases.

Figure 8.3.4-3 presents the delay times from 100 WAPDEG V4.0 realizations as CDFs. Each function is based on the results for 400 waste packages for each realization. Note the large variability in the results, indicative of the large variability in corrosion rates and package-to-package variability for the corrosion models in the WAPDEG V4.0 model (CRWMS

M&O 2000 [DIRS 151566], Section 6.5.1). Although many realizations have zero bathtub delay times in 50 percent of the waste packages, there is one outlier with zero bathtub delay in approximately 90 percent of the waste packages. This realization probably has very slow corrosion rates for the drip shield in comparison to the waste package, so patches have already formed on the underside of the waste package by the time the drip shield fails. Note that the maximum delay time is over 200,000 years.

These results provide for a broad range of uncertainty. The WAPDEG V4.0 model provides an efficient analysis with multiple realizations to obtain mean values and variance. It also provides a CDF that can be used directly in the TSPA model to determine the appropriate bathtub delay time.

#### **8.4 SUMMARY AND ABSTRACTION PROVIDED TO TOTAL SYSTEM PERFORMANCE ASSESSMENT**

The preceding sections outline the submodels and uncertainties that should be quantified in further uncertainty analyses of water flow in the EBS. Where possible, reasonable ranges and/or distributions of uncertain TSPA input parameters are provided.

The following recommendations are made. The waste package heat rate that contributes to evaporation off the drip shield should be set to a fraction  $\chi$  (nominally one-half), as governed by Equation 8-2. The drip shield condensation model states the principle that condensation can only occur if the invert temperature exceeds the drip shield temperature. The results of EBS Pilot Scale Test #3 suggest that the invert temperature did not exceed the drip shield temperature for the simulated test conditions. Other arguments presented in Section 8.3.2.3.3 support the recommendation that drip shield condensation not be included.

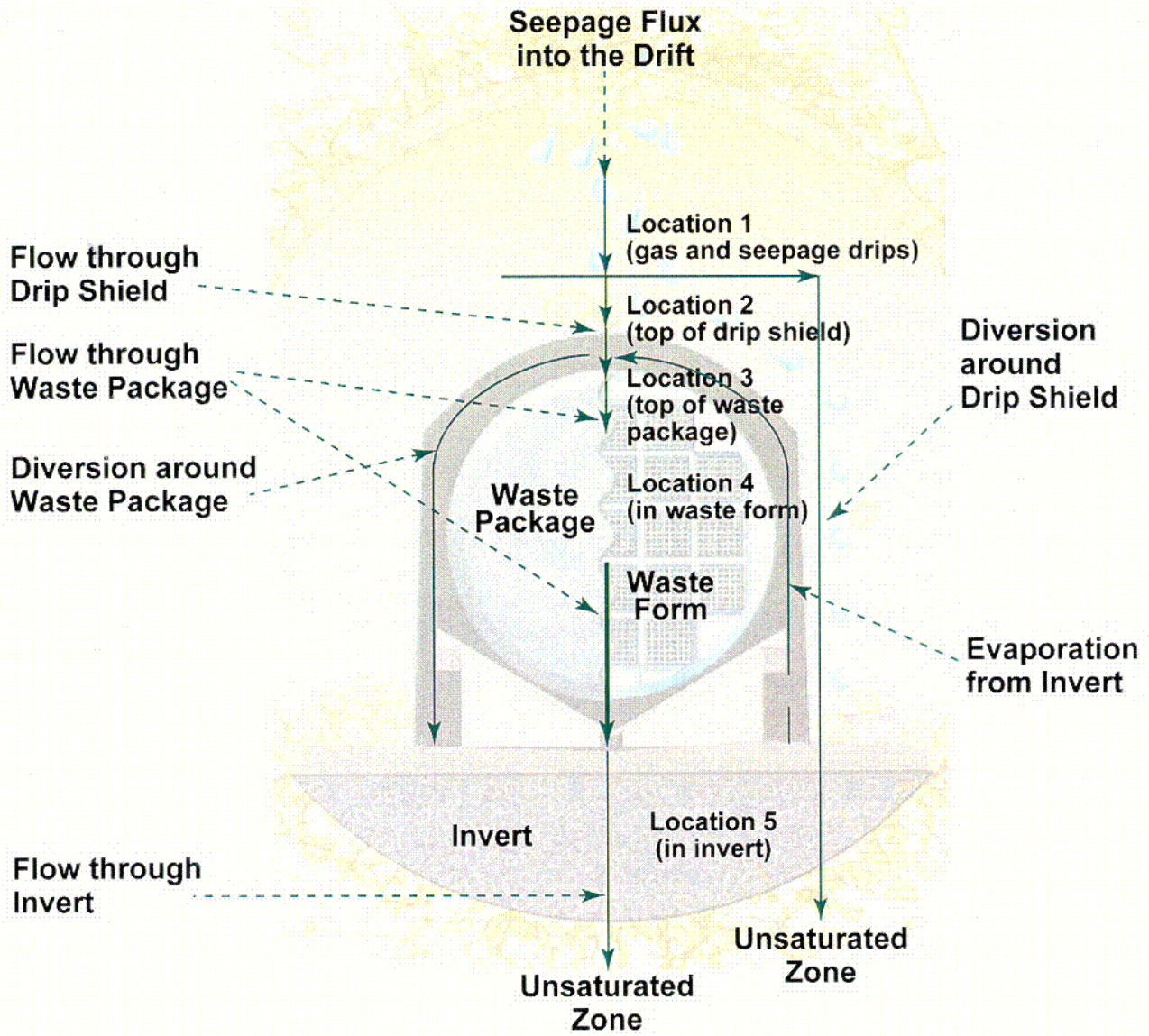
The following list summarizes the assignment of probabilities for the drip shield and waste package flux models:

- Assign the probability of flow directly onto the drip shield ( $P_{FDS}$ ) by the simple geometric ratio of the drip shield footprint to the tunnel footprint, or by the ratio of the projected width of the drip shield ( $D$ ) to the tunnel diameter ( $D_T$ ).
- Assign the probability of flow droplets impinging directly into breaches and displacing water ( $P_{FDIB}$ ) by the ratio of the breached area of the drip shield ( $A_{B,DS}$ ) to the projected area of the drip shield ( $A_{DS}$ ) (Equation 8-8).
- Assign the probability for sheet flow into breaches ( $P_{SFIB}$ ) on the top of the drip shield over the waste packages based on the square root of the breached area of the drip shield multiplied by half the drip shield width in plan ( $D$ ) and divided by the area of the drip shield ( $A_{DS}$ ). To account for the fact that in-drift seepage drips on the drip shield below the location of the crevice, the probability  $P_{SFIB}$  can be multiplied by a random  $f_{DS}$  between zero and one. It should be noted that there is uncertainty in the assignment of this probability, and that it could alternatively be assigned as the ratio of the breached area to the area of the drip shield.

- Assign a modification to the probability for sheet flow into breaches ( $P_{SFIB}$ ) to account for retention of water in breaches. The modification to the probability is based upon the relative humidity that would result in no flow reduction at 100 percent relative humidity and some reduction at lower relative humidities.
- Assign the probability for flow onto the waste package ( $P_{FOWP}$ ) on the basis of the relative humidity inside the drip shield. At high relative humidities, the probability is one to reflect the potential for pendant water to fall on the drip shield. At lower relative humidities, flow is much more likely to be dominated by film flow on the inside surface of the drip shield.
- Assign the flow onto the waste package using a similar approach to that of the drip shield for sheet flow and flow through the waste package using the waste package flow geometry.

It is recommended that the bathtub release model not be used because the flow-through model is conservative for the reasons cited in Section 8.3.4.2.

INTENTIONALLY LEFT BLANK

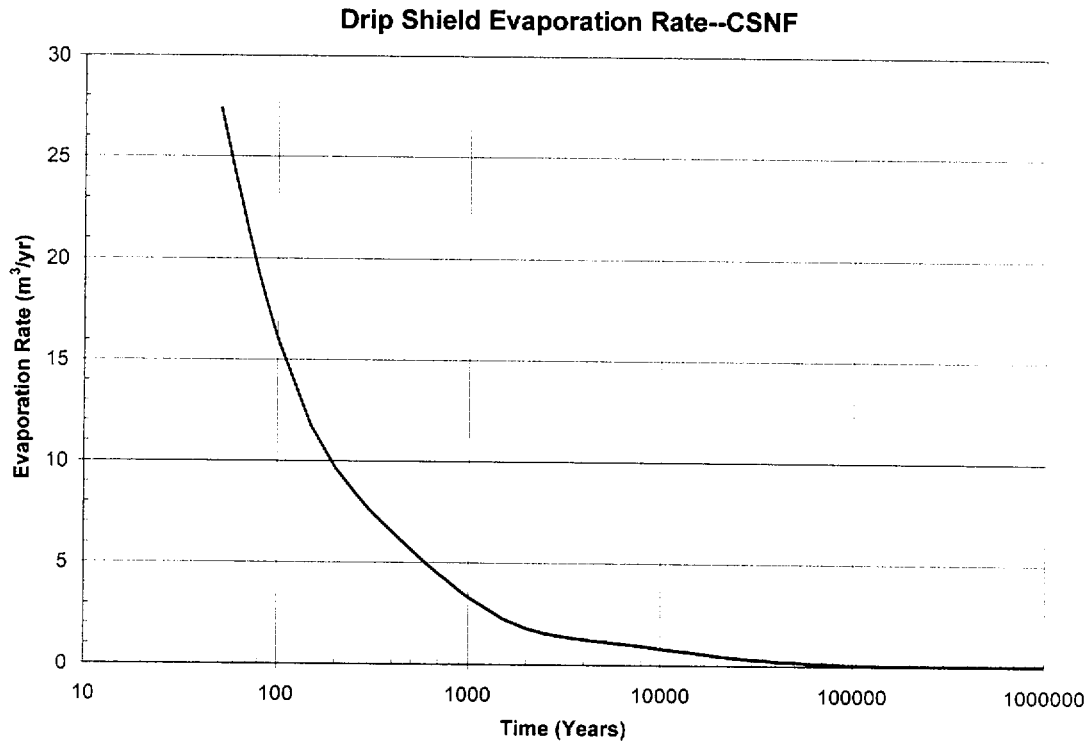


154\_0261.ai

154\_0261.ai

Figure 8.2-1. Schematic Diagram of Engineered Barrier System Flow Pathways

CO2

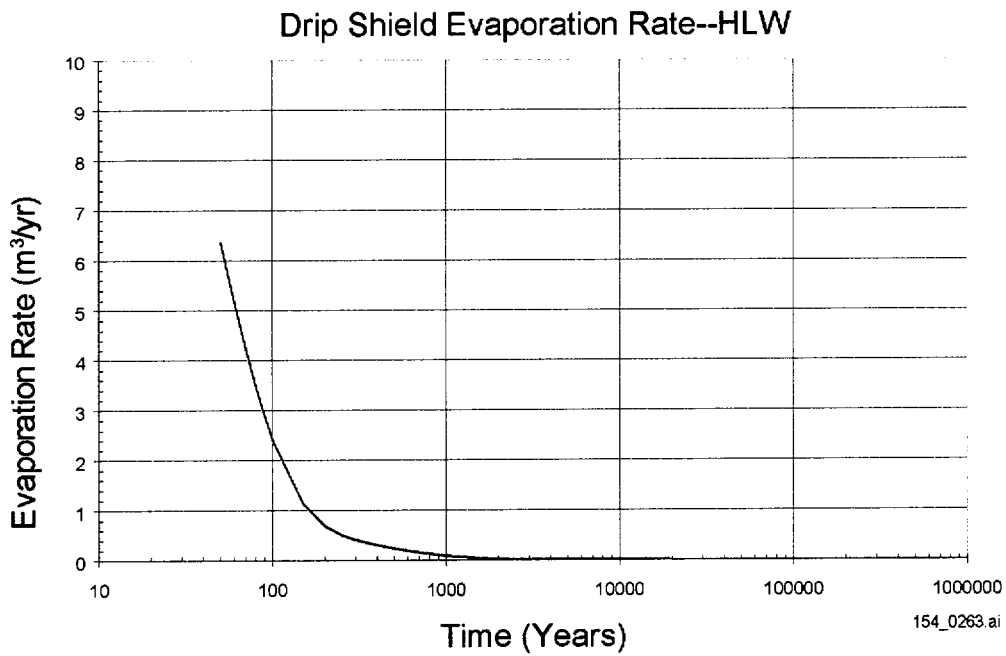


154\_0262.ai

154\_0262.ai

Source: CRWMS M&O 2001 [DIRS 154594], Figure 53.

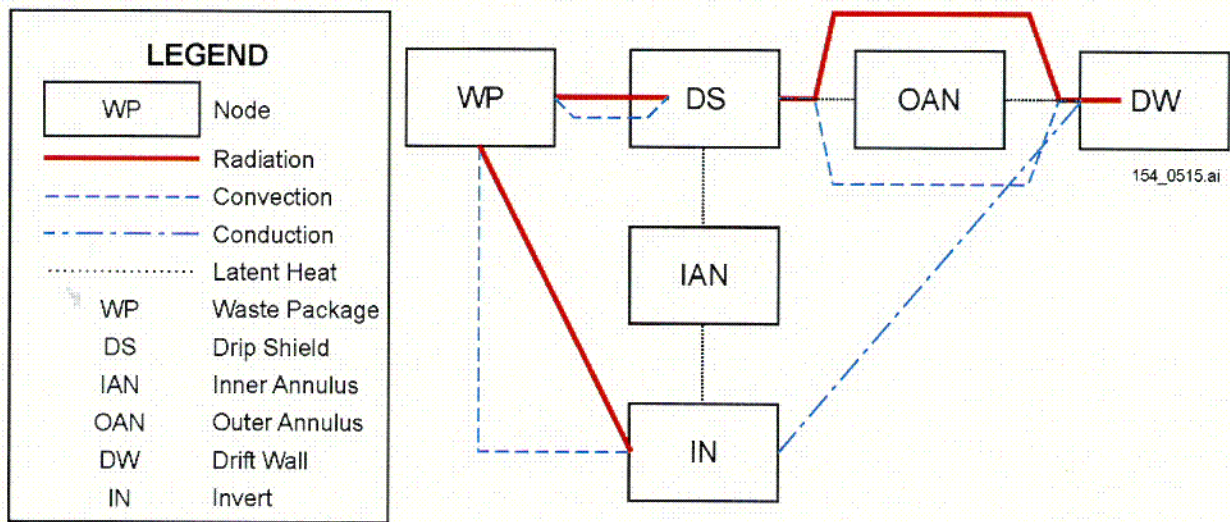
Figure 8.3.1-1. Average High Level Radioactive Waste Drip Shield Evaporation Rate



154\_0263.ai

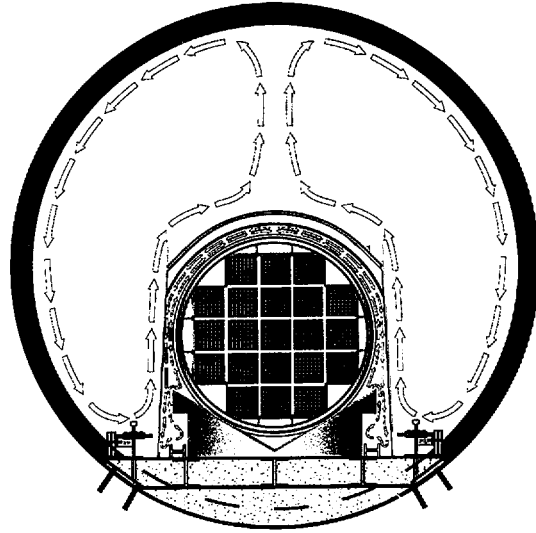
Source: CRWMS M&O 2001 [DIRS 154594], Figure 54.

Figure 8.3.1-2. Average Non-Commercial Drip Shield Evaporation Rate



154\_0515.ai

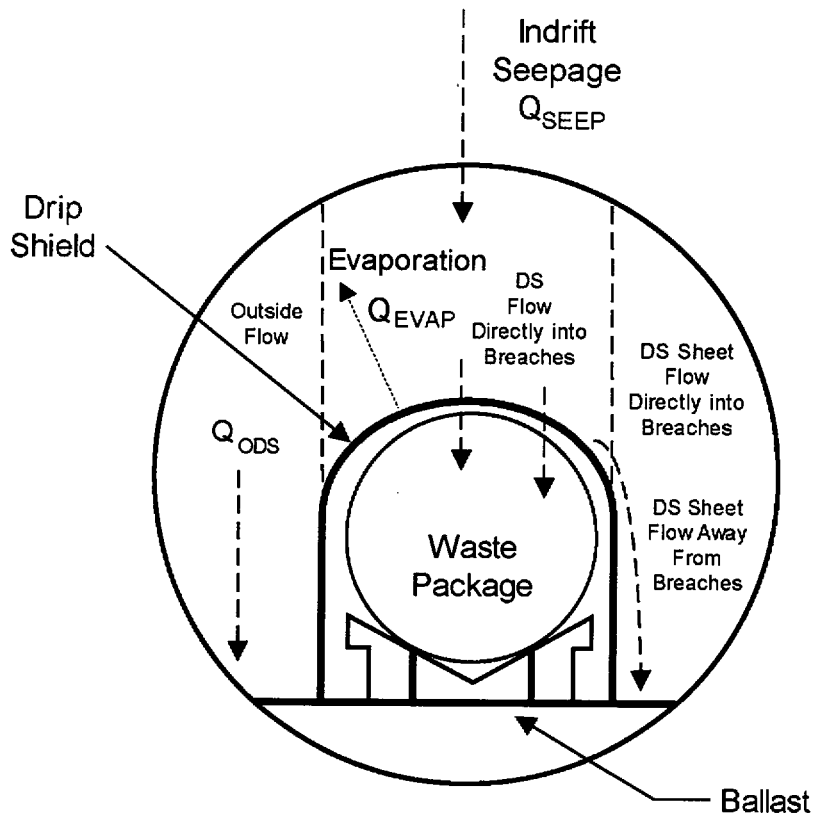
Figure 8.3.2.3-1. Conceptual Model for EBS Sensible and Latent Heat Flow Paths and Drip Shield Condensation



Drawing Not To Scale  
154\_0516.ai

154\_0516.ai

Figure 8.3.2.3.1-1. Main Convection Cells within the EBS



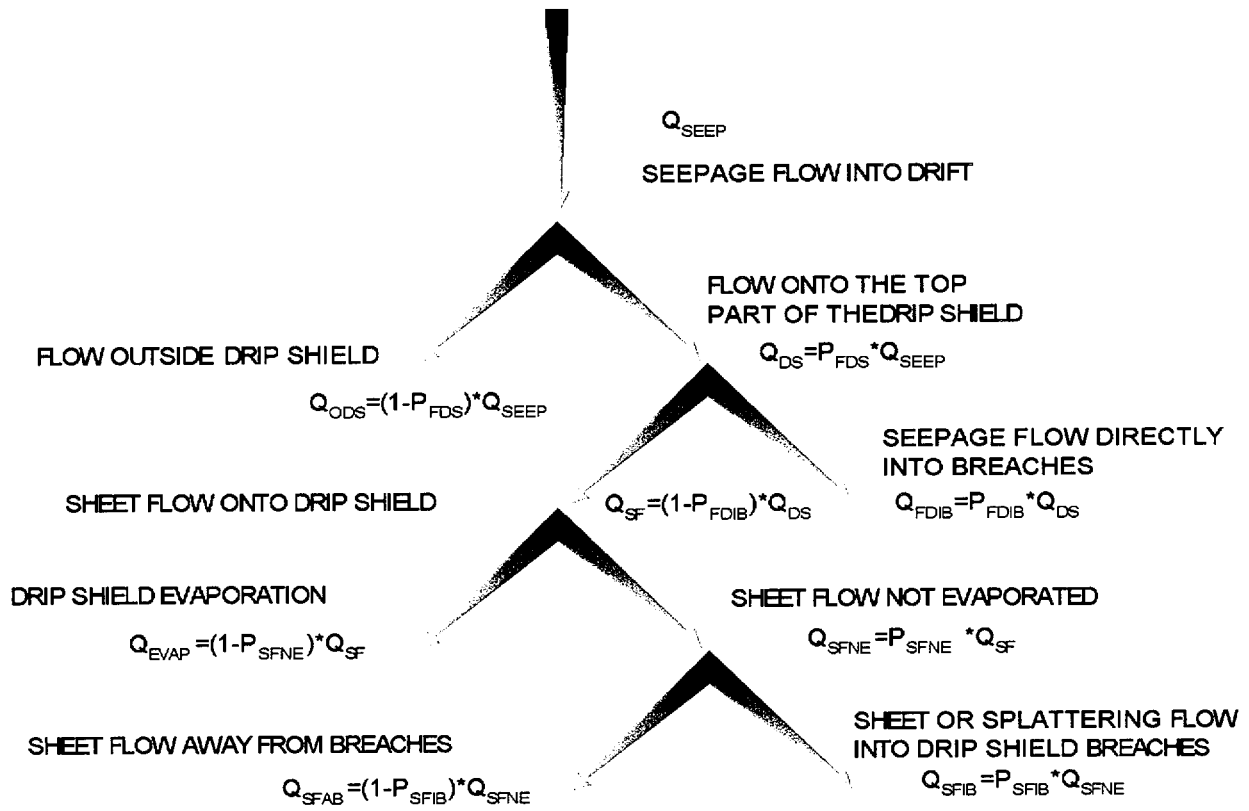
$$Q_{EVAP} = \frac{\left(\frac{1}{2}\right) q_{wp}}{\rho_l h_{fg}} f_{evap}$$

Eq. 8.3

154\_0453.ai

154\_0453.ai

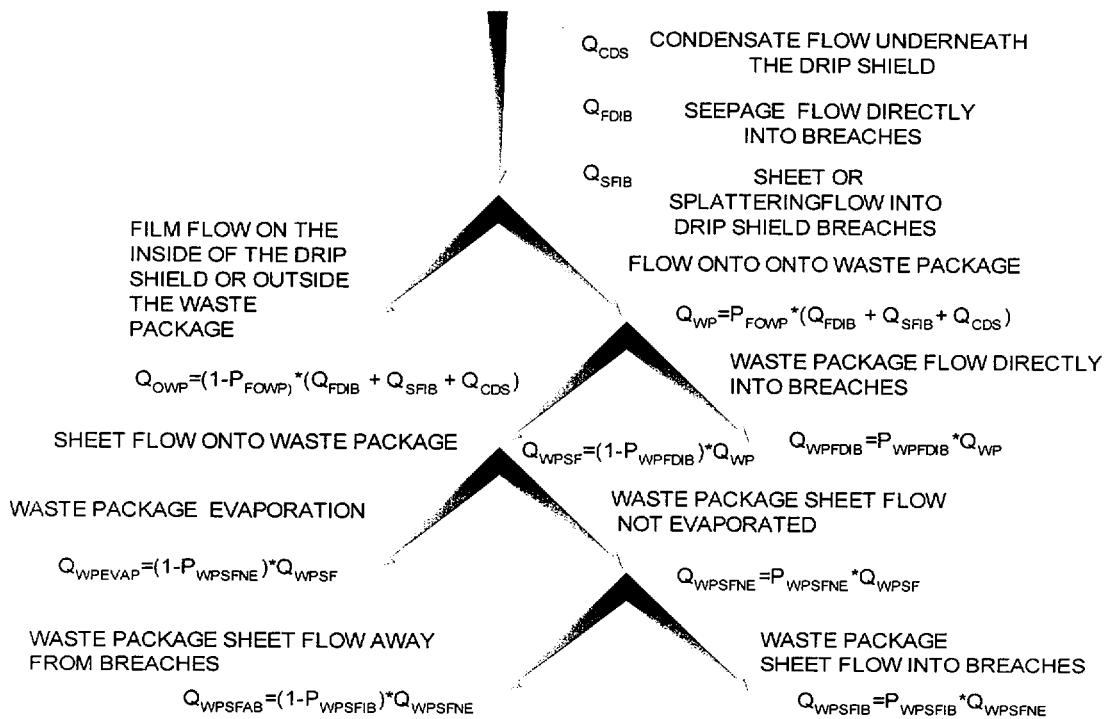
Figure 8.3.3-1. Conceptual Drip Shield Flux Model



154\_0454.ai

154\_0454.ai

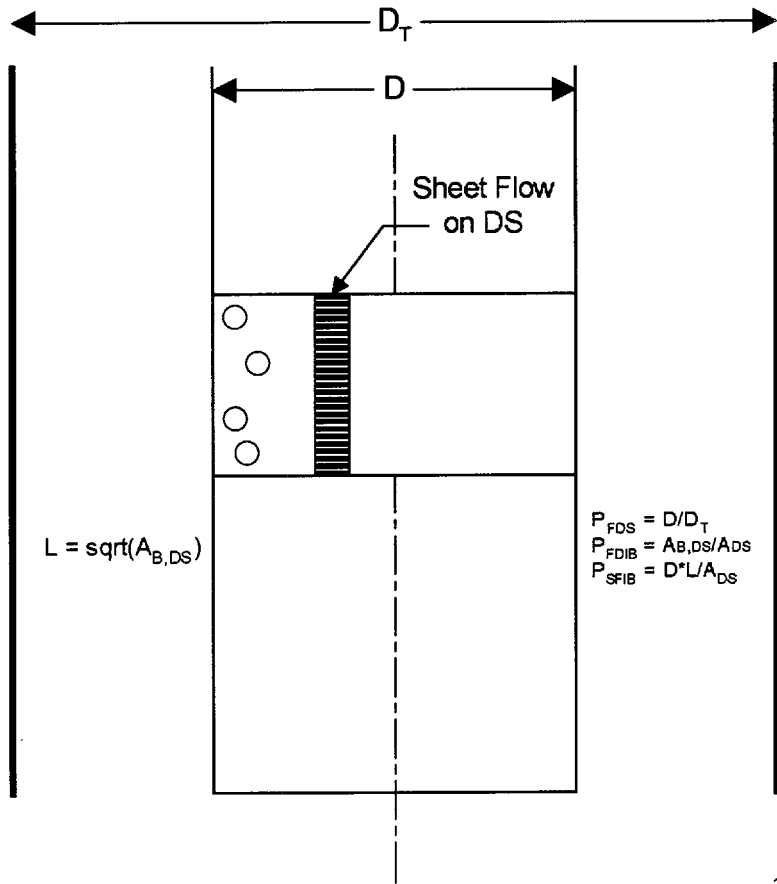
Figure 8.3.3-2. Event Tree for the Drip Shield Flux Model



154\_0547.ai

154\_0547.ai

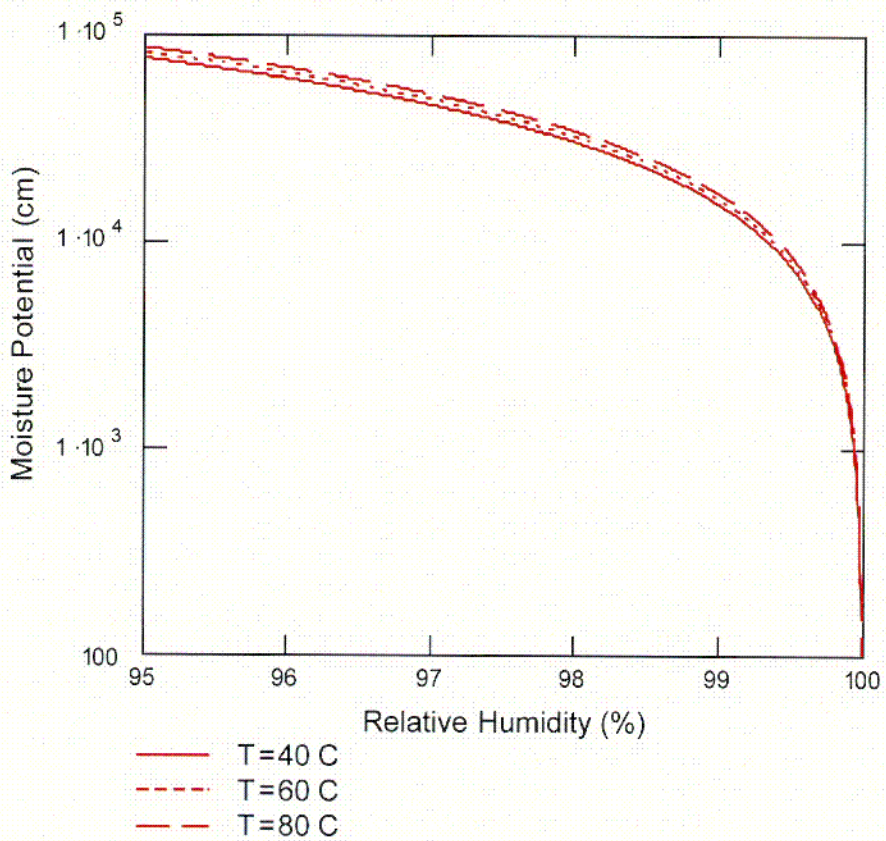
Figure 8.3.3-2b Event Tree for the Waste Package Flux Model



154\_0455.ai

154\_0455.ai

Figure 8.3.3-3. Geometric Factors in the Assignment of Probabilities



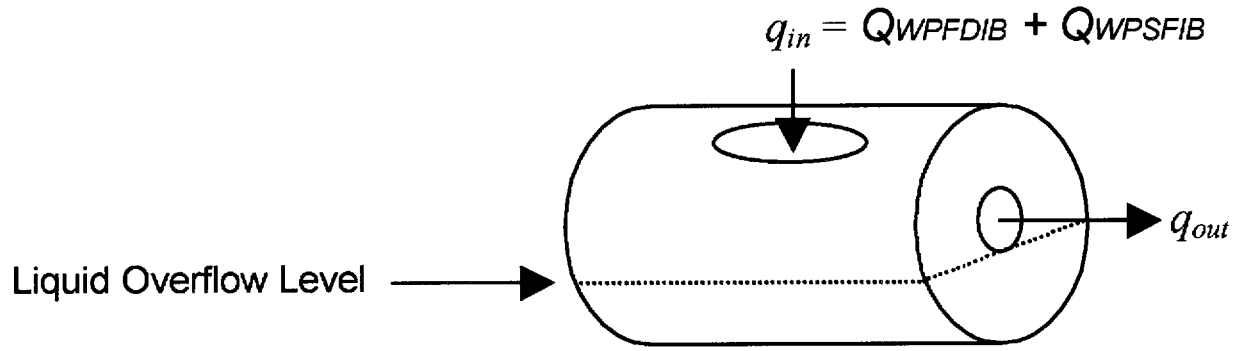
154\_0456.ai

154\_0456.ai

Source: CRWMS M&O 2000 [DIRS 131108], Figure 13.

Figure 8.3.3-4. Relationship of Moisture Potential to Relative Humidity

204

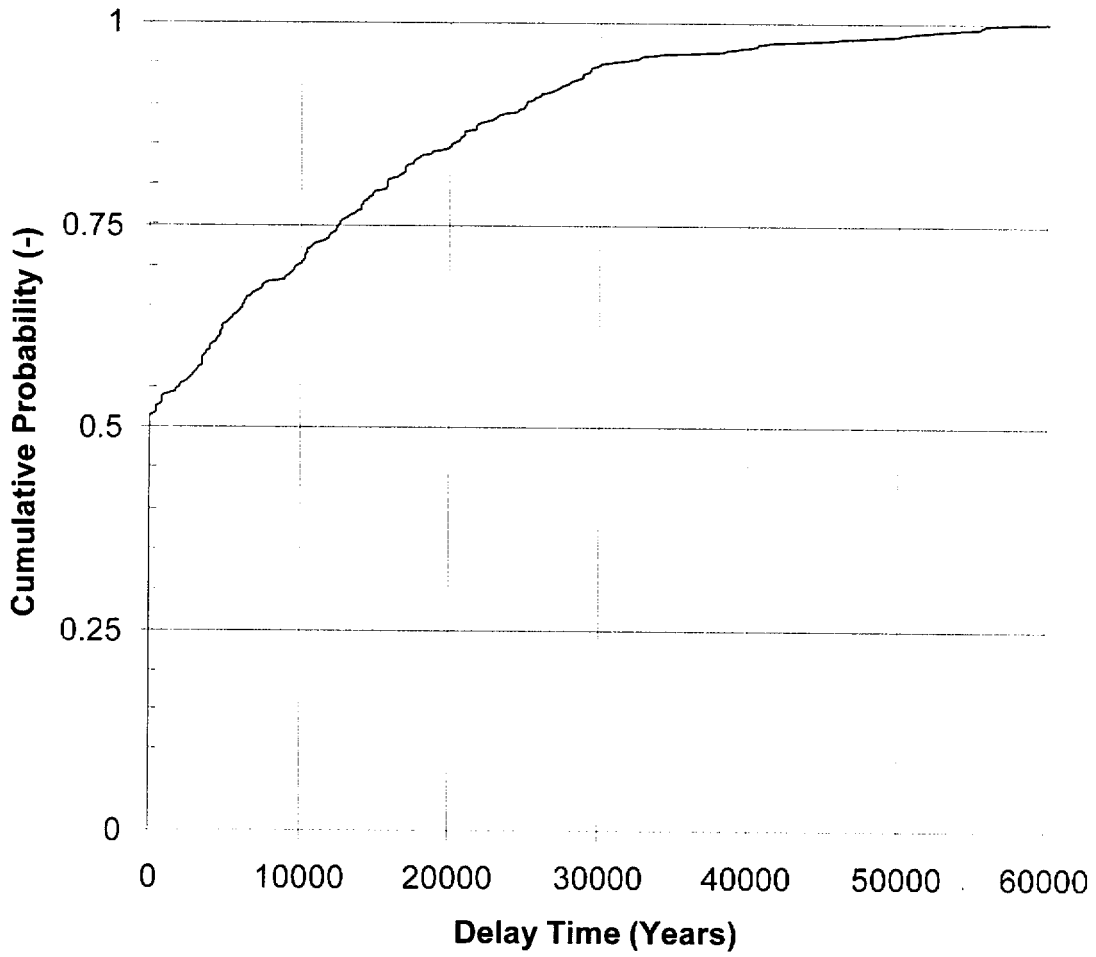


154\_0264.ai

154\_0264.ai

Note: See Section 8.3.3.3.2 for Waste Package Fluxes.

Figure 8.3.4-1. Schematic of the Bathtub Geometry for the Waste Package

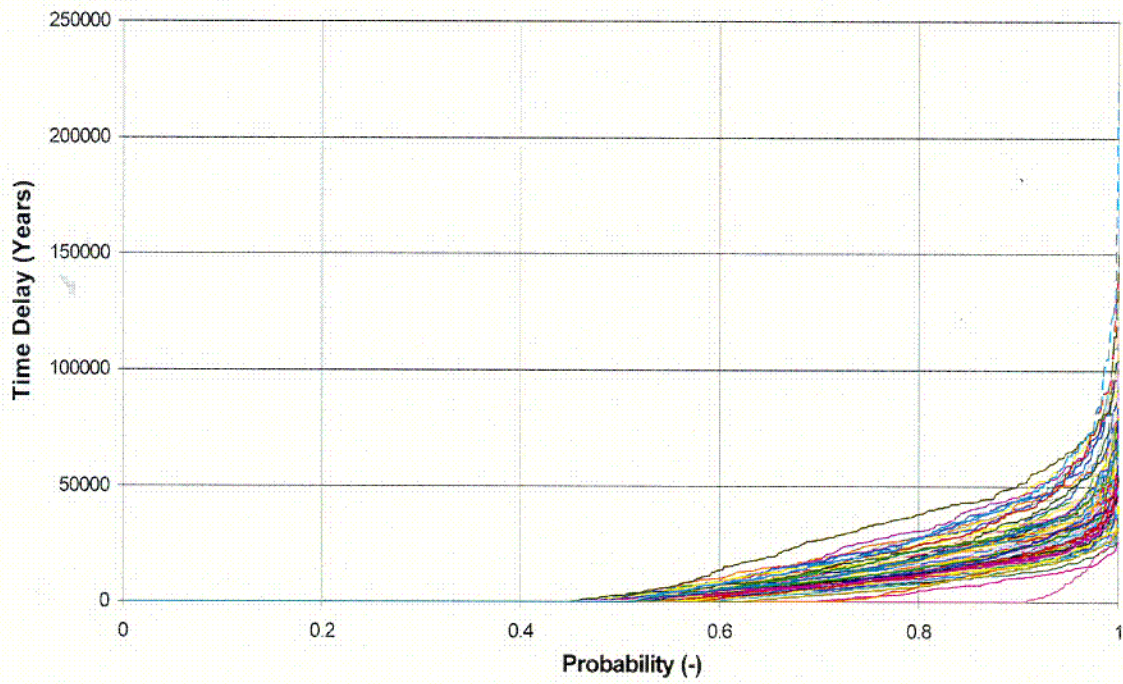


154\_0265.ai

154\_0265.ai

Source: Case 2001 [DIRS 155053], Figure 1.

Figure 8.3.4-2. Cumulative Distribution Function for the Bathtub Delay Time for a Single WAPDEG Realization with 400 Packages



154\_0266.ai

154\_0266.ai

Source: Case 2001 [DIRS 155053], Figure 2.

Figure 8.3.4-3. Cumulative Distribution Function for the Bathtub Delay Time for 100 WAPDEG Realizations. Each Curve is Based on the Results for 400 Waste Packages

205

INTENTIONALLY LEFT BLANK

## 9. WASTE FORM DEGRADATION AND RADIONUCLIDE RELEASE

### 9.1 INTRODUCTION AND CONCEPTUAL BASIS

The function of the waste form degradation model is to determine three outputs over time: dissolved radionuclide concentration, reversible colloidal radionuclide concentration, and irreversible colloidal radionuclide concentration. To do this, the model synthesizes eight major modeling/analysis efforts: radioisotope inventory, in-package chemistry, commercial spent nuclear fuel (SNF) degradation, commercial SNF cladding degradation, U.S. Department of Energy (DOE) SNF degradation, high-level radioactive waste (HLW) degradation, radioisotope dissolved concentration (solubility), and radioisotope colloidal concentration, as summarized in the *Yucca Mountain Science and Engineering Report (S&ER)* (DOE 2001 [DIRS 153849], Section 4.2.6). The radionuclides most important to human dose were identified and quantified per waste package design for inclusion in a total system performance assessment (TSPA) (DOE 2001 [DIRS 153849], Section 4.2.6.4.1). Reaction-path modeling of the breached waste form environment was used to assess the long-term evolution of in-package chemistry using as input water flux into the waste package; degradation of the steel, aluminum, DOE and commercial SNF, and HLW inside the package; and a chemical thermodynamics database (DOE 2001 [DIRS 153849], Section 4.2.6.3.2). Water chemistry parameters such as hydrogen ion concentration, total carbonate concentration, ionic strength, fluoride, and chloride concentrations are estimated for subsequent use in models used to predict commercial SNF cladding and matrix degradation, HLW degradation, radionuclide solubility, and colloid availability and stability.

The waste form models implemented in *Total System Performance Assessment for the Site Recommendation* (TSPA-SR) (CRWMS M&O 2000 [DIRS 153246]) were in most cases conservative models that bounded significant uncertainties. Table 9-1 shows the five waste form models that were chosen for further analysis because they were most likely to affect system performance. The waste form models implemented in this study differ from the TSPA-SR model in the following respects:

- **In-Package Chemistry** (Section 9.3.1)—The effects of HLW glass degradation rate and steel degradation rate on in-package chemistry were evaluated because sensitivity studies showed that degradation rates of in-package steels and glass have an impact on pH-time trajectories, which in turn can influence actinide solubilities. Lower degradation rates were investigated to quantify uncertainties associated with the conservative assignment of glass and steel degradation rates used in the TSPA-SR (CRWMS M&O 2000 [DIRS 153246]). Revised pH-time trajectories for commercial SNF and codisposal packages provided the basis for new TSPA runs and sensitivity analyses. As shown in Table 9-1, the distributions were based, in part, on updated scientific information, but this work was not prompted by thermal operating mode issues. The in-package chemistry model was developed when early waste package failures were screened out based on low probability (DOE 2001 [DIRS 153849], Section 4.2.4.3.1).

Table 9-1. Summary of Supplemental Models and Analyses

Key Attributes of System	Process Model (Section of S&ER)	Topic of Supplemental Scientific Model or Analysis	Reason For Supplemental Scientific Model or Analysis			Section of Volume 1	Performance Assessment Treatment of Supplemental Scientific Model or Analysis <sup>a</sup>	
			Unquantified Uncertainty Analysis	Update in Scientific Information	Lower-Temperature Operating Mode Analysis		TSPA Sensitivity Analysis	Included in Supplemental TSPA Model
Limited Release of Radionuclides from the Engineered Barriers	In-Package Environments (4.2.6)	Effect of HLW glass degradation rate and steel degradation rate on in-package chemistry	X	X		9.3.1	X	X
	Cladding Degradation and Performance (4.2.6)	Effect of initial perforations, creep rupture, stress corrosion cracking, localized corrosion, seismic failure, rock overburden failure, and unzipping velocity on cladding degradation	X	X		9.3.3	X	X
	DHLW Degradation and Performance (4.2.6)	HLW glass degradation rates	X	X		9.3.1		
	Dissolved Radionuclide Concentrations (4.2.6)	Solubility of neptunium, thorium, plutonium, and technetium	X	X		9.3.2	X	X
	Colloid-Associated Radionuclide Concentrations (4.2.6)	Colloid mass concentrations	X			9.3.4	X	

NOTE: S&ER = *Yucca Mountain Science and Engineering Report* (DOE 2001 [DIRS 153849]).

<sup>a</sup> Performance assessment treatment of supplemental scientific model or analysis discussed in SSPA Volume 2 (McNeish 2001 [DIRS 155023]).

Waste packages started failing between 10,000 and 100,000 years (DOE 2001 [DIRS 153849], Figure 4-92) when the chemical system was well into the extended cool-down period with a representative temperature of 50°C (DOE 2001 [DIRS 153849], Table 4-17). Because the in-package chemistry model presumed waste package breach after any thermal pulse had passed (BSC 2001 [DIRS 153724], Section 1), it was insensitive to front-end thermal conditions.

- **Dissolved Concentrations** (Section 9.3.2)—The dissolved concentrations of thorium, neptunium, plutonium, and technetium are evaluated because sensitivity studies in support of TSPA-SR (CRWMS M&O 2000 [DIRS 153246]) show these elements to have the largest effect on dose. As shown in Table 9-1, the distributions are based, in part, on updated scientific information. Differing alternative thermal operating modes do not affect the models for these elements.
- **Cladding** (Section 9.3.3)—Cladding degradation is evaluated because sensitivity studies in support of TSPA-SR (CRWMS M&O 2000 [DIRS 153246]) showed several uncertain cladding degradation parameters as important to peak dose. As shown in Table 9-1, the distributions are based, in part, on updated scientific information, but were not prompted by the consideration of a cooler thermal-operating mode. The behavior of the cladding within the repository is not expected to differ significantly between a low and high temperature-operating mode as long as a cladding temperature of 350°C is not exceeded (CRWMS M&O 2001 [DIRS 151662], Section 6.2.4 and Figure 14). Waste package temperature is treated as an independent variable in the creep cladding degradation abstraction (CRWMS M&O 2001 [DIRS 151662], Section 6.2.4, Table 8) and the intrinsic dissolution part of the unzipping rate abstraction (CRWMS M&O 2001 [DIRS 151662], Section 6.6.2)). This abstraction is applicable for a hot (backfill) design such as that considered in the total system performance assessment for the viability assessment (TSPA-VA) (CRWMS M&O 1998 [DIRS 100362], Figure 6-10), the TSPA-SR higher-temperature design, and any future cool repository design. Alternative thermal operating modes do not affect the waste form model as parameterized for the TSPA-SR or for this evaluation.
- **Colloids** (Section 9.3.4)—The effect of colloids is evaluated because of the significant uncertainties within the model. Thermal effects are being evaluated, but are expected to be overwhelmed by other uncertainties within the system.

The assessments made in the following sections are based upon a series of documented program scientific analyses and calculations, as well as assumptions, expert judgement, and best estimates. The purpose of their collection is to provide a means for establishing the sensitivity of system performance to various chemical and physical inputs describing waste form behavior.

## 9.2 REVIEW OF SCIENCE AND ENGINEERING REPORT TREATMENT

Conservatism and bounding analyses are used in the TSPA-SR (CRWMS M&O 2000 [DIRS 153246]) to address a number of uncertainties that were unquantified. Some of the latter are prompted by simplified conceptual models for waste form degradation processes, while others reflect uncertainty in the ranges of inputs to reasonably well-agreed-upon models. In each

case, the intention has been to err on the side of maximizing radionuclide transport in the calculation.

### 9.3 UNCERTAINTY ANALYSES

Efforts to address unquantified uncertainties have focussed on several areas: the in-package chemistry model (BSC 2001 [DIRS 153724]) and abstraction (BSC 2001 [DIRS 154620]), which are used to estimate in-package chemical conditions over the life of the potential repository and over a range of bounding conditions; the dissolved concentration abstraction (CRWMS M&O 2001 [DIRS 154286]), which develops functions describing dissolved radionuclide concentrations as a function of in-package fluid compositions; the glass degradation model (CRWMS M&O 2001 [DIRS 153846]), which provides a glass degradation rate law that is used as input in the in-package chemistry calculation; the cladding model (CRWMS M&O 2001 [DIRS 151662]), which provides estimates describing the persistence of cladding protection in waste forms containing commercial SNF; and the waste form colloid model (CRWMS M&O 2001 [DIRS 153933]), which develops a method for estimating fluxes of colloidally-transported radionuclides.

The waste form models were developed when early waste package failures were screened out based on low probability (DOE 2001 [DIRS 153849], Section 4.2.4.3.1). Further analysis, however, indicated that improper heat treatment of waste packages could result in failure of up to two waste packages with the failure assumed to be at the time of closure (see Section 7.3.6). These early failures have implications on degradation processes within the waste packages and require re-evaluation for the in-package chemistry model, the cladding degradation model, and the screening of criticality. The scenario after early breach indicates that the materials within the waste package will be exposed to hot air, with humidity increasing and temperature decreasing with time (Figures 5.2-4 and 5.2-5). The waste package model predicts the drip shield will prevent ground water from dripping onto the waste package during the regulatory 10,000-year period (Figure 7.4-2). Consequently, only humid air or condensed water will enter the package during the regulatory period.

The temperature dependence of the most important thermodynamic data used in the in-package chemistry model is being evaluated for future use of the model for early waste package failures. Other inputs such as  $f_{CO_2}$  and water vapor influx rates are being considered. For the cladding degradation model, early waste package failures require the re-evaluation of the rate of possible dry or humid unzipping. However, changes in these models to cover the early waste package failures may not significantly change the dose in the regulatory period because of the limited transport in this scenario. Continued functioning of the drip shield prevents advective releases, and breach at the waste package welds limits diffusive releases.

Criticality during the regulatory period was screened out when early failures were screened out. Even in the unlikely event of early waste package failures the conditions required for criticality are not likely. The failure mode postulated for early failures (e.g., cracks in the closure weld) is not sufficient for criticality to occur. Criticality would require the occurrence of additional low-probability events including the transport of a sufficient quantity of water through a waste package to cause the removal of criticality controlling material to form a critical configuration. Water transport into a waste package during the regulatory period is expected to be limited by

the nature of the failure (i.e., small cracks through the closure weld on the side of a package are not conducive to water flow through a package), by the presence of a drip shield (DOE 2001 [DIRS 153849], p. 4-219), and by the evaporation of water entering the package due to the decay heat of the waste (CRWMS M&O 2000 [DIRS 149626]). Criticality evaluations for various waste forms will be conducted prior to license application to confirm that the repository system will meet the criticality probability criterion of less than  $1 \times 10^{-4}$  per year for the entire repository for the regulatory period.

The models presented in the remainder of Section 9 were developed for scenarios where the waste packages breach after the thermal pulse. The use of these models for waste packages with early failures has not been validated. However, given the large uncertainty in many of these models, the use of these models for sensitivity studies is reasonable.

### **9.3.1 In-Package Chemistry**

Unquantified uncertainties in the in-package chemistry model include uncertainties in the model inputs: degradation rates, masses and surface areas of waste form components, and the composition of the incoming fluid. Unquantified conceptual model uncertainties are also associated with the use of the mixing model, which ignores small-scale heterogeneities of fluid flow and water contact with the various in-package components. The discussions below focus on the quantification of the numerical uncertainty associated with model inputs.

#### **9.3.1.1 Goal of Model**

The goal of the in-package chemistry model is to identify the range of major element fluid compositions (pH, Eh, alkalinity, and ionic strength) likely to exist inside the waste package once drift fluids come into contact with breached waste forms. The transport rates of species in and out of the package and the reaction rates of materials within the package will control these important chemical parameters. Detailed modeling of this coupled system with reactive transport codes has not been attempted in part due to the large uncertainty in the transport properties of the degrading waste package and its contents. Random sampling of the important chemistry parameters can give parameter combinations that are impossible to achieve within the waste package based on mass balance constraints. Based on these considerations, the in-package chemistry model was built using a reaction path model and conservative carbon dioxide and oxygen concentrations. This type of model can predict a wide range of chemistries depending on the input parameters, but these chemistries are constrained by mass balance considerations, and the output can be used to provide insight into the processes controlling the chemistry. In-package fluid compositions are predicted using the reaction path model EQ6 V7.2bLV that estimates the reaction of in-package solids (steel and fuel elements) with incoming fluids over time. This mixing cell calculation assumes continual equilibration with ambient carbon dioxide and oxygen. The nature and abundance of waste form solids are determined from project design calculations. The rates at which the solids dissolve are derived from a number of supporting analysis model reports (AMRs).

The primary output of the in-package chemistry model is a series of pH-time trajectories for two waste types (commercial versus codisposal) and inflow boundary conditions. In general, equilibrium between fluids and secondary, uranium-bearing minerals is predicted for long

periods of time in commercial spent fuel packages. Eh is conservatively assumed to be oxidizing and fixed by equilibrium with atmospheric levels of free oxygen. Similarly, carbonate alkalinity levels are conservatively assumed to be controlled by equilibrium with atmospheric carbon dioxide. Output pH-time trajectories are abstracted as input for TSPA. Ultimately, these abstractions are used by TSPA to calculate the dissolved radionuclide concentration limits for a number of important radionuclides.

### **9.3.1.2 Identification of Unquantified Uncertainties in Total System Performance Assessment-Site Recommendation**

The inputs that have significant uncertainty for the in-package chemistry model include: incoming water composition, incoming water rate, and the component surface areas and reaction rates. The latter includes the exposed surface area of spent fuel under breached cladding. The uncertainty in fluid flow rates and exposed spent fuel surface area are handled explicitly by using a range of inputs and defining the output as a function of these input parameters. The S&ER (DOE 2001 [DIRS 153849]) models also used two corrosion rates for each of the major components, a high rate and a more likely rate 10 times lower (CRWMS M&O 2000 [DIRS 111880]).

The importance of incoming fluid composition was tested in a series of calculations (BSC 2001 [DIRS 153724], Section 4.1.2), using J-13 well water, evaporated J-13 well water, and an output composition from the Near Field Environment Process Model Report (CRWMS M&O 2000 [DIRS 146589], Table 3-5). The results of the sensitivity studies indicated that the chemical composition of the influent water did not impact the pH-time trajectories. Hence, J-13 well-water composition was used for subsequent analyses.

Critical unquantified uncertainties that remain in the in-package chemistry calculation include those associated with: steel and glass degradation rates, oxygen fugacity, and in-package sorption. New information (BSC 2001 [DIRS 154840]) developed since completion of the S&ER (DOE 2001 [DIRS 153849]) models includes a series of sensitivity studies to assess the impact of varying the individual dissolution rates of the various waste form components. This effort was prompted in part by the aforementioned observation of trajectory sensitivity to rates and the geochemical evolution of waters associated with localized environments inside the waste form. Also, a more thorough examination of in-package sorption has been performed (Section 10.3.4).

The S&ER (DOE 2001 [DIRS 153849]) in-package chemistry model presumes waste package breach after any thermal pulse has passed (BSC 2001 [DIRS 153724], Section 1). It is, therefore, insensitive to front-end thermal conditions, and there is no need for an explicit consideration of initial thermal configuration impacts on model outputs.

### **9.3.1.3 Quantification of Previously Unquantified Uncertainty**

A number of solids are expected to degrade after contacted by fluids that enter breached waste packages. The most important solids are 316 stainless steel, A516 steel, 304 steel, HLW glass, commercial SNF, borated 316 stainless steel, and aluminum alloy. Degradation of these solids will alter the chemical composition of in-package fluids. The effect on pH depends on the

chemical composition of the particular solid, its mass, and its rate of dissolution. Dissolution of steels tends to cause pH to decrease; the magnitude of the decreases depends on the composition and degradation rate of the particular steel. Glass degradation causes increases in pH. Generally, one degradation process tends to dominate over individual time spans. Ultimately, influx of J-13 water causes in-package fluid to have a pH greater than 7. A secondary control over pH is the presence of degradation products (in particular, iron hydroxides from steel corrosion), which, when present, can buffer pH.

#### **9.3.1.3.1 High-Level Waste Glass Degradation**

The HLW degradation component developed for TSPA-SR (CRWMS M&O 2000 [DIRS 153246]) uses bounds on parameters of a phenomenological model to develop a simplified (Arrhenius-type) rate equation of degradation that is dependent only upon pH and temperature. Conservative estimates of the model parameters are based upon experimental data for the degradation of borosilicate glass (CRWMS M&O 2000 [DIRS 143420], Section 6.2).

Glass and mineral degradation rates tend to decrease with time (e.g., White et al. 1996 [DIRS 154473]). A more realistic treatment of glass degradation would implicitly account for the possibility of much lower rates. Therefore, for the purposes of sensitivity assessment, an uncertainty multiplier ranging from zero to one was used in the glass degradation model (BSC 2001 [DIRS 154840], Section 6.3). A lower end of zero corresponds to the case where formation of passivating alteration products completely halts dissolution. Rates may also drop with time because of dissolution of active surface sites and decreases in reactive surface area (e.g., White and Brantley 1995 [DIRS 154492]). The triangular distribution with a peak of  $10^{-4}$  allows evaluation of the expected range of dissolution and is consistent with engineering judgement that the peak value is more likely than the bounds.

#### **9.3.1.3.2 Steel Degradation Rates**

The steel degradation rates used in the TSPA-SR in-package chemistry calculations were chosen to be high and, therefore, conservative, as discussed in *Effect of Waste Package Materials Surface Area and High-Level Waste Glass Reaction Rate on In-Package Chemistry* (BSC 2001 [DIRS 154840]). A more realistic range in rate equations for each steel type would be anchored at the low end by a value of zero and at the high end by the values used in *In-Package Chemistry for Waste Forms* (BSC 2001 [DIRS 153724]). The mechanistic explanation for the low end is the common observation of metallic components becoming coated by passivating oxide or hydroxide layers that might potentially halt corrosion by inhibiting the transport of reactants to, or products from, the metal interface (e.g., ASM International 1987 [DIRS 103753]). The long-term persistence of such iron oxides as magnetite at Yucca Mountain lends some credence to the picture of steel passivation. Moreover, the long-term persistence of such natural analogue metallic objects as josphinite, iron-nickel meteorites, and various iron artifacts suggest at least qualitatively that the values used in performance assessment are indeed high and consequently conservative. A series of scoping calculations were performed (see section that follows) to assess the impact of lower steel degradation rates on in-package chemistry.

### 9.3.1.3.3 Impact of Glass and Steel Degradation Unquantified Uncertainties on In-package pH

EQ6 calculations have been done to assess the impact of the degradation rate uncertainties on in-package chemistry, in particular on in-package pH (CRWMS M&O 2000 [DIRS 111880]; BSC 2001 [DIRS 153724]; BSC 2001 [DIRS 154840]). These calculations provide insight into the importance of input parameter uncertainty and the effect of heterogeneous flow and reaction inside the waste form on effluent chemistry. Since the S&ER (DOE 2001 [DIRS 153849]), two sets of calculations have been performed. The first set of calculations were performed to update the chemistry model with a new glass degradation model and focused on lower fluid flow rates (BSC 2001 [DIRS 153724]). The second set was performed to further explore the sensitivity of the pH on individual degradation rates (BSC 2001 [DIRS 154840]). The most important input parameters used in the three cases (S&ER, updated expected, and sensitivity cases) are summarized in Table 9-2. Details of other varied input parameters may be found elsewhere (BSC 2001 [DIRS 153724]; BSC 2001 [DIRS 154840]). Because the glass degradation functions are V-shaped with pH (DOE 2001 [DIRS 153849], Figure 4-104), they are evaluated here at pH = 2 and pH = 7 for comparison. For the sensitivity calculations, the effective dissolution rates (rate multiplied by surface area) of the metal components were lowered by an order of magnitude or the component was removed from the calculation. The rates for the glass were decreased by two, and four orders of magnitude, or the glass was removed.

The 10,000-year pH-trajectories calculated for the S&ER case are shown in DOE (2001 [DIRS 153849], Figures 4-100 and 4-101). The million-year pH-trajectories of the updated expected case and the sensitivity case are shown in Figures 9-1 through 9-4. The model results for the commercial spent fuel package for the S&ER and the updated expected cases (Figure 9-1) were abstracted for TSPA as sets of response surfaces of pH as a function of water flux, fuel exposure and steel corrosion rates. The pH ranges covered by these response surfaces are summarized in Tables 9-3 and 9-4. The model results for the codisposal package (Figure 9-2) showed little dependence on flow rate or DOE SNF fuel types. Consequently, these results were abstracted as ranges only for each time period (Figure 9-2, Table 9-5). Because the sensitivity cases included unphysical scenarios where components were removed, these abstractions were also only provided as uncertainty ranges (Table 9-5).

The abstraction of in-package pH has been considerably refined since the S&ER (DOE 2001 [DIRS 153849]) model. In particular, pH values have been abstracted into four time periods instead of the original two. The goal of the abstractions is to simplify the observed pH histories into a format that is compatible for implementation in TSPA while honoring the fundamental trends observed in the pH histories. The time discretization was chosen based on the analyst judgement of the magnitude of change in pH. For example, if all of the modeled scenarios were reaching low pH values over a specific time period, followed by a trend of increasing pH, a time division was inserted at that point of change. The pH criteria chosen for each time period are shown in the last column in Tables 9-4 and 9-5. These criteria were chosen based on whether all of the pH-time histories were trending toward minimum or maximum pH values during a particular time interval. Although this method only provides a coarse discretization of the pH-time history, it still honors the overall observed pH trends in the data.

The commercial spent fuel package results (Figure 9-1) show two pH lows, in the early time (about 1 to 50 years), and again in the period between about 10,000 to 200,000 years, that bracket a period of near neutral pH. These pH lows can be attributed to dissolution of carbon steel for the early time and 316 stainless steels for the latter. The carbon steel contains a small amount of sulfur, which is calculated to oxidize to sulfuric acid and drive the pH down. The 316 stainless steels contain a significant amount of chromium and molybdenum, which are calculated to liberate protons upon oxidation/hydrolysis. The period of neutral pH is facilitated primarily by the buffering by  $\text{Fe}(\text{OH})_3(\text{s})$ , which precipitated during dissolution of the carbon steel.

As in the commercial spent fuel packages, the carbon steel in the codisposal packages is calculated to drive the pH down at early times (Figure 9-2). After the carbon steel has been depleted, the pH steadily increases as high-level waste glass tends to dominate the effluent chemistry with release of several alkalinity generating species (e.g., sodium, potassium, phosphate, and borate).

The two sensitivity cases that have the most discernible impact are zero dissolution of A516 steel (Figure 9-3) and zero degradation of glass (Figure 9-4). In both cases, the minimum in-package pH tends to drop to between  $\text{pH} = 2$  and  $\text{pH} = 3$ . For the first case, the pH drop occurs because in the absence of A516 dissolution, there is little accumulation of ferric hydroxides, which tend to buffer the in-package pH. For the zero glass degradation case, the pH drop occurs because the acid consumption, which would otherwise occur with glass degradation, cannot counter the acidity production that occurs from steel degradation. These two unlikely cases increase the abstracted uncertainty range from the updated expected case model to the sensitivity model.

#### **9.3.1.4 Other Lines of Evidence to Support Models**

Analogs (natural and other) were used to assess more realistic ranges for degradation rates for the steels and glasses (see Sections 9.3.1.3.2 and 9.3.1.3.1). As discussed in Section 7.3.2.4.2, steel analogs show remarkable phase stability.

Section 9.3.2.3 provides a qualitative discussion of pH trajectories observed in Argonne National Laboratory (ANL), spent nuclear fuel (SNF), and HLW tests, which are consistent with the first years of the much longer term pH ranges predicted by the in-package chemistry model.

#### **9.3.2 Dissolved Concentrations**

The goal of the dissolved concentration component is to predict concentrations of radioisotopes of interest as a function of fluid composition inside the waste form. Specifically, the solubilities of radionuclides that might affect dose were considered. The sources of information include EQ3/6 V7.2b simulations of in-package chemistry for three categories of radionuclides (CRWMS M&O 2001 [DIRS 154286], Section 6). Three radioisotope solubilities were abstracted as a function of in-package chemistry (neptunium, uranium, and americium), and three radionuclide solubilities (actinium, curium, and samarium) were set equal to that of americium. Four additional radioisotope solubilities were defined by probability distributions (plutonium, lead, protactinium, and nickel). The solubilities of the remaining screened-in radioisotopes were set at bounding values.

### 9.3.2.1 Identification of Unquantified Uncertainties

The radionuclides considered most important to dose and which are conservatively modeled in TSPA-SR (CRWMS M&O 2000 [DIRS 153246]) are thorium, neptunium, plutonium, and technetium. Uncertainties in the dissolved levels of these radioelements are associated with uncertainties in the thermodynamic data, in the assumed in-package oxygen fugacity (which has a profound effect on the solubilities of some radionuclides (Chen 2001 [DIRS 155247]), and in the identity of the concentration-limiting solid. Solubility calculations used to estimate dissolved concentration limits depend on assumed system boundary conditions (e.g., pH, carbon dioxide, and oxygen fugacity), a known set of chemical species, and reasonably precise thermodynamic relations describing equilibrium between them all. There are uncertainties associated with each of these quantities and with the assumption of thermodynamic equilibrium itself. The primary species identity uncertainty is mainly associated with the choice of what is to be the solubility-limiting solid phase. In the dissolved concentration AMR (CRWMS M&O 2001 [DIRS 154286]), the most soluble oxyhydroxide was conservatively assumed to control dissolved concentrations, and atmospheric oxygen levels were conservatively assumed to prevail. Over time though, soluble, hydrated minerals tend to dehydrate and become more crystalline and less soluble (CRWMS M&O 2001 [DIRS 154286], Section 6.5.2). Moreover, pooling of water, oxygen consumption by steel degradation, or the passivation of otherwise oxidizable surfaces by degradation products would tend to lead to local reduced zones inside the waste package. The unquantified uncertainty effort consequently focussed on these concentration-decreasing effects for the radionuclides of most concern to dose.

### 9.3.2.2 Quantification of Previously Unquantified Uncertainties

The accumulated unquantified uncertainties in dissolved radionuclide concentrations were constrained by setting the upper limit of dissolved levels to either the value set by the most soluble hydroxide phase in equilibrium with atmospheric levels of oxygen and ambient levels of carbon dioxide ( $10^{-3}$  bar) or, where no such phase exists, by inventory limits. The lower dissolved concentration limit was calculated by setting oxygen fugacities 40 log-units lower and letting dissolved levels of a particular radionuclide be set by the most stable solid phase(s) and calculating equilibrium concentrations from about pH = 3 to about pH = 10 (Chen 2001 [DIRS 155247]). The lower oxygen fugacity was chosen for the purposes of sensitivity studies to assess radionuclide solubilities that might be observed in natural waters under reducing conditions. Work focussed on thorium, technetium, and plutonium.

#### 9.3.2.2.1 Thorium

The *Summary of Dissolved Concentration Limits* AMR (CRWMS M&O 2001 [DIRS 154286]) does not provide a thorium solubility range because of uncertainties in the nature and extent of thorium-carbonate complexation (Chen 2001 [DIRS 155247]). Instead, a fixed solubility of  $10^{-5}$  mol/L (2.3 mg/L) was used in TSPA-SR (CRWMS M&O 2000 [DIRS 153246]).

Two thorium-carbonate species,  $\text{Th}(\text{CO}_3)_5^{6-}$  and  $\text{Th}(\text{OH})_3\text{CO}_3^-$ , were added to data0.ymp.R0, the qualified thermodynamic database (DTN: MO0009THRMODYN.001 [DIRS 152576]). Using this database and the EQ3NR software code from the EQ3/6 V7.2b code suite, thorium solubility in J-13-derived water was calculated (Chen 2001 [DIRS 155247]). The calculation assumes

ThO<sub>2(am)</sub> is the solubility-controlling mineral. The environmental conditions for the calculations are pH ranges from 3.4 to 9.8, log *f*<sub>CO<sub>2</sub></sub> ranges from -5.0 to -1.5, log *f*<sub>O<sub>2</sub></sub> = -0.7, and temperature is 25°C. The results have a maximum of 7.19 × 10<sup>-4</sup> mol/kg (1.65 × 10<sup>2</sup> mg/L) and a minimum of 2.74 × 10<sup>-9</sup> mol/kg (6.3 × 10<sup>4</sup> mg/L), with a geometric mean of 6.30 × 10<sup>-7</sup> mol/kg (1.45 × 10<sup>-1</sup> mg/L), which is about two orders of magnitude lower than the TSPA-SR (CRWMS M&O 2000 [DIRS 153246]) value of 1.0 × 10<sup>-5</sup> mol/kg [2.3 mg/L].

Because actinides tend to form many types of carbonate complexes (e.g., Langmuir 1997 [DIRS 100051]), it is possible that more thorium-carbonates will be reported. Less soluble, more stable thorium-bearing phases may form (Chen 2001 [DIRS 155247]) and limit the dissolved thorium concentrations to lower values. To establish the lower range of possible thorium concentrations, EQ6 calculations were done in which the most stable thorium-bearing phase (among the thorium phases given in the thermodynamic database) was considered (CO<sub>2</sub> fugacity was fixed at 10<sup>-3</sup> bars). The results are plotted in Figure 9-5 along with the thorium solubility controlled by ThO<sub>2(am)</sub>. The two solubility curves have similar shapes, and the most stable phase (thorianite) yields thorium solubility 4 to 6 orders of magnitude lower than that given by ThO<sub>2(am)</sub> (Figure 9-5). For pH less than 6, the difference is about 4 orders of magnitude, while for pH greater than 6, the difference is about 5.5 orders of magnitude.

The ThO<sub>2(am)</sub> curve (for log *f*<sub>CO<sub>2</sub></sub> = -3.0) can be represented by Equation 9-1 (Chen 2001 [DIRS 155247]). Equation 9-1 describes predicted thorium concentrations (mg/L) as a function of solution composition and was derived by fitting individual EQ3NR predictions of dissolved thorium concentrations. Although the latter are calculated output, the thermodynamic parameters that are used in the individual calculations were derived largely from experimental measurements. Nevertheless, the model parameters (e.g., numerical coefficients and exponents) and their precision do not imply any specific mechanistic basis or particular level of process understanding. The expressions are not valid outside of the range of fluid compositions from which the model was derived. Note lastly that the same approach is applied subsequently for other radionuclides.

$$\begin{aligned} \log[\text{Th}] = & 11891 - 2781.5\text{pH} + 354.02\text{pH}^2 \\ & - 23.309\text{pH}^3 + 0.62247\text{pH}^4 - 26221/\text{pH} + 23348/\text{pH}^2 \end{aligned} \quad (\text{Eq. 9-1})$$

where [Th] is thorium solubility in mg/L. The uncertainty in thorium solubility associated with the controlling phase is accounted for based on the above equation. Specifically, moving this curve down 2 orders of magnitude gives the mean of thorium solubility (mg/L), with a term of plus-or-minus 2.0 to cover the ranges. That is (Chen 2001 [DIRS 155247]):

$$\begin{aligned} \log[\text{Th}] = & 11889 \pm 2 - 2781.5\text{pH} + 354.02\text{pH}^2 \\ & - 23.309\text{pH}^3 + 0.62247\text{pH}^4 - 26221/\text{pH} + 23348/\text{pH}^2 \end{aligned} \quad (\text{Eq. 9-2})$$

Equation 9-2 predicts thorium concentrations [Th] at high and low pHs to be higher than is physically realistic. Dissolved thorium levels will be limited by the absolute availability of solvating water molecules. An upper bound of 1 mol/L (2.3 × 10<sup>5</sup> mg/L) is thus applied in addition to Equation 9-2. The upper bound for uranium, neptunium, and plutonium solubility is for the same reasons set at 1 mol/L (see below).

### 9.3.2.2.2 Technetium

Under oxidizing conditions, technetium is highly soluble (e.g., Langmuir 1997 [DIRS 100051]). Therefore, technetium levels are unlikely to be controlled by the formation of a technetium-containing solid. For TSPA-SR (CRWMS M&O 2000 [DIRS 153246]), technetium solubility is set to 1.0 mol/L ( $9.9 \times 10^4$  mg/L), which will allow the waste inventory to control its release. However, under reducing conditions ( $\log f_{O_2} = -40.7$  bar), EQ6 calculations show that  $TcO_2$  could precipitate and limit technetium solubility (Chen 2001 [DIRS 155247]). Over the pH range from 4.75 to 9.5, technetium solubility varies from  $5.59 \times 10^{-6}$  to  $4.13 \times 10^{-1}$  mol/kg ( $5.53 \times 10^{-1}$  to  $4.09 \times 10^4$  mg/L). A log-triangular distribution for technetium is proposed based on the judgement that oxidizing conditions are more likely than reducing conditions. The lower end of the distribution is, therefore, the minimum value of technetium calculated above:  $\log [Tc \text{ (mg/L)}] = -0.254$ , where [Tc] is the concentration of technetium. The distribution has a peak equal to its higher end (i.e.,  $\log [Tc] = (\text{mg/L}) = 5$ ).

### 9.3.2.2.3 Neptunium

For TSPA-SR (CRWMS M&O 2000 [DIRS 153246]), neptunium solubility was evaluated with the conventional solubility evaluation approach and  $Np_2O_5$  was assumed as the solubility-controlling mineral (CRWMS M&O 2001 [DIRS 154286], Section 6.4.2). However,  $Np_2O_5$  has not been identified in spent fuel dissolution experiments, nor have other neptunium pure phases been identified (CRWMS M&O 2000 [DIRS 146677], Section 6.7.2). Moreover, neptunium concentrations measured in spent fuel experiments are several orders of magnitude lower than the neptunium concentrations predicted by  $Np_2O_5$  solubility model (CRWMS M&O 2001 [DIRS 154286], Figure 2). Neptunium release from spent nuclear fuel may not be controlled by dissolution of  $Np_2O_5$  or other neptunium pure phases but by a different mechanism. Based on analyses of the crystal-chemical properties of the uranium-oxygen bond, neptunium-oxygen bond, and plutonium-oxygen bond, Burns et al. (1997 [DIRS 100389]) predicted that the substitutions  $Pu^{6+} \leftrightarrow U^{6+}$  and  $(Np^{5+}, Pu^{5+}) \leftrightarrow U^{6+}$  are likely to occur in most  $U^{6+}$  structures. Later, Buck et al. (1998 [DIRS 100388]) confirmed the prediction by transmission electron microscopy analyses of the corrosion products of spent fuel drip-tests. In that study, neptunium was found to be incorporated into dehydrated schoepite (Buck et al. 1998 [DIRS 100388]). However, the mechanism(s) for neptunium retention in spent fuel dissolution experiments were not firmly established. Retention of neptunium in the ANL drip experiments may be explained (CRWMS M&O 2000 [DIRS 146677], Section 6.7.2) by one or more of several factors, including:

- Incomplete oxidation of Np(IV) in the fuel to Np(V) under the experimental conditions in the ANL drip tests
- Coprecipitation of neptunium in U(VI) compounds
- Sorption of neptunium onto solid corrosion products or components of the fuel holder in the test vessel (or both)
- Ion exchange of neptunium species with cations in existing minerals (e.g.,  $NpO_2^+$  replacing  $Na^+$  in Na-boltwoodite).

Pending clearer identification of the mechanism(s) responsible for neptunium release from spent fuel, an empirical neptunium solubility model, which is documented in a calculation (Chen 2001 [DIRS 155247]), has been developed for the sensitivity studies. The model defines a concentrating factor  $F_c$  to describe the solution ratios of neptunium to uranium compared to the ratios in spent fuel with which it is in contact:

$$F_c = \frac{(Np/U)_{soln}}{(Np/U)_{fuel}} \quad (\text{Eq. 9-3})$$

which rearranges to:

$$[Np] = F_c (Np/U)_{fuel} [U] \quad (\text{Eq. 9-4})$$

where Np is neptunium and U is uranium. Equation 9-4 links dissolved neptunium levels to dissolved uranium levels and the measured ratio of neptunium to uranium in the fuel, through a concentrating factor,  $F_c$ , determined from spent fuel dissolution experiments. Figure 9-6 shows  $F_c$  from the ANL drip tests (Chen 2001 [DIRS 155247], Figure 4) as a function of time. The solid lines are tests with ATM-103 fuel while the dashed lines are tests for ATM-106 fuel. Two significant features can be observed. First, in those four tests,  $F_c$  of neptunium fluctuates around 1.0; the geometric mean of  $F_c$  is about 1.0. Secondly, in the tests conducted to date, the highest  $F_c$  occurs in the first sample, and then  $F_c$  decreases and reaches the lowest value within 2 years. In other words, large transient variations in  $F_c$  occur primarily in the first 2 years and dampen with time.

Figure 9-6 shows that  $F_c$  of neptunium fluctuates around 1.0 and appears to dampen to 1.0 as time increases. The fact that  $F_c$  of neptunium fluctuates around 1.0 suggests that neptunium and uranium enter water congruently. This has been observed elsewhere, for example in Pacific Northwest National Laboratory Series 2 and Series 3 steady-state tests results (CRWMS M&O 1997 [DIRS 100348]), and in experiments conducted by the Spanish Nuclear Waste Program (Bruno et al. 1998 [DIRS 101565]). Incorporation of neptunium into uranyl minerals is the simplest explanation for this relation.

Using only long-term data (longer than 2 years) from the four drip tests (28 data points) (Chen 2001 [DIRS 155247]) suggests that  $F_c$  can be approximated using a normal distribution of  $\log(F_c)$  with a mean of 0 and a standard deviation of 0.5. The ratio of neptunium/uranium in the fuel can be calculated from the average waste inventory (BSC 2001 [DIRS 154841], Table 34). After adjusting for decay of americium-241,  $(\text{neptunium/uranium})_{fuel} = 0.00194$ . Using schoepite as the uranium solubility-controlling mineral, uranium solubility (in mg/L) is represented as a function of pH, temperature, and fugacity of  $\text{CO}_2$  (Chen 2001 [DIRS 155247]):

$$\log [U] = 7.9946 - 2.6963 \cdot \text{pH} + 0.42918 \cdot \text{pH}^2 - 1.6286 \cdot \log f_{\text{CO}_2} + 9.5352 \cdot 10^{-3} \cdot T + 0.41613 \cdot \text{pH} \cdot \log f_{\text{CO}_2} - 5.1148 \cdot 10^{-3} \cdot \text{pH} \cdot T - 2.1621 \cdot 10^{-3} \cdot \log f_{\text{CO}_2} \cdot T \quad (\text{Eq. 9-5})$$

Combining values of  $F_c$ , (neptunium/uranium)<sub>fuel</sub>, and the solubility of uranium, [U], the abstracted neptunium solubility for the sensitivity studies was calculated, letting  $\log F_c$  have a normal distribution with a mean of 0 and a standard deviation of 0.5:

$$\log [\text{Np}] = 5.2806 - 2.6963 \cdot \text{pH} + 0.42918 \cdot \text{pH}^2 - 1.6286 \cdot \log f_{\text{CO}_2} + 9.5352 \cdot 10^{-3} \cdot T + 0.41613 \cdot \text{pH} \cdot \log f_{\text{CO}_2} - 5.1148 \cdot 10^{-3} \cdot \text{pH} \cdot T - 2.1621 \cdot 10^{-3} \cdot \log f_{\text{CO}_2} \cdot T + \log F_c \quad (\text{Eq. 9-6})$$

where [Np] is the neptunium solubility in mg/L.

Figure 9-6b compares abstracted neptunium solubility models with EQ3/6 calculation output and experimental data. The TSPA-SR abstraction (CRWMS M&O 2000 [DIRS 153246], Table 3.5-8) is shown as a solid pink line over the black crosses showing the EQ3/6 calculated values for the solubility of  $\text{Np}_2\text{O}_5$  (CRWMS M&O 2000 [DIRS 143569], Table 14, third column, with units converted). This model was only valid for the pH range plotted. Revision 1 of this analysis (CRWMS M&O 2001 [DIRS 154286], Table 14) calculated the  $\text{Np}_2\text{O}_5$  solubility over a larger pH range shown by the black circles. The sensitivity model presented in Equation 9-6 including plus and minus three standard deviations is plotted as red lines. These lines fall over the black squares showing the ANL experimental data from the spent fuel drip tests. Because this model is concave upward outside the range of data, and it includes a cap on the largest concentrations possible, it is valid for use at any pH within the TSPA sensitivity studies. The mean of the sensitivity model is up to four orders of magnitude lower than the TSPA-SR model at acid pHs, and the uncertainty has been increased by three orders of magnitude.

#### 9.3.2.2.4 Plutonium

Despite numerous studies of plutonium solubility, the stabilities of many plutonium-containing solids remain poorly known. The most studied are  $\text{PuO}_2$  and  $\text{PuO}_2 \cdot 2\text{H}_2\text{O}_{(\text{am})}$  (or equivalently  $\text{Pu}(\text{OH})_{4(\text{am})}$ , where am stands for amorphous). Solids precipitated from over-saturation experiments (CRWMS M&O 2001 [DIRS 154629], Section 6.1) have a dark green color, which is characteristic of Pu(IV) solid phases. X-ray diffraction data match the data reported for  $\text{PuO}_2$ . However, the diffuse and broad X-ray diffraction peaks suggest poor crystalline structures. Nonetheless, precipitates at higher temperatures (90°C) have a sharper X-ray pattern than solids precipitated at lower temperatures. Therefore, the solubility-controlling minerals in these laboratory experiments are believed to be plutonium hydroxides and/or plutonium colloids, aging towards  $\text{PuO}_2 \cdot x\text{H}_2\text{O}$  (CRWMS M&O 2001 [DIRS 154629], Section 6.1). The value of X should vary from 2 to zero. For  $X = 2$ , it is  $\text{Pu}(\text{OH})_{4(\text{am})}$ , the amorphous end member. For  $X = 0$ , it is  $\text{PuO}_2(\text{c})$  (where c refers to crystalline), the crystalline end member. Rai and Ryan (1982 [DIRS 112060]) reported that in 1,300 days,  $^{238}\text{PuO}_2(\text{c})$  was found to convert to a less crystalline form of  $\text{PuO}_2$ , denoted as  $\text{PuO}_2(\text{lc})$ , (where lc refers to less crystalline) due to  $\alpha$ -decay of plutonium isotopes. That means the crystal structure of  $\text{PuO}_2(\text{c})$  may be damaged by  $\alpha$ -decay and a less crystalline form of  $\text{PuO}_2$  would control plutonium solubility. Because the thermodynamic properties of the less crystalline  $\text{PuO}_2$  forms are unknown, it is not possible to use it as the solubility-controlling phase in plutonium solubility calculations. To be conservative, for the TSPA-SR (CRWMS M&O 2000 [DIRS 153246]),  $\text{PuO}_2 \cdot 2\text{H}_2\text{O}_{(\text{am})}$  was selected as the controlling solid for plutonium.

More realistic calculations of plutonium solubility require consideration of more crystalline, less hydrated plutonium solids and lower oxygen fugacities. Rai and Ryan (1982 [DIRS 112060]) observed that plutonium hydroxide gradually converted to anhydrous crystalline material; therefore, over geological time, plutonium hydroxides are expected to convert to  $\text{PuO}_{2(c)}$ . The calculation (Chen 2001 [DIRS 155247]) is conducted for J-13 derived water, and other environmental conditions considered are: pH from 5.0 to 9.8;  $\log f_{\text{CO}_2}$  from  $-5.0$  to  $-1.5$ ;  $\log f_{\text{O}_2} = -0.7$ ; and temperature is at  $25^\circ\text{C}$ . The results have a maximum of  $3.6 \times 10^{-2}$  mol/kg ( $8.6 \times 10^3$  mg/L) and a minimum of  $5.48 \times 10^{-6}$  mol/kg (1.31 mg/L) with a geometric mean of  $6.27 \times 10^{-4}$  mol/kg ( $1.5 \times 10^2$  mg/L). The results for  $\log f_{\text{CO}_2} = -3.0$  are the top line with black circles plotted in Figure 9-7, and can be represented as function of pH:

$$\log[\text{Pu}] = 26.952 - 7.0629 \times \text{pH} + 0.49436 \times \text{pH}^2 \quad (\text{Eq. 9-7})$$

where [Pu] is plutonium solubility in mg/L. The solubility of  $\text{PuO}_{2(c)}$ , shown in Figure 9-7 has a similar pH-dependence to  $\text{PuO}_2 \cdot 2\text{H}_2\text{O}_{(\text{am})}$  but is 2 to 3 orders of magnitude lower.

Also shown in Figure 9-7 are plutonium solubilities estimated under reduced conditions ( $\log f_{\text{O}_2} = -40.7$ ) for conditions where  $\text{PuO}_{2(c)}$  (red squares) or  $\text{PuO}_{2(\text{am})}$  (green circles) controls solubility. Under these reduced conditions, plutonium solubilities are less dependent on pH and drop by six orders of magnitude.

Data from degradation of commercial spent nuclear fuel are also shown in Figure 9-7. The plutonium concentrations measured at ANL and PNNL overlap the values calculated under reducing conditions. These results suggest that in a potential repository at Yucca Mountain, plutonium concentration from spent fuel dissolution will be close to  $1.0\text{E-}5$  mg/L.

For the sensitivity studies, the uncertainties in plutonium solubility associated with the controlling phase and redox conditions are modeled with an equation similar to Equation 9-7, but with an uncertainty term ( $\epsilon$ ):

$$\log[\text{Pu (mg/L)}] = 20.952 - 7.0629 \times \text{pH} + 0.49436 \times \text{pH}^2 + \epsilon \quad (\text{Eq. 9-8})$$

where  $\epsilon$  is a random variable with a normal distribution, a mean of 0, and a standard deviation of 2. Figure 9-7b shows the abstraction for the sensitivity studies with plus or minus three standard deviations plotted on top of the data and calculations used in development of the abstraction. This range covers all of the experimental data, the theoretical concentrations from the amorphous solid in air, the crystalline material at  $\log f_{\text{O}_2 (\text{atm.})}$  of  $-40.7$ , and honors the pH dependence in air. Because this model is concave upward outside the range of data, and it includes a cap on the largest concentrations possible, it is valid for use at any pH within the TSPA sensitivity studies. This abstraction has a lower mean and a wider range than the log-uniform distribution ( $10^{-4.62}$  to  $10^{+1.68}$  mg/L) used in the TSPA-SR (CRWMS M&O 2000 [DIRS 153246], Table 3.5-8) shown by the bar on the left side of Figure 9-7b.

#### 9.3.2.2.5 Upper Bound Concentrations

Application of the dissolved concentration expressions for plutonium, uranium, neptunium and thorium beyond the pH regions in which they were calculated (typically between  $\text{pH} = 4$  and

pH = 9) generally leads to the prediction of physically unattainable results. For this reason the dissolved concentration limits for these elements are capped at 1 mol/kg bound. The physical justification for the bounding value is illustrated using the case of plutonium levels being set by equilibrium with  $\text{PuO}_2 \cdot 2\text{H}_2\text{O}$ . Dilute water with a molecular weight of about 18 g/mole and a density of about  $1 \text{ g/cm}^3$  (Lide 1991 [DIRS 131202], p. 6-10) contains about 55 moles of water in a liter (110 moles of hydrogen atoms, 55 moles of oxygen atoms). If every oxygen atom in solution were associated with a dissolved plutonium ion, there would be 27.5 moles of plutonium (neglecting changes in the specific volume of water). However at pH = 9 and above, plutonium forms a soluble carbonate species and each plutonium tends to be associated with 11 oxygen atoms, in which case the limiting plutonium concentration would be 5 mol/kg. Even 5 mol/kg is too high because water molecules will associate with other salts dissolved in the water as well. Consequently, substantially fewer water molecules will be available for association with dissolved plutonium. The limited supply of water in concentrated mixed solutions sets a physical upper bound approximated as 1 mol/kg (239,000 mg/L) for dissolved plutonium. A similar analogy was applied to bound the upper limit for dissolved levels of uranium (238,000 mg/L), thorium (230,000 mg/L), and neptunium (237,000 mg/L).

#### 9.3.2.2.6 In-Package Sorption

At present, TSPA-SR (CRWMS M&O 2000 [DIRS 153246]) conservatively takes no account of sorption inside breached waste packages or along the transport pathway to the invert, allowing pure or mixed phase solubility to control the concentration of radionuclides leaving the package. In reality, plutonium, and to a lesser extent neptunium, sorb strongly and irreversibly to most minerals and in particular to iron hydroxides (Lu et al. 2000 [DIRS 154422]), the primary degradation product predicted to occur in waste packages. Irreversible sorption refers to the fraction of the initially sorbed contaminant that becomes embedded or buried in the host surface and no longer available for subsequent desorption followed by aqueous transport.  $K_d$ s describe radionuclide transport in only limited situations. Their present-day use is primarily a numerical convenience. Dozens of technical articles, presentations, and books have accumulated over the past half century pointing to the extreme association of bomb-pulse fallout with particle surfaces and the resulting sharp attenuation of plutonium transport in soil profiles (e.g., Brady et al. 1999 [DIRS 154421], Appendix E and F; Bunzl et al. 1995 [DIRS 154468]; Coughtrey et al. 1986 [DIRS 154494]; Coughtrey et al. 1983 [DIRS 132164]). These observations (i.e., fallout data, hazardous waste sites, and laboratory experiments) suggest that plutonium (and to a lesser extent neptunium) will sorb strongly to solid surfaces, and they will do so irreversibly (i.e., not by a  $K_d$ -type model), possibly never leaving the waste package and invert, except as colloids.

Pertechnetate, which is usually assumed to have a  $K_d$  of zero and is therefore estimated to contribute significantly to dose, may sorb on copper oxides, the most likely alteration product of copper rails beneath the waste package. Conservative neglect of in-package sorption in general, and irreversible sorption of plutonium and neptunium in particular, may dwarf all other conservatisms in waste form. For the sensitivity studies, in-package sorption was added as an additional control of radionuclide concentrations. Further discussion is presented in Section 10.

### 9.3.2.3 Other Lines of Evidence to Support Models

As noted in Section 9.3.1.4, SNF and HLW tests done at ANL constitute another line of evidence to support the model (CRWMS M&O 2000 [DIRS 131861]). The range of leachate chemistries observed in laboratory studies of aqueous corrosion of unirradiated  $\text{UO}_2$  and commercial spent  $\text{UO}_2$  fuel (commercial SNF) provides confidence that the potential water chemistries that are modeled to develop in breached waste packages are realistic. Such corrosion studies conducted at ANL are of two types: drip tests and batch tests. The drip tests are dynamic flow-through studies in which the solids being studied are exposed to periodic injections of tuff-equilibrated J-13 well water (EJ-13) at a flux low enough to allow precipitation of solid corrosion products (secondary phases). The batch studies expose crushed solids with relatively high surface areas ( $\text{UO}_2$  and SNF) to small volumes of EJ-13 water. While the experimental conditions do not exactly match those modeled in the in-package chemistry calculation, the reactions affecting major element fluid compositions are the same in both, as are the broad trends observed.

A plot of dissolved uranium as a function of pH from the ANL drip and batch tests on unirradiated  $\text{UO}_2$  and commercial SNF is displayed in Figure 9-8. Also shown in Figure 9-8 are thermodynamic stability fields for some U(VI) silicates and predominance fields for aqueous U(VI) species. Dissolved uranium and pH measured in the leachates fall within the range suggesting that uranium solids may play an important role in controlling uranium concentrations (and possibly pH), qualitatively similar to what is observed in the in-package chemistry calculations. Figure 9-8 illustrates the wide range of dissolved uranium concentrations and pH values that have been observed in the ANL drip and batch tests. Total dissolved uranium spans a range of more than six orders of magnitude, and pH values span a range of more than four log units.

#### 9.3.2.3.1 Pure and Mixed-Phase Concentration Control

**Neptunium**—The potential influence that solid uranium(VI) corrosion products may have on dissolved radionuclide concentrations is currently under study. Microscopic examinations of radionuclide-bearing corrosion products taken from the ANL unsaturated drip and vapor tests on commercial SNF have shown that U(VI) solids may incorporate certain radioelements into their structures under the experimental conditions. Perhaps most notable among these discoveries is the identification of neptunium in the uranyl oxyhydroxide “dehydrated schoepite” that formed on commercial SNF that had reacted in humid air at  $90^\circ\text{C}$ . To date, neptunium-bearing dehydrated schoepite has not been identified from any drip tests with spent fuel; however, dissolved uranium and neptunium concentrations appear to be correlated in the ANL drip experiments (Figure 9-9). This correlation has been suggested as indicating that neptunium-bearing U(VI) corrosion products help limit the concentration of dissolved neptunium in leachates from the ANL drip tests.

**Technetium**—Technetium is released at a nearly constant rate in the ANL high drip-rate tests, consistent with the hypothesis that technetium is not solubility-limited in those tests. Analyses of solid corrosion products indicate that technetium is not incorporated into U(VI) solids in significant amounts. Electron energy loss spectra of the uranyl silicate,  $\beta$ -uranophane, formed in one ANL high drip-rate tests, reveal only a trace amount of technetium in this U(VI) compound; however, technetium was close to the detection limit for electron energy loss spectra (Finn

et al. 1998 [DIRS 100392], p. 9), and uranophane is not believed to significantly limit the release of technetium in the ANL drip tests.

**Plutonium**—The cumulative release behavior of plutonium in the ANL drip tests, like those of the actinides uranium, neptunium, and americium, exhibits early rapid release followed by substantial slowing after approximately 1.5 years of reaction. This behavior is consistent with plutonium release being limited by saturation with a plutonium-bearing solid. Transmission electron microscope examinations have identified plutonium-rich amorphous solids on the surfaces of reacted fuel grains in the ANL tests, and these may explain plutonium release behavior in the drip tests. Over long times (100,000 years) plutonium may display geochemical behavior similar to that of thorium in natural waters and may precipitate in minerals analogous to naturally occurring thorium minerals.

### **9.3.3 Cladding**

Since the 1950s, most commercial SNF has been clad in 600 to 900  $\mu\text{m}$  of zircaloy, a zirconium alloy. This material was selected for reactor use because it is corrosion-resistant and has attractive neutronic properties. The cladding was not considered as a barrier to the release of radionuclides in early TSPAs. However, information has accumulated in the literature indicating that cladding plays a major role in delaying the release of radionuclides to the environment.

#### **9.3.3.1 Goal of Model**

Clad degradation modeling is currently used as the basis for extending the period of wet storage, for licensing dry storage facilities, and for licensing shipping cask for commercial SNF by the Nuclear Regulatory Commission (NRC). The zircaloy cladding is not an engineered barrier of the Yucca Mountain disposal system but rather is an existing characteristic of the commercial SNF that is important to determining the rate of release of radionuclides once the waste package has breached. For TSPA-VA (CRWMS M&O 1998 [DIRS 100362], Section 6.3.1.1), several cladding degradation modes were combined into a time-varying function to evaluate failure.

The commercial SNF cladding degradation component is potentially important in reducing the peak dose because it restricts the amount of commercial spent fuel that is exposed to water and available for dissolution. Inventories of the two most important commercial SNF radionuclides in the nominal scenario, technetium-99 and neptunium-237, represent over 86 percent and 95 percent of the total inventory of these nuclides in the repository, respectively. Hence, the commercial SNF cladding degradation component can directly influence the peak dose by reducing the release of rate of these two radionuclides. The goal of the commercial SNF cladding degradation component is to determine the quantity of commercial SNF matrix that is exposed and, thereby, ready for radionuclides to dissolve into any available water.

### 9.3.3.2 Identification of Unquantified Uncertainties in Total System Performance Assessment for Site Recommendation

For TSPA-SR (CRWMS M&O 2000 [DIRS 153246]), two steps of cladding degradation were included, perforation and unzipping. The perforation of the cladding was modeled to occur because the cladding:

- Is damaged (initial perforations) before being received at the potential repository (during reactor operation and storage, dry storage, or transportation periods)
- Experiences creep rupture or stress corrosion cracking (SCC) during dry storage or initial disposal in the repository
- Experiences localized corrosion over time
- Experiences mechanical damage because of shaking from earthquakes or crushed by rock overburden.

Once perforated, the cladding may split along the axis (unzip) because the underlying uranium dioxide oxidizes further to uranium minerals that take up much more volume.

Some aspects of cladding perforation were evaluated using available data and therefore were realistic in TSPA-SR (CRWMS M&O 2000 [DIRS 153246]). However, many aspects of cladding perforation and unzipping were simply bounded.

The cladding degradation component of the model samples six parameters for the TSPA-SR (CRWMS M&O 2000 [DIRS 153246]). These parameters are represented by mathematical distributions covering the expected range of values of the parameter. The parameters used are:

- The number of rods initially perforated in a commercial SNF waste package
- The fraction of cladding perforated because of creep rupture and stress corrosion cracking
- The uncertainty in localized corrosion rate
- Uncertainty in mechanical damage (seismic). Rock overburden failures have been added for sensitivity calculations since the TSPA-SR model
- The uncertainty of the commercial SNF degradation rate
- The uncertainty in the unzipping velocity of the cladding, which represents the uncertainty in the surface area of the commercial SNF matrix inside the cladding that is available for degradation.

In TSPA-SR (CRWMS M&O 2000 [DIRS 153246], Section 3.5.4), the parameters that show importance in determining uncertainty in the dose in the first 100,000 years are those associated with initial cladding perforation and the unzipping velocity of the cladding. This is because in

this model the only cladding perforated is that initially perforated (i.e., as received) in that time period. However, between 100,000 years and 1,000,000 years, localized corrosion and mechanical damage perforation of the cladding become important. Predictions past the regulatory period are needed to address peak dose issues for the Environmental Impact Statement. During this period, uncertainties in two parameters show up as important: the order of magnitude uncertainty in the commercial SNF degradation rate and the two orders of magnitude uncertainty in the unzipping rate (i.e., active surface area).

Waste package temperature is treated as an independent variable in the cladding model and the lower temperature design does not affect the model.

### **9.3.3.3 Quantification of Previously Unquantified Uncertainty**

Table 9-6 lists the primary uncertainties that were considered in TSPA-SR (CRWMS M&O 2000 [DIRS 153246], Section 3.5.4) and subsequently.

#### **9.3.3.3.1 Initial Cladding Perforation**

The TSPA-SR (CRWMS M&O 2000 [DIRS 153246]) uncertainty on the percentage of cladding initially perforated is a triangular distribution with a mode of 0.0948 percent and range between 0.0155 percent and 1.285 percent. This upper range was determined by assuming that around any rod, the four closest were also damaged. The lower range was determined by assuming the distribution was symmetrical. The assumption that the upper limit is a factor of four is conservative since this represents all of the surrounding rods. A triangular distribution is proposed based on engineering judgement that the most likely percentage of perforated clad is well known and more likely than the upper and lower bounds. No refinement of this uncertainty is considered at this time.

#### **9.3.3.3.2 Creep and Stress Corrosion Cracking Perforation**

The TSPA-SR (CRWMS M&O 2000 [DIRS 153246]) repository design is cool enough that little or no creep rupture or stress corrosion cracking perforation are expected in the potential repository. The conservative creep model used in TSPA-SR, however, predicted failures during dry storage. This model used an unirradiated creep correlation for irradiated cladding and a lower-limit failure criteria of 0.4 percent creep strain. The percent failure range was defined as a triangular distribution, with a mode of 2.44 percent and mean of 7.5 percent and a range between 1.05 percent and 19.4 percent. A revised calculation (CRWMS M&O 2001 [DIRS 151662], Section 6.2) used an irradiated cladding creep correlation and the NRC recommended lower limit creep failure criteria of 1 percent creep strain (NRC n.d. [DIRS 147797]). This revised calculation does not predict creep failures during vacuum drying, dry storage, or in the repository with lower waste package temperatures. It does predict an upper limit of 0.47 percent of the rods failing from SCC. Based on these new calculations, a more realistic range between 0 percent and 0.5 percent with a uniform distribution was chosen for the sensitivity calculations (CRWMS M&O 2001 [DIRS 151662], Section 6.2.5).

#### **9.3.3.3.3 Localized Corrosion Perforation**

The conditions necessary for localized corrosion of zircaloy are not predicted to occur in the in-package bulk solutions but have not been ruled out for localized and/or non-equilibrium effects such as microbially induced corrosion, galvanic coupling, radiolysis, or extreme concentration by evaporation. Because the probability of damage from any of these mechanisms is difficult to quantify, a simplified model was utilized for TSPA-SR (CRWMS M&O 2000 [DIRS 153246]). This model assumes the amount of localized corrosion of the cladding is proportional to the amount of water that seeps into the waste package because most of these effects require seepage. A log-uniform distribution from 0.0041 to 0.41 percent localized failure per m<sup>3</sup> water seeping into the waste package was used. Although this model is generally conservative, it does not predict perforation from localized corrosion in packages that do not have water seeping into them. Thus, for about 87 percent of the waste packages (CRWMS M&O 2000 [DIRS 153246], Section 4.1.2), the intact cladding (i.e., cladding not initially damaged in the reactor or during dry storage) will not perforate until mechanically damaged.

To test the sensitivity of the peak dose on the localized corrosion model, the range of this simple model was lowered about an order of magnitude with greater probability in the low range (Table 9-7). In addition, a minimum failure rate of about 10<sup>-9</sup> of the rods/year was added for the packages without seepage.

#### **9.3.3.3.4 Seismic Failures**

For modeling perforation by shaking during earthquakes, TSPA-SR (CRWMS M&O 2000 [DIRS 153246]) used a bounding model, which perforated all cladding whenever large ground motion (frequency less than  $1.1 \times 10^{-6}$  per year) was sampled to occur. To test the sensitivity of TSPA to this parameter, the complementary cumulative distribution function for the frequency of seismic cladding failure (Table 9-8) was used.

#### **9.3.3.3.5 Rock Overburden Failures**

In TSPA-SR (CRWMS M&O 2000 [DIRS 153246]) calculations, the cladding was protected from rock falls or rock overburden by the drip shield and waste package during the regulatory time period of 10,000 years. For the sensitivity calculations, damage to cladding from rock fall or rock overburden was added for the period when the waste package no longer protects the cladding. After severe degradation of the drip shield and waste package, the static load of the overburden resting on the cladding within areas of the waste package that have structurally failed, have been conservatively modeled and calculated to breach (CRWMS M&O 1999 [DIRS 136105], Section 5.3). In the sensitivity model, the cladding perforation from rock overburden starts to occur when 50 percent of the modeled waste package surface area has been corroded through by generalized corrosion. The fraction of breached cladding increases linearly with the fraction of the waste package that is corroded until all cladding is breached when the entire waste package has been corroded by general corrosion.

#### **9.3.3.3.6 Cladding Unzipping**

In TSPA-VA (CRWMS M&O 1998 [DIRS 108000]), most of the radionuclide inventory in a rod was assumed available for dissolution once the cladding on a rod was perforated. For TSPA-SR

(CRWMS M&O 2000 [DIRS 153246]), only the fast release fraction (gap inventory and initial fuel dissolution) is modeled to be available at initial perforation. The remaining inventory is made available only as the cladding splits open, thus representing a more realistic approach. A simple model based on swelling of the fuel was developed, which predicted the splitting rate to be 40 times the intrinsic dissolution velocity (uncertainty is triangular shape 1, 40, and 240 times).

For the sensitivity calculations, the distribution of the unzipping velocity has been reevaluated and summarized (CRWMS M&O (2001 [DIRS 151662], Section 6.6.1; see also Table 9-9). The lower limit is set at the intrinsic dissolution velocity (velocity multiplier = 1). This is equivalent to the fuel being dissolved at the intrinsic dissolution velocity at the face of the pellets and propagate axially along the fuel rod. The upper range, 15,000 times the intrinsic dissolution velocity, is introduced to represent axial splitting of the cladding in an anoxic environment. This type of unzipping has occurred in an ANL fuel dissolution test with clad fuel (Cunnane 2001 [DIRS 154818]). It is occasionally observed in boiling water reactors (BWRs) (Edsinger 2000 [DIRS 154433]; Lysell et al. 2000 [DIRS 154432]) and is associated with oxygen starvation and the collection of hydrides in the cladding leading to a type of delayed hydride cracking. This type of unzipping is quick, exposing the pellets in tens of days. Armijo (1994 [DIRS 154411], p. 411), reports that axial splitting occurs in 22 percent of the 48 failed BWR rods that he studied. For the sensitivity model, it is assumed that oxygen starved conditions, similar to BWR conditions, are generated in all waste packages for a short time. A probability of 22 percent is assumed for all the failed rods to unzip quickly. When this occurs, the pellets are available to dissolve using a surface area for irradiated pellets developed by Barner (1985 [DIRS 109194], Table 4.6, p. 4.16). Bare fuel has an equivalent wet unzipping velocity multiplier of 15,000.

### **9.3.3.7 Thermal Operating Mode**

The behavior of the cladding within the repository is not expected to differ significantly between a low and high temperature-operating mode as long as the cladding temperature limit of 350°C is not exceeded. The revised *Clad Degradation - Summary and Abstraction* AMR (CRWMS M&O 2000 [DIRS 147210], Section 6.2.4 and Figure 14) shows that with the cladding below 350°C, cladding failure is not expected. There are some secondary temperature effect included in the abstraction. The waste form dissolution rate is weakly temperature dependent and is included in the cladding unzipping calculation. This feedback only occurs after water ingress into the waste package. The waste package temperature is treated as an independent variable in the cladding degradation abstraction (CRWMS M&O 2000 [DIRS 147210], Attachment I). This abstraction is applicable for a hot (backfill) design such as that considered in TSPA-VA (CRWMS M&O 1998 [DIRS 108004]), the TSPA-SR (CRWMS M&O 2000 [DIRS 153246]) warm design, and any future cool repository design.

### **9.3.3.4 Other Lines of Evidence to Support Model**

The direct and indirect evidence that supports the various features of the DOE cladding degradation model can be found in the extensive experimental literature on zircaloy and zirconium. Earlier studies (Ahn et al. 1999 [DIRS 135894]; Henningson 1998 [DIRS 112089]; Manaktala 1993 [DIRS 101719]; Pescatore et al. 1990 [DIRS 101230]; Rothman 1984 [DIRS 100417]) evaluated cladding degradation under repository conditions. Others

(Cunningham et al. 1987 [DIRS 101591]; Einziger and Kohli 1984 [DIRS 101605]; Peehs 1998 [DIRS 109219]) evaluated fuel performance under dry storage conditions similar to early repository conditions. As part of the development of U.S. Environmental Protection Agency environmental standards, S. Cohen & Associates (1999 [DIRS 135910]) did a detailed study of cladding degradation, before receipt at, and emplacement in, a potential repository. Sanders et al. (1992 [DIRS 102072]) reviewed the condition of cladding after reactor operation and reviewed the potential of damage from external mechanical loading. Experiments (Wilson 1985 [DIRS 102147]; Wilson 1987 [DIRS 102150]; Wilson 1990 [DIRS 100793]) also measured the releases of radionuclides from damaged cladding under possible repository conditions. The latest TSPA by the Electrical Power Research Institute (EPRI 2000 [DIRS 154149]) included cladding degradation. Other sources address specific degradation mechanisms. An International Atomic Energy Agency report (IAEA 1998 [DIRS 150560]) summarizes work on water side corrosion and gives 538 references and a bibliography of 45 books. Cox (1990 [DIRS 152954]) summarizes the pellet-clad work (235 references). Cox (1990 [DIRS 152778]) also summarizes the stress corrosion cracking work (106 references).

### **9.3.4 Colloids**

#### **9.3.4.1 Goal of Model**

The goal of the colloid model is to quantify the impacts of uncertainties in the behavior of colloids generated from the degradation of HLW glass, commercial SNF, and DOE SNF, as well as colloid-facilitated transport of radionuclides from the waste package. It is anticipated that colloids will also be mobilized as a result of corrosion of waste package components, in addition to the degradation of HLW and SNF waste forms. The abundance of colloids within the breached waste package will depend on the extent of waste form alteration and the nature of the alteration products formed.

Colloid abundance and stability also depend on many environmental factors, including the ionic strength, pH, cation concentrations, colloid content of groundwater entering the waste package from the drift, presence of fulvic and humic acids, and microbe fragments (CRWMS M&O 2001 [DIRS 153933], Section 1.0). Suspended colloids may subsequently flocculate and settle by gravity, be chemically or mechanically filtered, or dissolve. If environmental factors change, colloids may be peptized; colloid-sized particles may precipitate; or other natural processes may occur. In addition, colloids may sorb readily at the interfaces between air and water in rocks and engineered barriers and, depending upon the degree of saturation of the porous medium as well as its configuration, may be retarded, immobilized or transported (CRWMS M&O 2001 [DIRS 153933], Section 6.1.5). These issues are of concern within the engineered barrier system in the drift and in the near- and far-fields (CRWMS M&O 2001 [DIRS 153933], Section 6.1.5). They are relevant as well to transport within the waste package. The colloid source term is defined here as the total of those radionuclides associated with colloids that: are mobilized at the surface of the waste form, are transported within the waste package to the waste package wall, leave the waste package at a breach (or breaches) in the waste package wall, and enter the drift. The present discussion is restricted to the in-package portion of the potential repository system.

### **9.3.4.2 Identification of Unquantified Uncertainties Total System Performance Assessment for Site Recommendation**

To begin with, large-scale uncertainties burden the collective understanding of colloidal fate and transport. For the colloidal radioisotope concentration component, the conceptualization used YMP-relevant experimental results from YMP-specific work and from the published literature as summarized in *Waste Form Colloid-Associated Concentrations Limits: Abstraction and Summary* (CRWMS M&O 2001 [DIRS 153933], Section 6.1). The conceptualization identified the availability and the stability of three categories of colloids: existing colloids in the groundwater, colloids generated during degradation of the waste form, and colloids generated during degradation of the waste package. A number of unquantified uncertainties were identified in the TSPA-SR (CRWMS M&O 2000 [DIRS 153246]) and subsequently. They can be roughly grouped as pertaining to: amounts of colloids available, nature and extent of sorption to colloids, and colloid retardation. Generally, in TSPA-SR, uncertainties were addressed by following bounding approaches and choosing conservative inputs and/or conceptual models. A number of uncertainties, bounding assumptions, and conservatisms are outlined below.

#### **9.3.4.2.1 DOE Spent Nuclear Fuel Degradation Colloids**

The potential for colloid-facilitated migration of radionuclides derived from the degradation of metallic uranium fuel is not considered in the current colloid model and will be addressed by ongoing laboratory experiments. Preliminary unpublished results from the experimental degradation of metallic uranium fuels indicate that the fuel degrades rapidly, to generate fine particles, some of them colloidal in size (CRWMS M&O 2001 [DIRS 153933], p. 33, Section 6.1.1.1).

#### **9.3.4.2.2 Commercial Spent Nuclear Fuel Degradation Colloids**

The uncertainty associated with the potential contribution of irreversibly attached radionuclides on colloids generated from commercial SNF degradation will be addressed by ongoing laboratory experiments. The only existing data on irreversibly attached plutonium concentrations are from those generated from the degradation of defense high level waste (HLW) glass (CRWMS M&O 2001 [DIRS 154071], Table 4); data from commercial SNF have been inconclusive because insufficient numbers of colloids have been collected from degradation experiments (CRWMS M&O 2001 [DIRS 154071], pp. 31 to 36).

#### **9.3.4.2.3 Air-Water Adhesion**

Colloids adhere strongly to the interface between air and water, such as thin films and bubbles (CRWMS M&O 2001 [DIRS 153933], Section 6.1.5). The analysis of this important process is site specific (i.e., must be tailored specifically to the system under investigation) and can be quite complex. Leaving colloid sorption onto the air-water interface out of the colloid model is likely conservative. Adhesion to a fixed interface (e.g., as part of a water film on a component in the waste package) would serve to immobilize the colloid as long as the interface remained intact. Adhesion to the surface of a freely suspended bubble, on the other hand, would enable the colloid to be transported with the bubble, although the relatively large size of the bubble may

cause it to become filtered out at constrictive passageways. Air-water interface adhesion of colloids is neglected in the present model.

#### **9.3.4.2.4 Waste Package Retardation**

Colloid retardation in the waste package is ignored. The development of defensible parameters describing retardation of colloids in the waste package is challenging because of uncertainty in the detailed nature of flow paths and pore structures. Changing ratios of divalent to monovalent cations along this initial flow path might also cause destabilization of colloids (e.g., Stumm and Morgan 1996 [DIRS 125332]).

#### **9.3.4.2.5 Microbes**

Microbial effects have been ignored. These effects might include: organic coatings on mineral colloids, which would tend to sorb radionuclides as well as destabilize the colloid suspension and cause the colloids to agglomerate, and development of colloids comprised of monocellular microbes and fragments, which could sorb and transport radionuclides and/or agglomerate and immobilize radionuclides (CRWMS M&O 2001 [DIRS 153933], Section 6.1.8). Thus, either of two competing processes, one that encourages colloid mobilization, another that encourages colloid agglomeration and flocculation, may prevail. It is uncertain which process would dominate at a particular location or point in time within the repository. Microbial effects are discussed at greater length in Section 10.

#### **9.3.4.2.6 Temperature**

Thermal effects on colloidal transport are largely unknown, but colloid stability is generally expected to decrease with increasing temperature. Actinide and metal sorption onto metal hydroxides colloids tends to increase with temperature paralleling temperature-dependent increases in metal hydroxide anionic surface charge (Machesky 1990 [DIRS 145046]).  $K_{ds}$  of uranium, neptunium, plutonium, and americium on hematite, montmorillonite, and silica increase roughly one order of magnitude as temperature increases from 20° to 80°C in J-13 well water for 10-day runs (Lu et al. 2000 [DIRS 154422]).

#### **9.3.4.2.7 Mineralogy**

In TSPA-SR (CRWMS M&O 2000 [DIRS 153246]), the properties of groundwater colloids flowing into the drift are assumed to be bounded by smectite. Other colloids may be present, including silica, zeolites, feldspars, iron-(hydr)oxides, etc. Smectite has a higher affinity for radionuclides than many of these other minerals, and, therefore, this assumption may overestimate colloidal uptake of radionuclides and be conservative. Information on colloid mineralogy collected from YMP-area wells may justify use of a mixture of mineralogies including less sorptive minerals (e.g., silica). A preliminary review of data presented in Lu et al. (2000 [DIRS 154422]) suggests that while  $K_d$  values for plutonium and americium sorption are generally higher for montmorillonite than silica, the difference is less than one order of magnitude. For TSPA, it is critical that enough different colloids are modeled to capture the overall behavior of the system. The waste form and waste package degradation product colloids, and the uncertainty associated with their parameters (formation, abundance, and sorption), might outweigh any uncertainty in the groundwater colloid parameters.

#### **9.3.4.2.8 Steel Degradation Colloids**

Degradation of waste packages will generate large quantities of iron hydroxides that may collectively constitute the most significant source of colloids in the system. Although the nature and reactivity of these colloids is discussed in greater detail in Section 10, a number of the implications of waste form colloidal export will be touched on below.

#### **9.3.4.2.9 Consideration of Radionuclides Other than Plutonium and Americium**

In the current waste form degradation model americium is assumed to behave similarly to plutonium (i.e., may be incorporated into a colloid as irreversibly attached). The quantities of plutonium and americium irreversibly attached to colloids are determined at each time step in TSPA by the radionuclide inventory remaining at each time step (CRWMS M&O 2001 [DIRS 153933], p. 51).

In the current colloid model, plutonium and americium are treated as irreversibly attached to waste form colloids. These two radionuclides were considered potentially the most significant sparingly soluble radionuclides that could readily become irreversibly attached to colloids and subsequently be transported from the waste package. In addition to plutonium and americium, two other radionuclides, protactinium and thorium, are considered for reversible attachment to waste form colloids and subsequent transport. The fractions of release from colloids associated with other dose-important radionuclides are considered insignificant relative to their dissolved concentrations.

#### **9.3.4.3 Quantification of Previously Unquantified Uncertainty**

##### **9.3.4.3.1 Combined Groundwater and Corrosion Colloid Concentrations**

Limited data exist for concentrations of iron-(hydr)oxide colloids in natural systems. At the Morro de Ferro natural analogue site (Poços de Caldas, Brazil) concentrations of iron-hydroxide [ $\text{Fe}(\text{OH})_3$ ] colloids were measured in deep groundwaters adjacent to an iron-rich rock body (CRWMS M&O 2000 [DIRS 150707], Section 3.8.2.3.1). The measured concentration, 0.25 mg/L, is similar to concentrations of other inorganic colloids found in natural waters at other deep sites (CRWMS M&O 2000 [DIRS 150707], Section 3.8.2.3.1). The upper end of the range used, 1.0 mg/L, imparts a four-fold conservatism relative to the concentration observed at the analogue site.

There are more abundant measurements of groundwater colloid concentrations than there are of corrosion colloid concentrations. Consequently uniform distributions were ascribed to a combined population of groundwater and corrosion colloids for two different ionic strength ranges. Reasonable ranges for this combined reversible colloid population are log uniform distributions between  $10^{-6}$  and  $10^{-1}$  mg/L (for ionic strength less than or equal to 0.05) and  $10^{-9}$  and  $10^{-3}$  mg/L (for ionic strength greater than 0.05 M).

##### **9.3.4.3.2 Plutonium Irreversibly Associated with Waste Form Colloids**

Reasonable distributions for plutonium irreversibly associated with waste form colloids are log-uniform distributions between  $10^{-11}$  and  $10^{-6}$  mol/L (for ionic strength less than or equal

to 0.05 M) and  $10^{-14}$  and  $10^{-8}$  mol/L (for ionic strength greater than 0.05 M). The upper range is roughly centered on the bounding concentration of  $8 \times 10^{-8}$  mol/L defined in CRWMS M&O (2001 [DIRS 153933], Figures 7 and 13). The minimum value is approximately four orders of magnitude lower. The maximum value of the distribution,  $10^{-4}$ , is approximately three orders of magnitude greater. Similarly, the lower range is centered on the minimum concentration measured experimentally,  $10^{-11}$  mol/L (CRWMS M&O 2001 [DIRS 154071], Table 4, p. 20). The minimum and maximum values of the higher ionic strength range are then plus-or-minus 3 orders of magnitude from  $10^{-11}$  mol/L.

### 9.3.4.3.3 Colloid Sorption of Plutonium and Americium

A recent review of the data presented in *Waste Form Colloid-Associated Concentrations Limits: Abstraction and Summary* (CRWMS M&O 2001 [DIRS 153933], Attachment XVI) and in Lu et al. (2000 [DIRS 154422]) corroborates the currently used  $K_d$  values for plutonium and americium sorption ( $10^4$  and  $10^5$  ml/g respectively) for sorption onto montmorillonite (proxy colloid mineral for waste form and groundwater colloids). In contrast, a preliminary review of the Lu et al. (2000 [DIRS 154422]) data suggest that the currently used  $K_d$  values for iron-(hydr)oxides (proxy colloid mineral for steel corrosion colloids) may be underestimated by as much as one to two orders of magnitude. One factor that may contribute to overly conservative  $K_d$  values is that materials used in the Lu et al. (2000 [DIRS 154422]) experiments probably optimize measurements of sorption, because they provided fresh, clean surfaces for actinide attachment, which would not likely be the case in the potential repository environment. Furthermore, the studies considered did not evaluate the impact of other solutes (including less critical radioisotopes) regarding competition for radionuclide uptake (the exception is the Lu et al. (2000 [DIRS 154422]) sorption determinations for a range of ionic strengths; only the monovalent cation  $\text{Na}^+$  was used in the solutions). These accumulated uncertainties are reflected in the recommended log-normal distribution of the  $K_d$  describing plutonium and americium sorption, namely a mean of  $10^5$  ml/g with a geometric standard deviation of plus-or-minus 2 log units.

## 9.4 SUMMARY AND PARAMETERS PROVIDED TO TOTAL SYSTEM PERFORMANCE ASSESSMENT FOR SENSITIVITY CALCULATIONS

The preceding sections outline the quantification of waste form model uncertainty since the TSPA-SR (CRWMS M&O 2000 [DIRS 153246]). Some of the sections (e.g., in-package sorption and colloidal transport) are treated in greater detail in Section 10. Complementary information is provided here to emphasize the integration among the sub-components. The new waste form models and parameters provided to TSPA for the sensitivity calculations are summarized here.

### 9.4.1 In-Package Chemistry

Two new in-package chemistry models were developed for TSPA: an updated expected case and a sensitivity case. The updated expected model has been implemented in TSPA for the supplemental studies, but the sensitivity model is presented for insight only. For the commercial SNF packages, the pH-time trajectories are abstracted using response surfaces for four time periods (BSC 2001 [DIRS 154620]) and are summarized in Section 9.3.1.3.3. The pH-time

trajectories for the codisposal packages were abstracted into four ranges (Table 9-5, first two columns). These models cover pH ranges similar to the TSPA-SR models, but provide better time discretization.

#### **9.4.2 Dissolved Concentrations**

New solubility models were provided for thorium (Equation 9-2), neptunium (Equation 9-6), plutonium (Equation 9-8), and technetium (a log-triangular distribution from 0.56 to a peak of  $10^5$  mg/L). In all four cases, the mean solubility was lower, and the distribution was larger, than in the TSPA-SR.

#### **9.4.3 Cladding**

Changes in the cladding models are discussed in Section 9.3.3.3 and summarized in Table 9-6. The most important changes are the lowering of initial failures due to creep during dry storage and the addition of late time rock load breaching.

#### **9.4.4 Colloids**

The colloid model was simplified, and the uncertainty ranges were expanded in the supplemental studies (see Section 9.3.4.3). The groundwater and corrosion product colloids were combined to provide a single colloid type with reversible radionuclide attachment. Over 5 orders of magnitude of uncertainty were added to the concentration of this colloid type. The new ranges were log-uniform distributions between  $10^{-6}$  and  $10^{-1}$  mg/L (for ionic strength less than or equal to 0.05 M) and  $10^{-9}$  and  $10^{-3}$  mg/L (for ionic strength greater than 0.05 M). Instead of using separate  $K_d$ s for each radionuclide, a single  $K_d$  for reversible sorption of plutonium, americium, protactinium, and thorium was defined. This  $K_d$  was chosen in the high range from the earlier modeling but with a broader uncertainty range. A log-normal distribution with a geometric mean of  $10^5$  ml/g and a geometric standard deviation of 2 log units was chosen.

Approximately 5 orders of magnitude of uncertainty were added to the modeled concentration of irreversibly attached plutonium. The new ranges were log-uniform distribution between  $10^{-11}$  and  $10^{-6}$  mol/L (for ionic strength less than or equal to 0.05 M) and  $10^{-14}$  and  $10^{-8}$  mol/L (for ionic strength greater than 0.05 M). The concentration of irreversibly attached americium was calculated in proportion to its inventory relative to plutonium.

Table 9-2. Important Input Parameters for the Impact of Glass and Steel Degradation Unquantified Uncertainties on In-package pH Calculations

Model	Parameter	High	Medium	Low	None
<b>Science and Engineering<sup>a</sup></b>					
	A516 rate ( $\mu\text{m}/\text{yr}$ )	72		7	
	flow rate (L/yr)	150	15	1.5	
	fuel exposed	0.99	0.8	0.01	
	glass rate (pH=2) ( $\mu\text{m}/\text{yr}$ )	36		3.6	
	glass rate (pH=7) ( $\mu\text{m}/\text{yr}$ )	0.007		0.0007	
<b>Updated Expected Case<sup>b</sup></b>					
	A516 rate ( $\mu\text{m}/\text{yr}$ )	72		7	
	flow rate (L/yr)	15	1.5	0.15	
	fuel exposed		0.1	0.01	
	glass rate (pH=2) ( $\mu\text{m}/\text{yr}$ )	0.5			
	glass rate (pH=7) ( $\mu\text{m}/\text{yr}$ )	0.007			
<b>Sensitivity<sup>c</sup></b>					
	A516 rate ( $\mu\text{m}/\text{yr}$ )	72		7 <sup>d</sup>	0
	flow rate (L/yr)			0.15	
	fuel exposed			0.01	
	glass rate (pH=2) ( $\mu\text{m}/\text{yr}$ )	5.00E-01	5.00E-03	5.00E-05	0
	glass rate (pH=7) ( $\mu\text{m}/\text{yr}$ )	7.00E-03	7.00E-05	7.00E-07	0

Source: <sup>a</sup> CRWMS M&O 2000 [DIRS 111880], Table 1 and p. 17 with units converted.

<sup>b</sup> BSC 2001 [DIRS 153724], Table 2 and p. 20 with units converted.

<sup>c</sup> BSC 2001 [DIRS 154840], Tables 1, 2, and 3 with units converted.

<sup>d</sup> Effective rate decreased by decreasing surface area.

NOTE: Glass and metal dissolution units were converted from  $\text{mol}/\text{cm}^2\text{-s}$  to  $\mu\text{m}/\text{yr}$  by multiplying by the defined molecular weight of 100 g/mol, dividing by the density (A516 =  $7.86 \text{ g}/\text{cm}^3$ ; glass =  $2.85 \text{ g}/\text{cm}^3$ ), and multiplying by  $10^4 \mu\text{m}/\text{cm}$ , and  $3.1558 \times 10^7 \text{ seconds}/\text{year}$ .

Table 9-3. Total System Performance Assessment Model Results for pH Ranges

<b>Total System Performance Assessment Model</b>		
<b>Time Period (years)</b>	<b>Process Model Range for CSNF</b>	<b>Process Model Range for Codisposal</b>
0-1,000	3.4-5.5 (minimum pH) (a)	4.8-6.4 (minimum) (c)
1,000 – 1,000,000	5.7-7.3 (average pH) (b)	8.1-10.0 (maximum) (d)

Source: CRWMS M&O 2000 [DIRS 129287], (a) Tables 2 and 3, (b) 4 and 5, (c) 7 and 9, and (d) 10 and 11.

Table 9-4. Model Results for Commercial Spent Fuel Package pH Ranges

<b>New CSNF Package Models</b>			
<b>Time Period (years)</b>	<b>Updated Expected Case Process Model<sup>a</sup></b>	<b>Sensitivity Abstraction<sup>b</sup></b>	<b>pH Criteria</b>
0-200	3.9-6.7	4.4-6.7	Minimum
200 - 10,000	6.0-7.3	4.3-7.5	Average
10,000 - 300,000	3.9-6.6	2.8-6.8	Minimum
300,000 - 1,000,000	6.1-6.7	6.0-6.8	Stabilized

Sources: <sup>a</sup> BSC 2001 [DIRS 154620], Tables 3 to 9.

<sup>b</sup> BSC 2001 [DIRS 154840], Table 6.

NOTE: Uncertainty of +/- 1 pH unit added to these ranges.

Table 9-5. Model Results for Codisposal Fuel Package pH Ranges

<b>New Codisposal Package Models</b>			
<b>Time Period (years)</b>	<b>Updated Expected Case Abstraction</b>	<b>Sensitivity Abstraction</b>	<b>pH Criteria</b>
0-300	3.3-3.6	2.6-4.5	Minimum
300 - 10,000	5.6-7.7	3-7.4	Average
10,000 - 400,000	9.1-10.0	4.7-10	Maximum
400,000 - 1,000,000	8.8-10.0	6.5-8.9	Stabilized

Source: BSC 2001 [DIRS 154840], Tables 8 and 9.

NOTE: Uncertainty of +/- 1 pH unit added to these ranges.

Table 9-6. Primary Cladding Uncertainties Considered

Description	Parameter	Parameter Distribution in TSPA-SR <sup>a</sup>	Parameter Distribution in Unquantified Uncertainty Analysis <sup>b</sup>
Percentage of cladding with initial perforation.	Initial_Rod_Failure fraction	Triangular (0.0155%, 0.0948%, 1.285%)	Triangular (0.0155%, 0.0948%, 1.285%)
Percent of cladding perforated due to creep rupture and stress corrosion cracking.	Creep_Used	Triangular (1.05%, 2.44%, 19.4%)	Uniform (0.0 to 0.5%)
Uncertainty in the localized corrosion rate.	% rods/m <sup>3</sup> water	0.041%/m <sup>3</sup> , uncertainty multiplier, Log-uniform (0.1, 10)	Specified CCDF (range 5 × 10 <sup>-4</sup> % to 5 × 10 <sup>-2</sup> %, minimum rate added)
Uncertainty in the CSNF intrinsic dissolution rate multiplier (10 <sup>Uncert_a0</sup> ).	Uncert_a0	Uniform (-1, 1)	Uniform (-1, 1)
Seismic failure.	Frequency	1.1 E-6 /yr, no uncertainty range	Specified CCDF (range 4.9 × 10 <sup>-6</sup> to 2.7 × 10 <sup>-12</sup> ).
Rock overburden failure.	Fraction f(pf, waste package patch fraction)	Not included	0, pf < 50% 2 x (pf-50), pf >= 50%
Uncertainty in unzipping velocity multiplier.	Unzip_uncert	Triangular (1, 40, 240)	Specified CCDF (range 1.0 to 15,000).

Sources: <sup>a</sup> CRWMS M&O 2000 [DIRS 153246], Sections 3.5.3.2 and 3.5.4.2.

<sup>b</sup> CRWMS M&O 2001 [DIRS 151662] and this work.

NOTE: CCDF = complementary cumulative distribution function.

Table 9-7. Complementary Cumulative Distribution Function for Fraction of Rods Failed per m<sup>3</sup> of Seepage

Complementary Cumulative Distribution Function	Percent of Rods Failed per m <sup>3</sup>
1.00	5 E-4
0.50	5 E-4
0.00	5 E-2

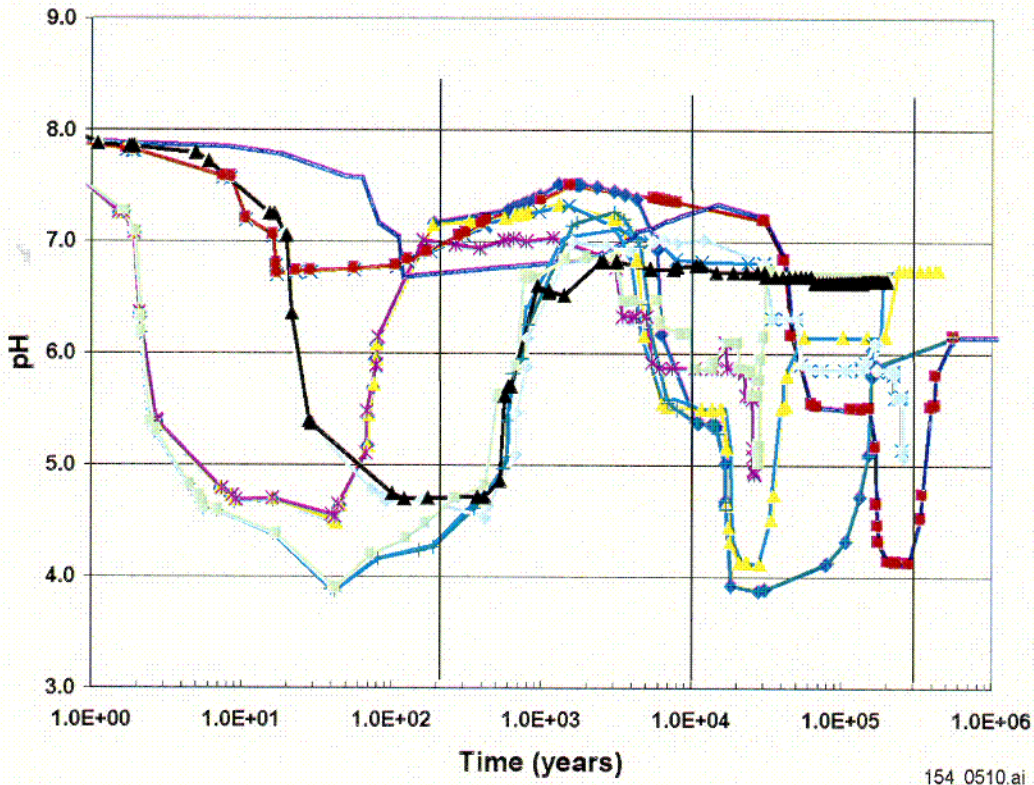
Table 9-8. Complementary Cumulative Distribution Function for Frequency of Seismic Cladding Failure

Complementary Cumulative Distribution Function	Frequency (/yr)
1.00	4.90 E-06
0.95	4.90 E-06
0.85	1.10 E-06
0.50	6.40 E-08
0.15	6.20 E-10
0.05	2.70 E-12
0.00	2.70 E-12

Table 9-9. Complementary Cumulative Distribution Function for Unzipping Velocity Multiplier

Complementary Cumulative Distribution Function	Velocity Multiplier
1.00	1
0.90	1
0.50	9
0.25	18
0.23	180
0.22	15,000
0.00	15,000

Source: CRWMS M&O 2001 [DIRS 151662], Section 6.6.1 and Section 9.3.3.3.6 of this document.



154\_0510.ai

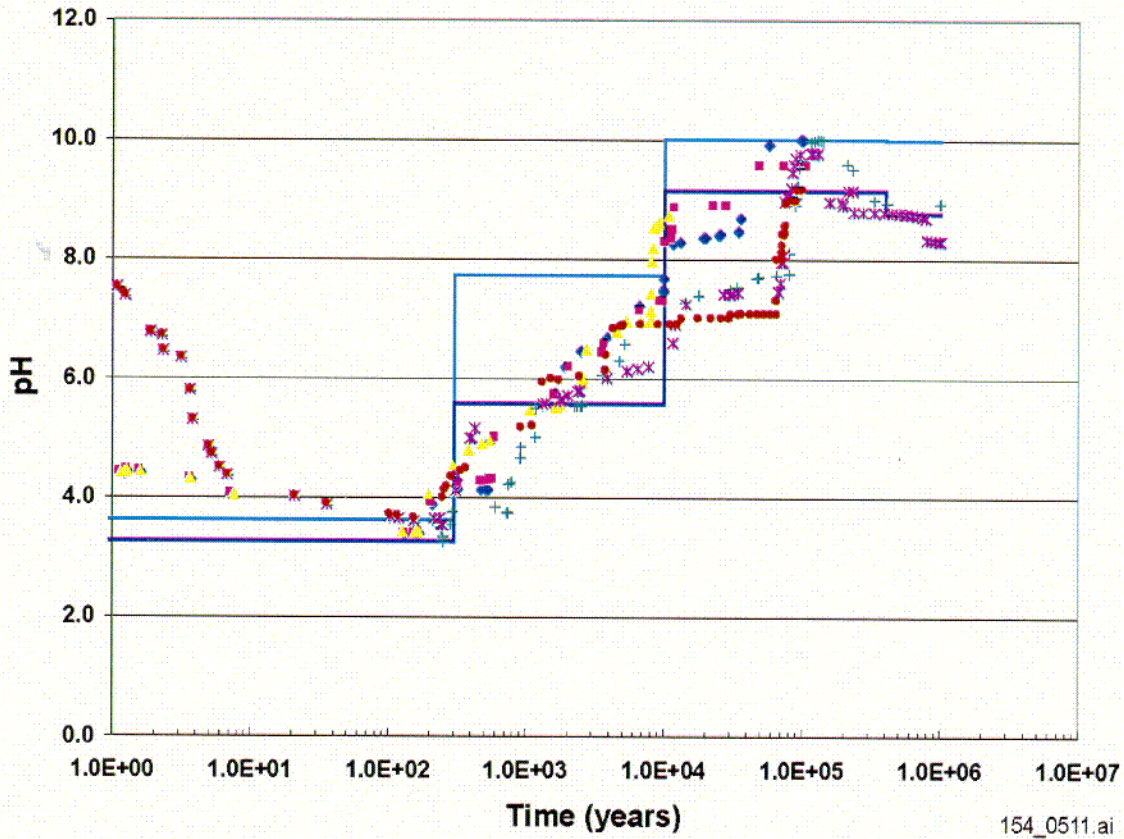
154\_0510.ai

Source: BSC 2001 [DIRS 154620], Figure 1.

NOTE: Updated base-case model pH-time trajectories for commercial spent nuclear fuel packages. Lines represent trajectories calculated over a range of water fluxes (15-0.15 L per waste package per year), clad exposures (1-10 percent) and steel degradation rates (BSC 2001 [DIRS 154620]).

Figure 9-1. Updated Expected Case Model pH-Time Trajectories for Commercial Spent Nuclear Fuel Packages

C06

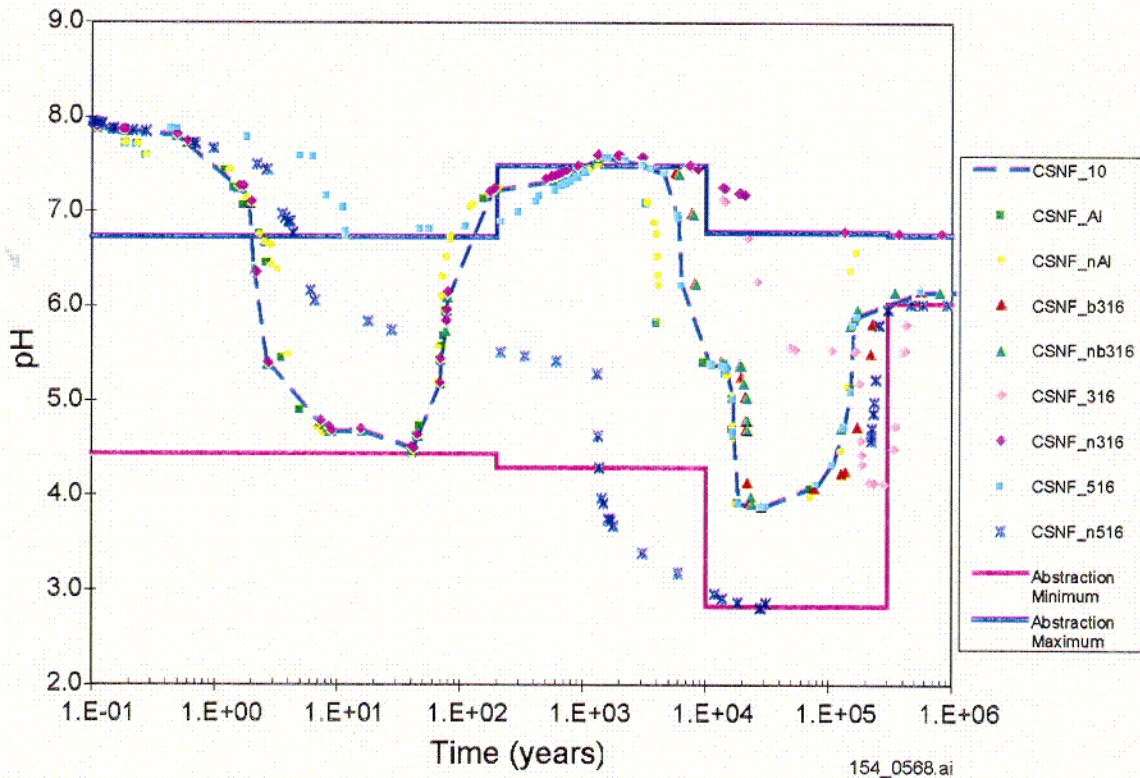


154\_0511.ai

Source: BSC 2001 [DIRS 154840], Figure 13.

NOTE: Updated base-case model pH-time trajectories for codisposal packages. Points represent Fast Flux Test Facility and Fermi waste package trajectories calculated over a range of water fluxes (15-0.15 L per waste package per year). The lines represent model abstractions of the minimum, maximum, and average pH ranges (BSC 2001 [DIRS 154620]).

Figure 9-2. Updated Expected Case Model pH-Time Trajectories for Codisposal Packages



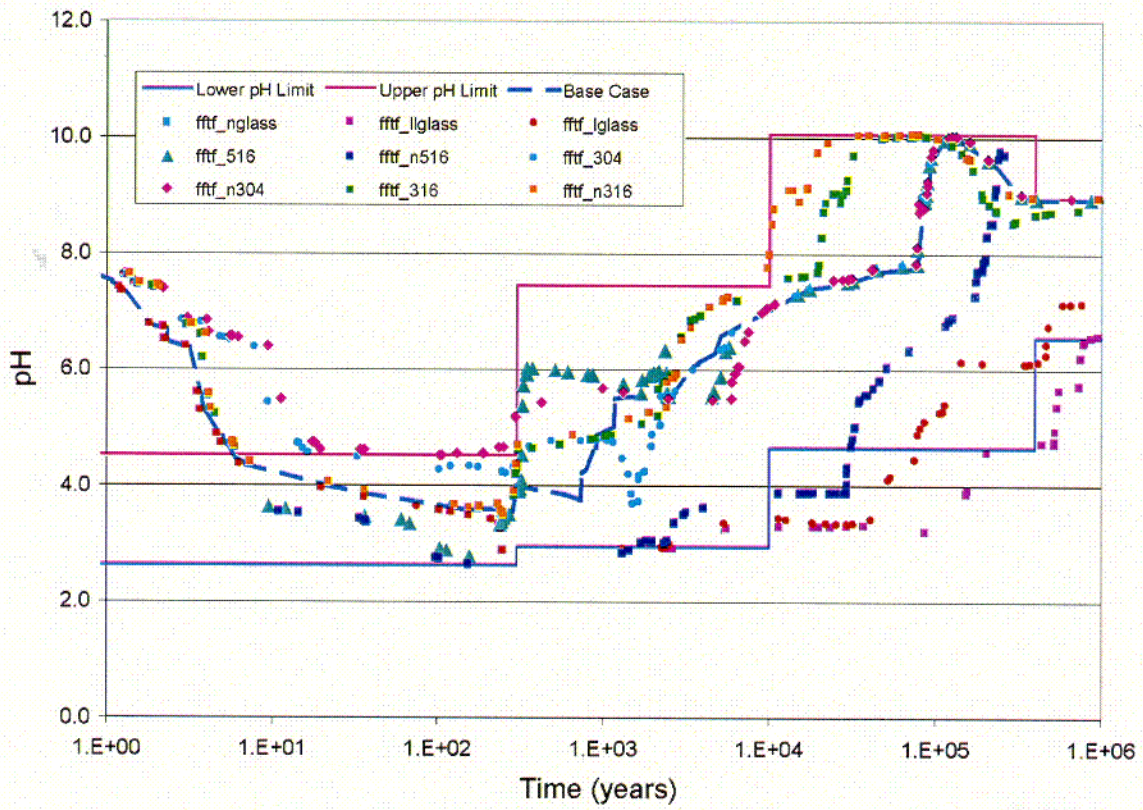
154\_0568.ai

Source: BSC 2001 [DIRS 154840], Figure 6.

NOTE: CSNF = Commercial Spent Nuclear Fuel.

Figure 9-3. Sensitivity Model pH-Time Trajectories for Commercial Spent Nuclear Fuel Packages

CO8

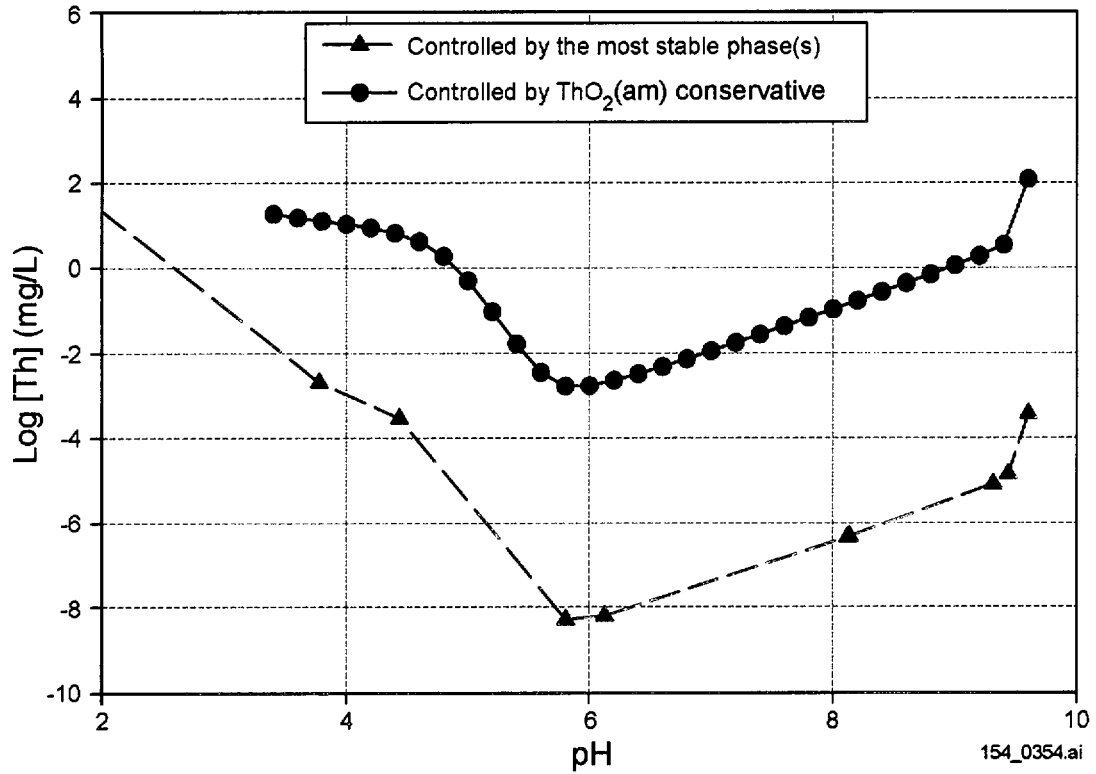


154\_0569.ai

Source: BSC 2001 [DIRS 154840], Figure 12.

Figure 9-4. Sensitivity Model pH-Time Trajectories for Codisposal Packages

C09



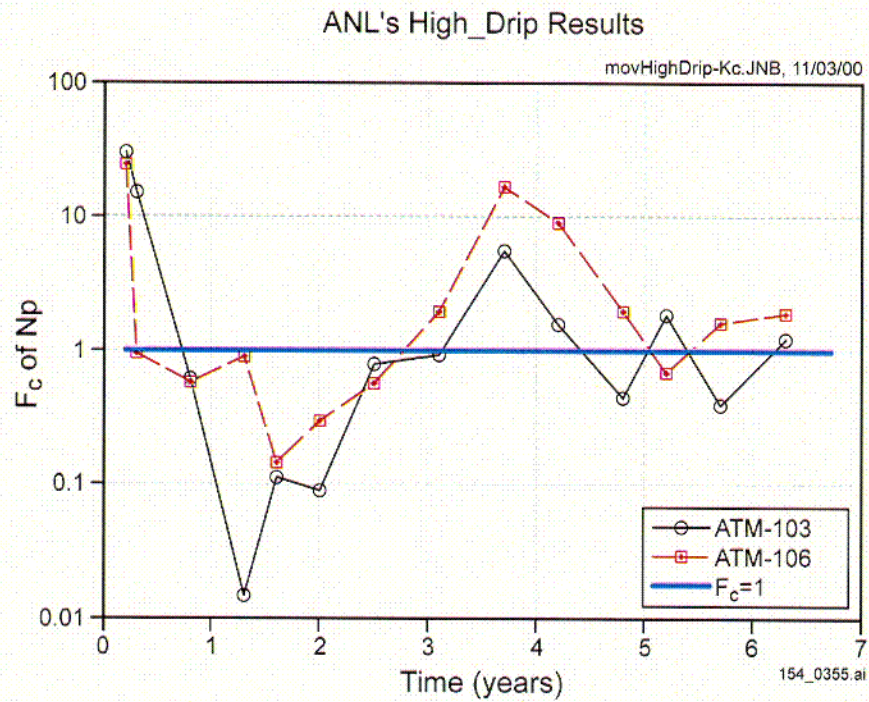
154\_0354.ai

Source: Chen 2001 [DIRS 155247], Figure 8.

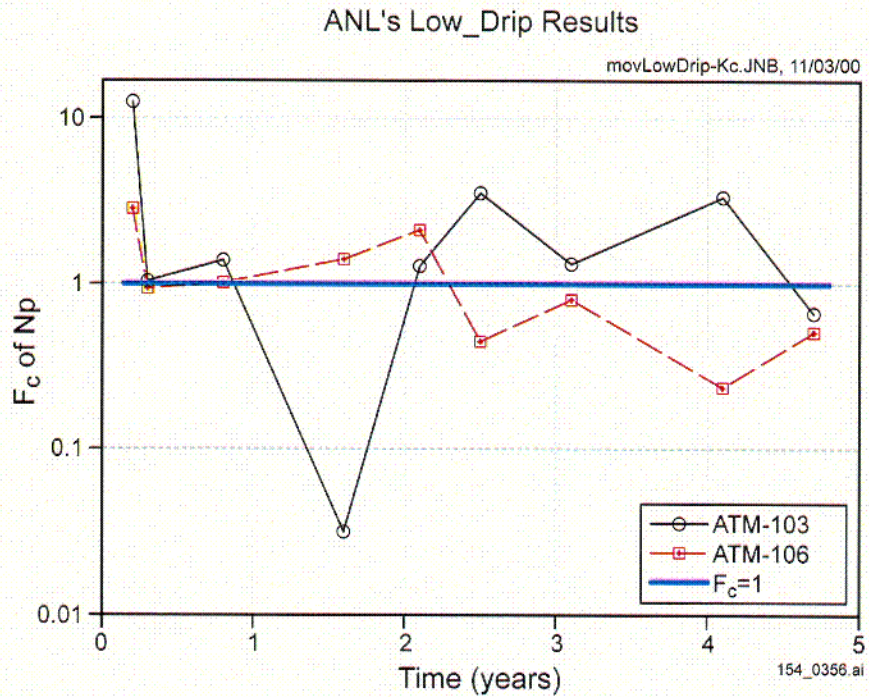
NOTE: The most stable phase (thorianite) yields thorium solubility 4 to 6 orders of magnitude lower than that for ThO<sub>2</sub>(am).

Figure 9-5. Thorium Solubility versus pH with Different Controlling Minerals

(a)



(b)



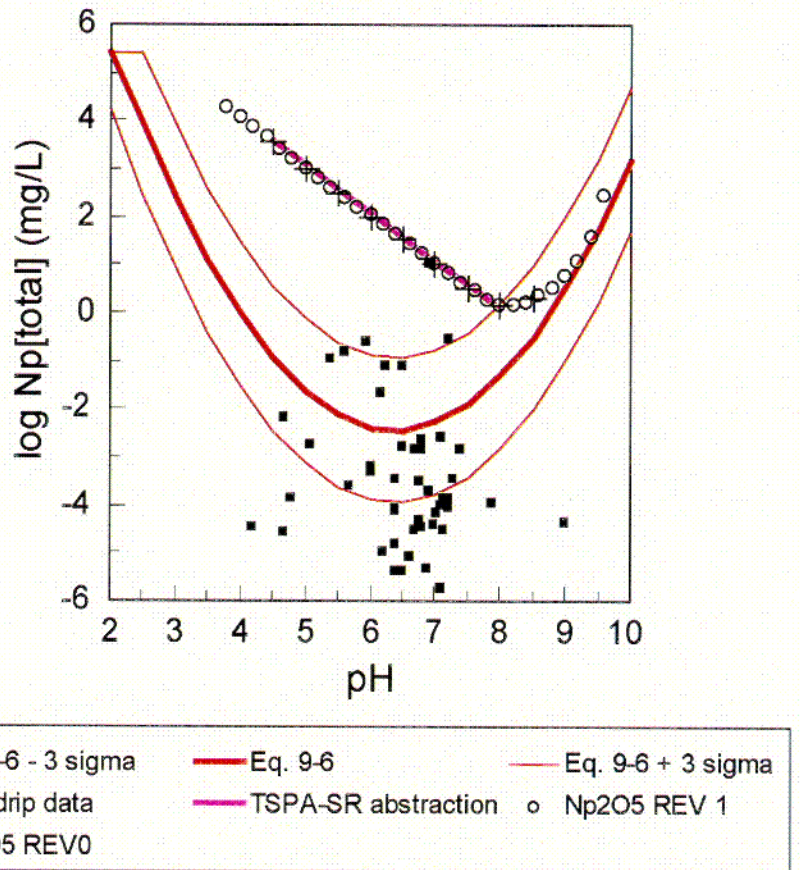
154\_0355.ai / 154\_0356.ai

Source: Chen 2001 [DIRS 155247], Figure 4.

NOTE: Argonne National Laboratory (ANL) (a) high-drip and (b) low-drip tests. The concentrating factor ( $F_c$ ) of neptunium (Np) fluctuates around 1.0 and appears to dampen to 1.0 as time increases. ATM = approved testing material

Figure 9-6. Concentrating Factors of Neptunium in Drip Tests

*cid*



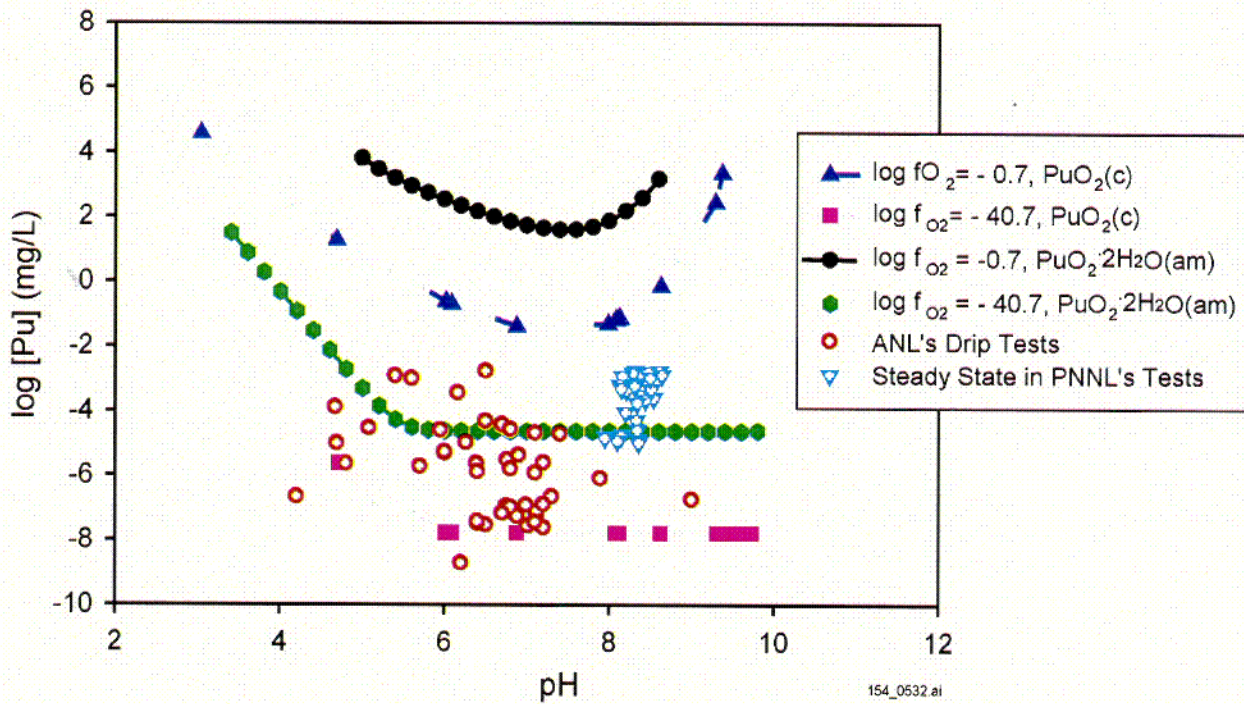
154\_0530.ai

154\_0530.ai

Source: Chen 2001 [DIRS 155247], Figure 6.

Figure 9-6b. Neptunium Dissolved Concentration Limit Models and Data

211



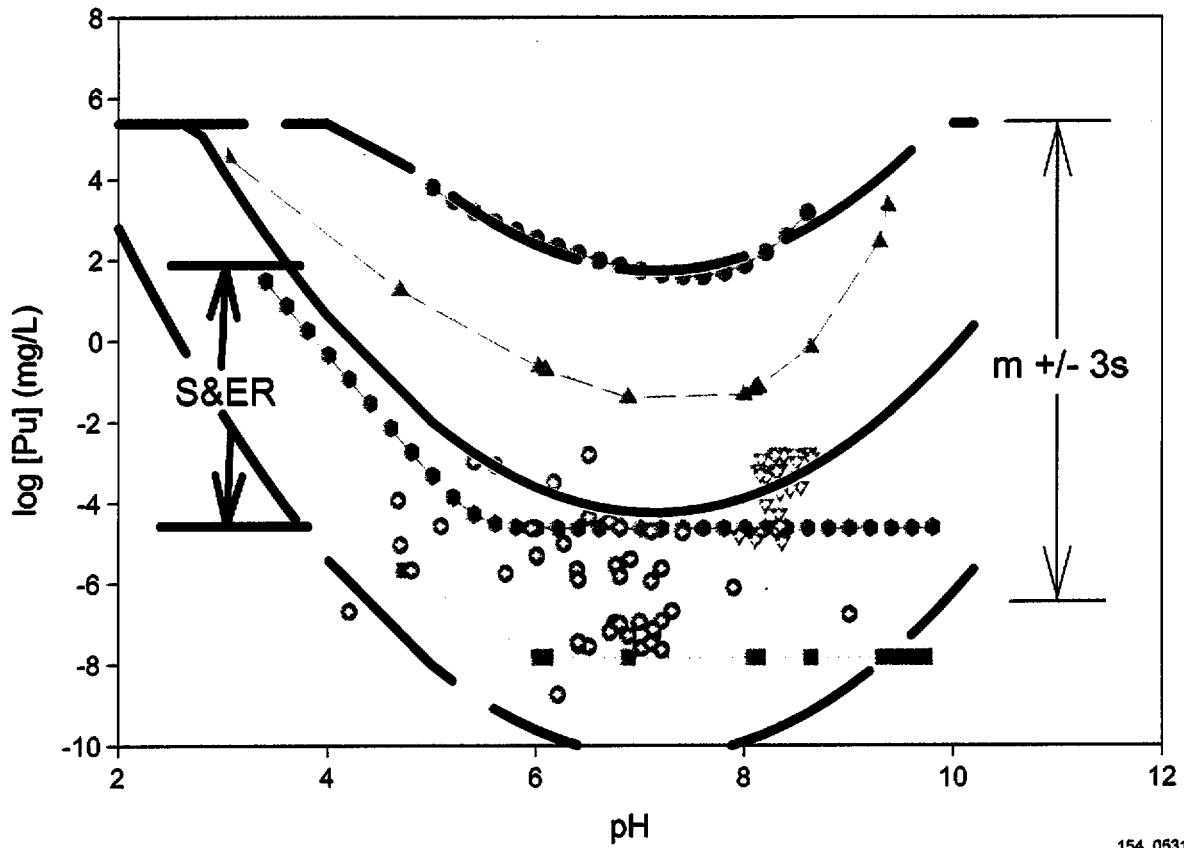
154\_0532.ai

Source: Chen 2001 [DIRS 155247], Figure 10.

NOTE: ANL = Argonne National Laboratory; PNNL = Pacific Northwest National Laboratory.

Figure 9-7. Plutonium Dissolved Concentration Limit Estimations and Data

C12



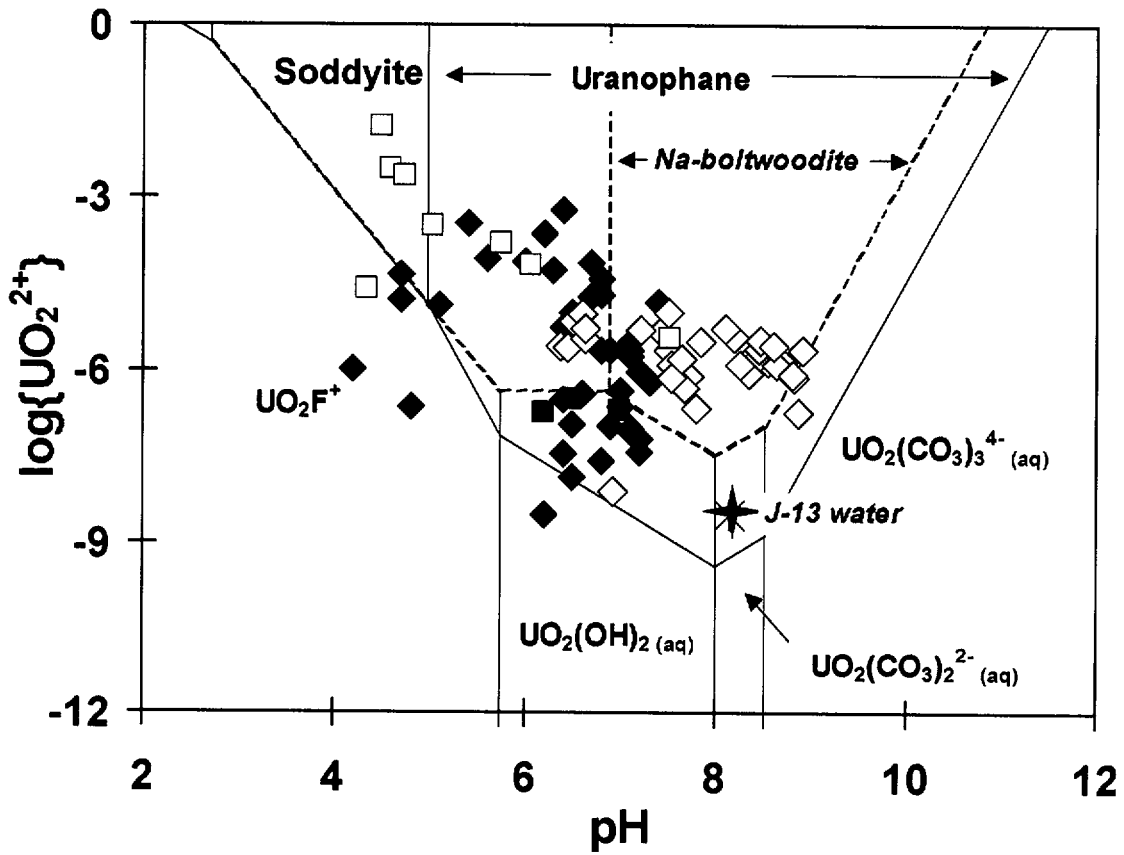
154\_0531.ai

154\_0531.ai

Source: Chen 2001 [DIRS 155247], Figure 11.

NOTE: S&ER = *Yucca Mountain Science and Engineering Report* (DOE 2001 [DIRS 153849]).

Figure 9-7b. Plutonium Dissolved Concentration Limit Abstraction and Data

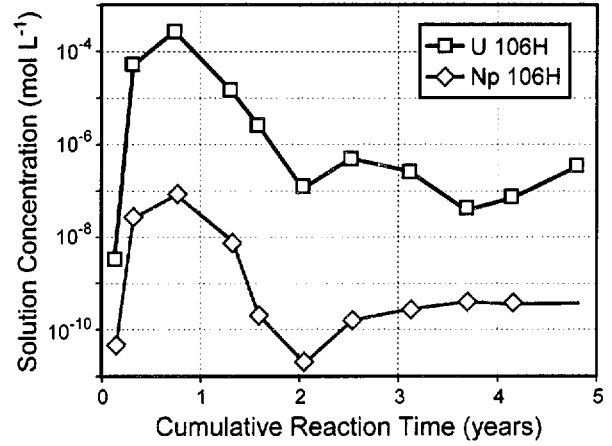
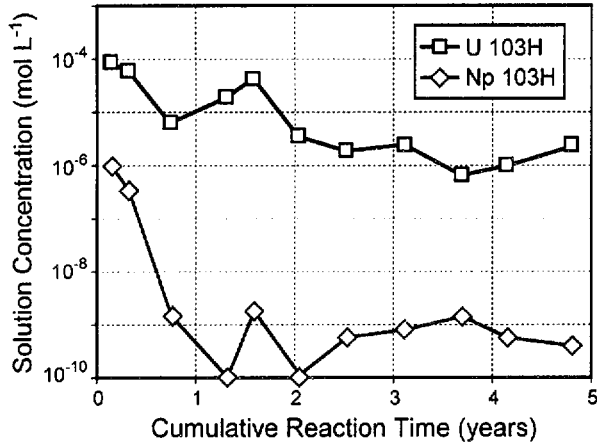


154\_0570.ai

154\_0570.ai

NOTE: Data from Argonne National Laboratory dip and batch studies of spent nuclear fuel and  $\text{UO}_2$  corrosion (CRWMS M&O 2000 [DIRS 131861]). Black diamonds: commercial spent nuclear fuel drip tests; black squares: commercial spent nuclear fuel batch tests; hollow diamonds:  $\text{UO}_2$  drip tests; hollow squares:  $\text{UO}_2$  batch tests. Also shown are thermodynamic stability fields for uranium(VI) solids and predominance fields for aqueous uranium (VI) species in equilibrium with Well J-13-like water chemistries over a range of pH values (Finn et al. 1998 [DIRS 100392], Figure 61).

Figure 9-8. Experimentally Measured pH and Dissolved Uranium of Leachates



155\_0571.ai

155\_0571.ai

Source: BSC 2001 [DIRS 154844], Figure A4.

NOTE: Data on neptunium (Np) and uranium (U) leachates from Argonne National Laboratory high drip-rate tests on commercial spent nuclear fuel. Left panel = ATM-103; right panel = ATM-106. ATM = approved testing material.

Figure 9-9. Temporal Variations in the Molar Concentrations of Neptunium and Uranium

INTENTIONALLY LEFT BLANK